DETECTION AND ISOLATION OF CIRCULATING TUMOR CELLS FROM WHOLE BLOOD USING A HIGH-THROUGHPUT MICROCHIP SYSTEM

by

Yuan Zhong

A Dissertation

Submitted to the Faculty of Purdue University

In Partial Fulfillment of the Requirements for the degree of

Doctor of Philosophy

School of Mechanical Engineering

West Lafayette, Indiana

May 2021

THE PURDUE UNIVERSITY GRADUATE SCHOOL

STATEMENT OF COMMITTEE APPROVAL

Dr. Cagri A. Savran, Co-Chair

School of Mechanical Engineering

Dr. Chun-Li Chang, Co-Chair

School of Mechanical Engineering

Dr. Jong Hyun Choi

School of Mechanical Engineering

Dr. Bumsoo Han

School of Mechanical Engineering

Dr. Babak Ziaie

School of Electrical and Computer Engineering

Approved by:

Dr. Cagri A. Savran

To my advisors, family, and girlfriend

ACKNOWLEDGEMENTS

First, I would like to acknowledge my advisor, Prof. Cagri Savran, for his continuously guidance and support. His profound knowledge, advocation for academic freedom, and sharp insights in plenty of scientific research area have inspired me throughout my graduate life. It is an honor and privilege to work with and be advised by him. I am also deeply grateful for his genuine caring and immense patience.

I would like to profoundly thank Prof. Chun-Li Chang for his unreserved help and encouragement in all aspects through my doctoral journey. He shares with me not only professional vision and skills, but also his worldview and philosophy, which influence me deeply. To me, he is a proficient academic mentor and a thoughtful friend at the same time.

I would like to acknowledge my esteemed advisory committee members, Prof. Jong Hyun Choi, Prof. Bumsoo Han, and Prof. Babak Ziaie for sharing their invaluable knowledges and suggestions that guided me through my doctoral career. I want to extend my acknowledgments to our collaborators, Prof. Milan Radovich's group from Indiana University School of Medicine and Prof. Philip Low's group from Purdue University Department of Chemistry for contributing their expertise and professional perspective.

I would like to thank my lab partners and colleagues, Dr. Norman David Brault, Dr. Wanfeng Huang, Dr. Onur Gur, and Dr. Rohil Jain, for their help and assistance throughout my research. We had many interesting and inspiring discussions in the lab, and I am grateful for the brilliant and insightful thoughts they shared with me.

I would also like to thank my friends: Dongxin Liu, Sikai Wang, and Haowei Yin for their companion and continued support that made my life more cheerful at Purdue.

My most sincerely appreciation goes to my parents, Dong Zhong and Dr. Yueming Yuan, and my beloved girlfriend Junyi Zhao, for their endless love and support, and for sharing my joy and sorrow.

TABLE OF CONTENTS

LIST OF TABLES

LIST OF FIGURES

ABSTRACT

Circulating tumor cells (CTCs) have been proved to possess great value and potential in detection, diagnosis, and prognosis of non-haematologic cancers. Their unique characteristics in providing both phenotypic as well as genotypic information make them highly valuable in liquid biopsy assays. At the same time, though numerous studies and research have been done, identification and enumeration of CTCs is still technically challenging due to their rarity and heterogeneity. The primary goal of the thesis is to develop a CTC detection and isolation system with ultra-high sensitivity and purity, while keeping it fast and scalable. We proposed a microfluidic system that integrates positive immunomagnetic capturing, high-throughput parallel flow and size filtration. In this thesis, two generations of the system have been developed to achieve the goal, and are approved to be able to effectively detect and isolate CTCs from hundreds of breast cancer blood samples in real clinical applications.

The first-generation system is based on a sandwich-structured microfluidic chamber, which has a micro-aperture chip as the core to detect and isolate immunomagnetically targeted CTCs. The system achieves high detection yield (>95%) and purity (>99.9998% depletion of leukocytes) by streamlining the workflow and using unprocessed whole blood (without centrifuging), as well as utilizing an advanced surface coating approach to passivate the microchip surface. We first demonstrate experiments for determining the optimal detection parameters. Then we characterize the system by isolating deterministically spiked 1, 10, and 100 single MCF-7 breast cancer cells into tubes of whole blood, and show that >95% of cells were captured. A detection yield of 100% from single cell spiking experiments (n = 6) demonstrates excellent detection capability and repeatability of the system. We finally demonstrate the use of the system for CTC detection in the context of a phase II clinical trial of early-stage triple-negative breast cancer (TNBC) patients. As a part of the trial, 182 blood samples were collected from 124 early-stage TNBC patients at high-risk of relapse. We detected CTCs in 36.3% of patients who had already completed chemotherapy and surgery for curative intent and were thus nominally expected to have very few to zero CTCs. Moreover, increasing CTC count from the same patients shows good correlation with their clinical course. The ability to detect CTCs' presence using this first-generation system illustrates its important clinical utility.

The second-generation system applies a similar detection strategy but employs an upgraded microchip and device, as well as a further streamlined process flow to achieve an even higher detection efficiency, especially for capturing the target cells with low surface marker expression level. We first did modeling and simulation of the new system to find the optimal magnet configuration and verify the detection sensitivity improvement on the first-generation system. Then we characterized the new system by detecting spiked JEG-3 and JAR cells in both cell culture medium and human blood. The result demonstrates that the detection yield increased by ~20% using the second-generation system under the same experiment condition. Next, we applied the system to a phase I clinical trial for CTC detection from metastatic triple-negative breast cancer (mTNBC) patient blood samples. CTCs of mTNBC are known to with in the low marker expression phenotype, which requires ultra-high detection sensitivity. Our system captured CTCs from 48 out of 102 (47%) blood samples, the positivity rate agrees with the conclusions from other studies and presents the reliability to the system. Finally, we explored a novel 4-marker panel for CTC detection from mTNBC patient blood samples. We conducted paired comparisons using the 4-marker panel versus a single marker for detection. The 4-marker panel yielded more CTCs in 5/8 complete paired assessments, and less CTCs in 1/8. The association missed the significance level only slightly ($p = 0.08$), and the result strongly illustrates the potential for using the panel to cover the mTNBC cells' heterogeneity for enhanced CTC detection. Furthermore, the presence of CTCs from blood samples correlates well with the patient's disease progression.

Finally, we demonstrated downstream analysis ability of the CTCs detected by the second-generation system. Captured CTCs can be readily released from our system without any loss or damage to a secondary microchip device to be further isolated as single cells, and picked up individually for downstream analysis like DNA/RNA sequencing or single-cell cultivation. Directions for future work is also discussed. We envision this versatile and efficient system to be highly beneficial in a broad range of clinical and research applications regarding CTCs.

1. INTRODUCTION

1.1 Motivation

1.1.1 Liquid Biopsy

Cancer is the second leading cause of death globally; it is responsible for about 10 million deaths in 2020 [1]. Cancer can be detected by certain symptoms or medical imaging methods, but almost the only way for definitive cancer diagnosis is biopsy, a procedure that involves extraction of sample tissues or cells from patients, for it offers a close medical examination opportunity to get hands on a real piece of the tumor to help differentiate between cancerous and noncancerous cells, and get vital genetic information about the cancer. However, the standard biopsy methods require invasive excisions that always cause great pain to the patients and more importantly, can cause complications that could be lethal. Hence the use of biopsy is restricted, and it cannot be performed routinely. Besides, cancer is a heterogeneous genetic disease, traditional biopsy methods can only give a limited (both spatial and temporal) snapshot of the primary tumor lesion and cannot effectively reflect the dynamic tumor progression or provide enough information about the metastases and genomic landscape [2].

Since 1990s, liquid biopsy has drawn more and more attention as a revolutionary alternative technique to traditional biopsies. Liquid biopsy, as the name suggests, is the sampling and analysis of patient-derived body liquid, primarily blood. It consists of the detection, isolation, and characterization of 1) circulating tumor cells (CTCs): a subset of aggressive tumor cells enters the bloodstream from the primary tumor and/or metastatic lesions; 2) circulating tumor DNA (ctDNA): tumor derived fragmented DNA from cells undergoing apoptosis and necrosis, or active release from viable tumor cells; and 3) exosomes: a type of extracellular vesicle that contains constituents (protein, DNA, and RNA) of the cells that secrete them [3]. As shown in Figure 1.1, CTCs, ctDNA and exosomes all come from the primary tumor or metastatic lesions and are shed into the bloodstream directly or indirectly (CTCs can further contribute to the release of ctDNA and circulating exosomes) and carried around body in the blood circulation. Therefore, these biomarkers can be treated as a tiny piece of their original tumor lesions, and have the same diagnostic and genetic information [4]. Liquid biopsy possesses multiple benefits including easy and frequent access, capability of providing much wider temporal and spatial information, and

great potential of aiding in therapeutic decisions. These not only make liquid biopsy a reliable alternate to, if not a better choice than, traditional biopsies, but also help open unprecedented perspectives in cancer pathology and clinical therapy [5,6].

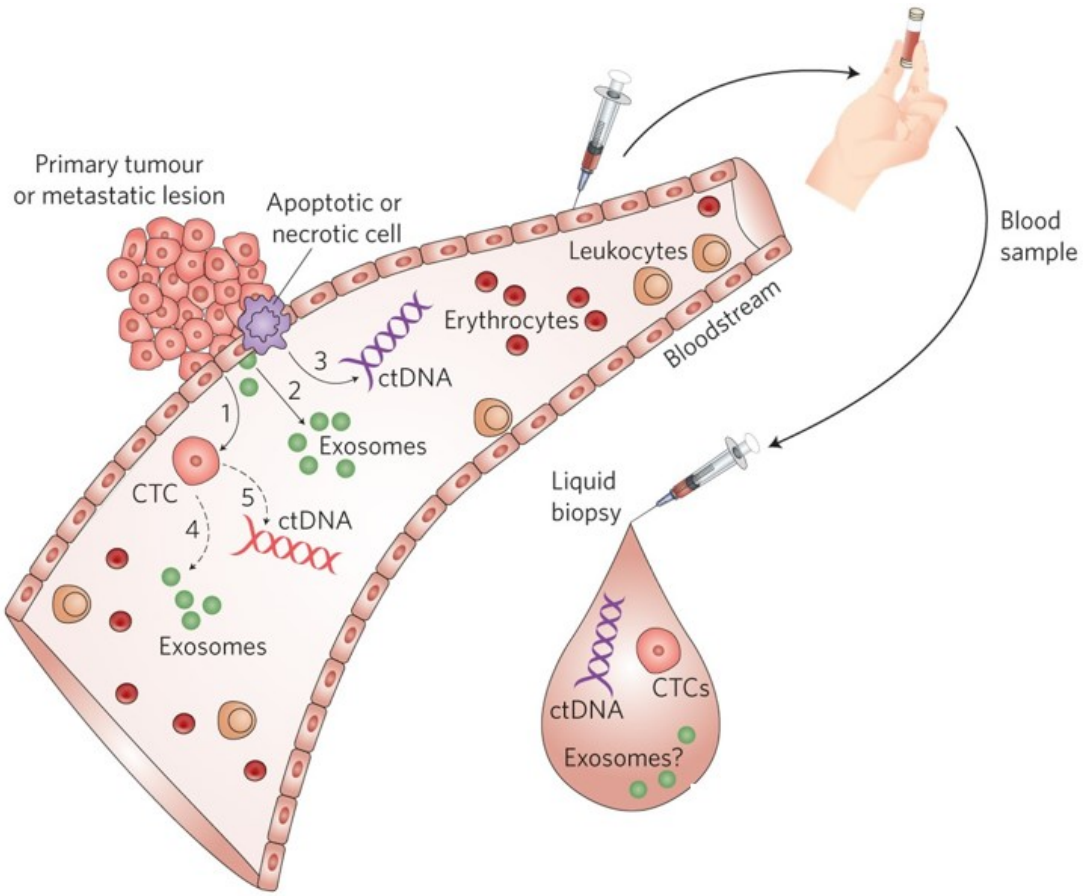

Figure 1.1. Liquid biopsy assays. (1) CTCs: a subset of aggressive tumor cells released to the bloodstream from the primary tumor and/or metastatic lesions, which will undergo apoptosis or circulate as isolated CTCs. (2) & (4) Exosomes: released by viable tumor cells, as well as CTCs. (3) & (5) ctDNA: fragmented DNA released by apoptotic or necrotic tumor cells, as well as apoptotic CTCs.

First, drawing blood for liquid biopsy is a non-invasive way. Therefore, liquid biopsy can be accessed rapidly and effectively avoid complications that occur after invasive biopsies, such as pain, bleeding, and infections. Due to this non-invasive nature, liquid biopsy can also be collected routinely for real-time monitoring of disease progression and treatment response, and providing a wealth information of metastasis risk and genomic evolution [7-9].

Second, liquid biopsy can serve as a diagnostic marker for early cancer detection. The chance of cancer survival depends largely on extent of the disease at the start of treatment: many localized cancers can be successfully cured by surgery and/or systemic therapies when detected before they have metastasized; but once distant metastasis (the cause of most cancer deaths) has occurred, surgical excision is rarely curative [10-13]. However, currently most people who develop cancer already have advanced disease at the time of diagnosis [12,13]. Therefore, early detection of cancer, especially before clinical symptoms appear, is very important and needs to be addressed promptly. Studies have shown that liquid biopsies can be detected in the blood of patients with very early-stage cancers and no metastasis [11,14,15], sometimes even before any primary solid tumor was detectable with current imaging methods, of which the detection threshold is $\sim 10^9$ cells [16,17]. Hence, liquid biopsy qualifies for a reliable early screening method, which can be done repeatedly and routinely, while medical imaging are costly and usually subject patients to radiation, and cannot be used regularly. Similarly, after surgical removal of the primary tumor, liquid biopsy can be used as an important prognostic marker for detecting residual disease and predicting metastatic recurrence risk, which promotes early therapy intervention to a great extent.

Third, liquid biopsy can provide more spatial information. Cancer is associated with mutated genes and is a very genetically heterogeneous disease. In almost all cases, tumors originate from a single cell, and tumor cells are always replicating, which results in tumors displaying startling phenotypic as well as genetic heterogeneity [18]. In other words, tumor cells could be very different from each other even when they are from the same lesion of the same patient. As mentioned above, liquid biopsy may originate from both primary and metastatic lesions, rendering it characteristics to provide information for the total tumor burden. Compared with a single tissue biopsy, liquid biopsy can not only give a wider genetic landscape of the cancer, but also identify specific mutations to reflect heterogeneity [16,19]. In addition, liquid biopsy is especially useful when the tumor lesion is in vital organs or tissues where it is impossible or difficult to extract a biopsy by traditional methods.

Finally, based on the information acquired from downstream analysis of liquid biopsy, personalized medicine or therapy can be designed and tested. For example, CTCs can be cultured and individually tested of cancer drug susceptibility [20], and ctDNA and exosomes are proved to be useful in the provision of personalized therapy [7,21].

The potential to detect and characterize cancers in such a non-invasive and repeatable way renders liquid biopsy considerable clinical implications to improve diagnosis and treatment of cancer. But there are still some limitations of liquid biopsy, among which the detection sensitivity is the biggest issue. Evidence have shown that patients with early-stage cancers or residual disease can have very few CTC or ctDNA, and the concentration of the liquid biopsy is highly variable in patients even of the same tumor types and stages.

1.1.2 Circulating Tumor Cell (CTC)

Among three liquid biopsy markers, we are most interested in CTCs. Circulating tumor cells (CTCs) are rare cells released to the blood from both primary tumor lesions as well as metastatic sites of cancer patients. They are carried around the body through blood or lymphatic circulation, in which most of them have a short half-life and are apoptotic, but a few of them can survive with increased resistance to apoptosis and contribute to metastasis [22-25]. CTC detection, isolation and downstream analysis have been widely studied and used in a broad range of clinical applications, such as cancer detection and diagnosis [26], treatment response monitoring and metastasis prediction [27,28], targeted therapy design [29], CTC cultivation [30,31], and genome analysis [32]. Evidence have shown that presence of CTCs and their enumeration in the blood can be used for primary diagnosis as well as prediction of unfavorable prognosis in a number of non-haematologic cancers [26,33-36].

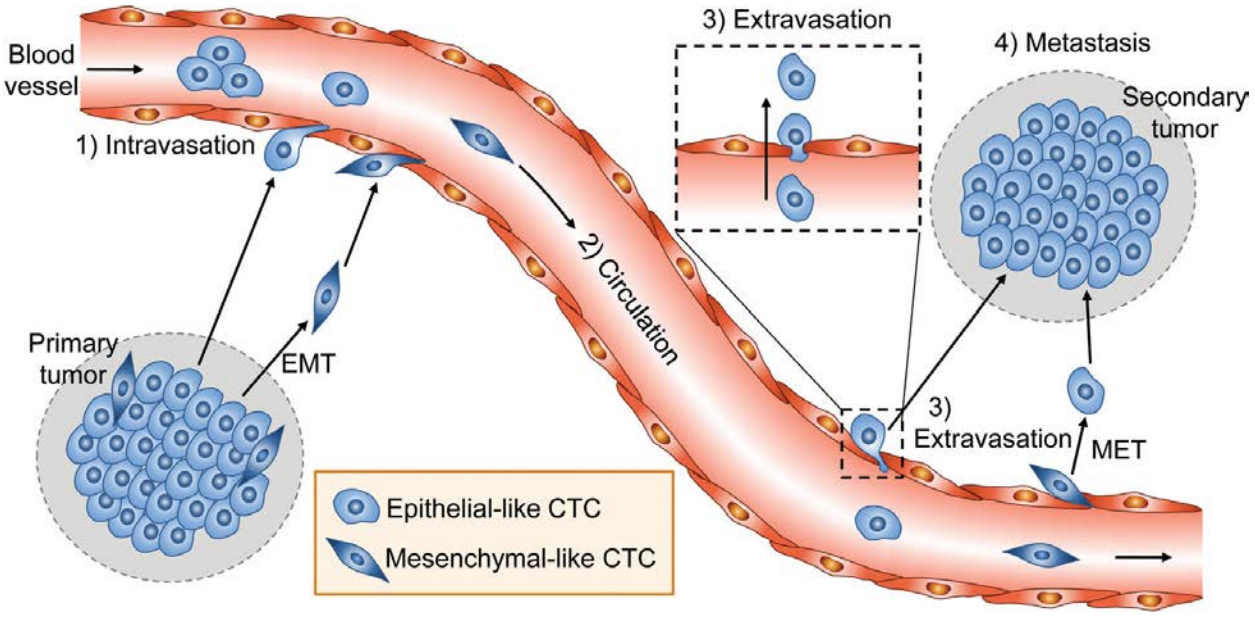

Figure 1.2. 1) CTCs are shed into blood circulation from tumor lesions. 2) CTCs circulate through and survive in the bloodstream. 3) CTCs adhere to blood vessel walls and extravasate to distant organs, resulting in metastasis. 4) Some of the metastatic tumor cells develop into secondary tumors. Some CTCs may go through EMT (epithelial–mesenchymal transition) and become more invasive.

Among liquid biopsy assays, though not abundant as ctDNA in blood, CTCs have great value of providing metastatic information, which the other biopsies (including traditional tissue biopsies) usually do not. CTCs are believed to play an important role in the development of distant metastases for they can extravasate, seed distant organs, and become a new malignant tumor [37-39], as shown in Figure 1.2 [40]. Metastasis is the most common cause and is estimated to be responsible for as high as 90% of cancer related deaths [13]. The pathways and mechanisms of metastasis have not been entirely clear to the scientific community. Due to the strong and unique correlation to metastasis, CTCs can provide crucial clinical information for diagnosis and treatment, and are keys to understanding the biology behind metastasis.

CTCs can be released from their origins and detected in the peripheral blood of patients of all cancer stages, even in the very early stage, which makes them especially powerful for early detections when the tumor is undetectable by imaging methods. Similarly, CTCs have shown great potential of providing prognostic information in early detection of minimal residual disease (MRD), which reflects the presence of malignant cells remain in patients whose primary tumors have been surgically removed and lacking any clinical symptoms of metastasis or recurrence. The

detection of CTCs allowing for the identification of patients at high risk of recurrence and enabling early therapeutic intervention. Previous published data has shown that CTCs can be detected in patients who eventually relapse, sometimes months earlier than using current imaging methods [5,41-43].

Tumor cell clones can be very genetically and phenotypically divergent within a tumor [18]. CTCs have unique values also because they can provide both more abundant genotypic information as well as phenotypic information at the same time [24]. Unlike ctDNA, which are DNA fragments that usually have only one or a few mutations, a single CTC possesses a whole set of genetic information of the original tumor under certain stage and progression. Another issue with ctDNA is lacking ability for identifying tumor origin, which is important especially in early-stage diagnosis. Multiple tumor types can be driven by the same gene mutations, hence ctDNA, which based on genomic analysis alone, usually cannot signal the location of the primary tumor [11]. While CTCs can identify a cancer's origin by phenotype identification and molecular analysis of expressed cell markers [44,45] or genome sequencing [46]. CTC phenotype (epithelial or mesenchymal) is proved to be able to predict recurrence and survival of the cancer [47].

Another advantage of CTCs is that they allow further downstream analysis. The DNA and RNA of captured CTCs can be sequenced to reveal multiple mutations or quantitate genetic variations [48,49]. Molecular analysis can be done to reveal the phenotypic information as discussed above. They can also be cultured after capturing to benefit clinical research like identification of biomarkers and exploring the mechanism of metastasis [50]. Furthermore, the cultured CTCs can be biochemically tested to help design targeted therapy and find personalized drugs for patients [32,51-53].

Except for the existence of CTCs, the enumeration of them is also an important prognostic marker. The presence of more CTCs (increased CTC number) is an independent predictor that is correlated with a shorter relapse-free and overall survival time in patients with metastatic cancer, therefore it can be used to monitor patients at risk of recurrence [42-44,54]. During treatment, the persistence or increase of CTC numbers from routine detections can indicate resistance to the current therapy, and the patients could then be offered a more effective therapy before there is further tumor progression.

In short, CTC detection is a powerful and crucial tool to help against cancer as well as understand the biology behind it. However, despite the great clinical implications and huge effort

that has been made in the related research, CTC has not been a standard clinical technique or an independent decision-making tool yet [55]. Studies have shown that CTC enumerations can be used as a reliable biomarker to determine therapy choices for metastatic patients, as an alternative to the clinical evaluation. But in many studies, the presence of CTCs is usually not significantly alone for decision making [43,54]. That is, when the number of CTCs are relatively large, the count of them can usually reflect the overall tumor burden and guide the treatment choices; but when the number is low (as small as one to a few CTCs per tube of blood) like under the circumstances of early-stage or MRD, current detection systems are not efficient enough. This leads to the main issue of CTC detection and isolation: sensitivity. Detection platforms are challenged by the very low concentration of CTCs in blood. In this regard, ctDNA usually has a higher sensitivity than CTCs. But when the index mutations are not covered by the ctDNA assay or the concentration of covered mutations is very low, CTCs can also be captured from blood in the absence of detectable ctDNA [43].

1.2 Current Systems for CTC Detection

Plenty of CTC detection and isolation systems have been developed over the past decade. Every system, in one way or another discriminates CTCs based on either biological or physical principle, or a combination of both [56-59], as shown in Figure 1.3 [58]. Depends on whether biomarker labels are used (for detection), the detection systems can be classified into two types, namely immunoaffinity-based and label-free methods. No matter in which type of method, after selection the detected cells need to be immuno-stained with antibody-dyes that target the subcellular and membrane markers for CTC identification.

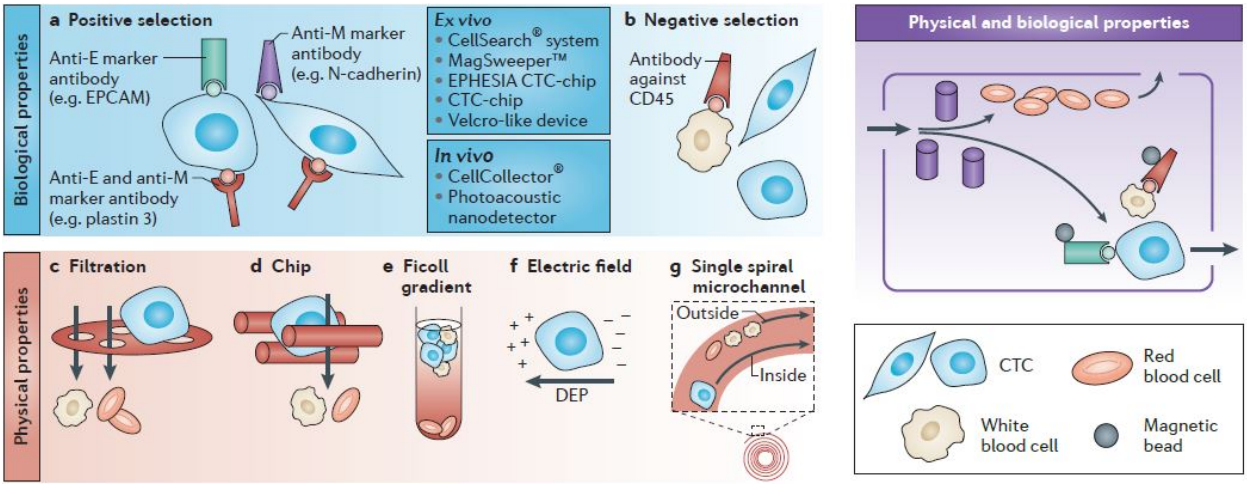

Figure 1.3. CTC detection principles. (1) Biological principles: based on immunoaffinity, CTCs can be either positively selected (using antibodies target CTC surface markers) or negatively selected (using antibodies target blood cell surface markers). (2) Physical principles: based on CTCs' dissimilar physical properties, such as size, deformability, density, or dielectrophoresis. (3) A combination of biological and physical principles.

1.2.1 Immunoaffinity-based Methods

Biological CTC detection methods utilize immunoaffinity, i.e., antibody-antigen affinity, to target CTCs. These technologies require a known protein marker (or a panel of markers) expressed on the target cell surface and recognize the target cells by corresponding antibody (or antibodies). CTCs can be either positively selected by using antibodies specifically targeting CTC surface markers (such as anti-EpCAM); or negatively selected by depleting unwanted white blood cells (WBCs) targeted by antibodies like anti-CD45.

Immunomagnetic capturing, also known as Magnetically Activated Cell Sorting (MACS), is one of the mainstream principles. In immunomagnetic capturing, blood sample first incubates with micro or nano magnetic particles coated with antibodies against a particular antigen, and cells expressing this antigen on their surface will attach to the magnetic particles. Then the sample is running through a device placed in magnetic field, in which the magnetic particle conjugated cells will be captured and those not bound any beads will flow through. In recent years, numerous microfluidic cell sorting systems that perform highly sensitive and efficient detection of CTCs using or involving immunomagnetic capturing have been reported.

Among all detection platforms, the CellSearch system, which isolates CTCs by positive immunomagnetic enrichment from whole blood samples, is the only one that is approved by FDA

for clinical use in metastatic breast, prostate, and colorectal cancers [60,61]. Using CellSearch system, CTCs are detected by anti-EpCAM and identified with pan-cytokeratin (CK)+, CD45−, and DAPI+. CD45− means the cells are not blood cells, while pan-CK+ (CK8, CK18, and CK19) representing epithelial cells. Studies suggest that the CellSearch can provide important prognostic information by monitoring the change of CTC numbers, which are predictive of disease progression and can help detect tumor recurrence in metastatic cancer patients [36,42]. Though widely accepted as the gold standard in CTC-related research, CellSearch system has not made a significant penetration into the clinical practices as it does not provide diagnostic or predictive information that can inform clinical decision-making. In addition, the CellSearch platform requires multiple instruments as well as manual sample preparation steps which reduce its scalability for high-throughput sample processing.

As a ground breaker, Toner and Haber Groups at Harvard Medical School developed "CTC-iChip" series of microfluidic device that captures CTCs by combining hydrodynamic size-based cell sorting, inertial focusing, and immunomagnetic isolation. The system can perform either positive or negative selection, depending on whether CTCs or WBCs are immunomagnetically labelled initially. The schematic of the system is shown in Figure 1.4 [62,63]. The whole blood sample is premixed with immunomagnetic beads and then flows through the chip. At the first stage, RBCs, platelets, and other blood components with small sizes are eliminated by hydrodynamic force, and only CTCs and WBCs are supposed to flow into the next stage. Then, the remaining cells go through a well-designed microfluidic channel, and were aligned in a single center stream by inertial focusing (which uses the effect of fluid inertia in shaped microchannels to align microparticles and cells at high flow rates [64]). At the last stage, an external magnetic field is applied to magnetically separate the CTCs from WBCs. The CTC-iChip series can achieve a high detection yield of 90%, with a fair detection purity of ~3.5-log WBC depletion. The system has shown convincing results of detecting CTCs from cancer patient samples. However, the flow speed and throughput of the system is not satisfied, it takes more than an hour to run one tube of whole blood through the chip, not including pre-processing and CTC immunostaining time. Besides, the system is rather complicated and lack resistance to errors like possibly introduced air bubbles.

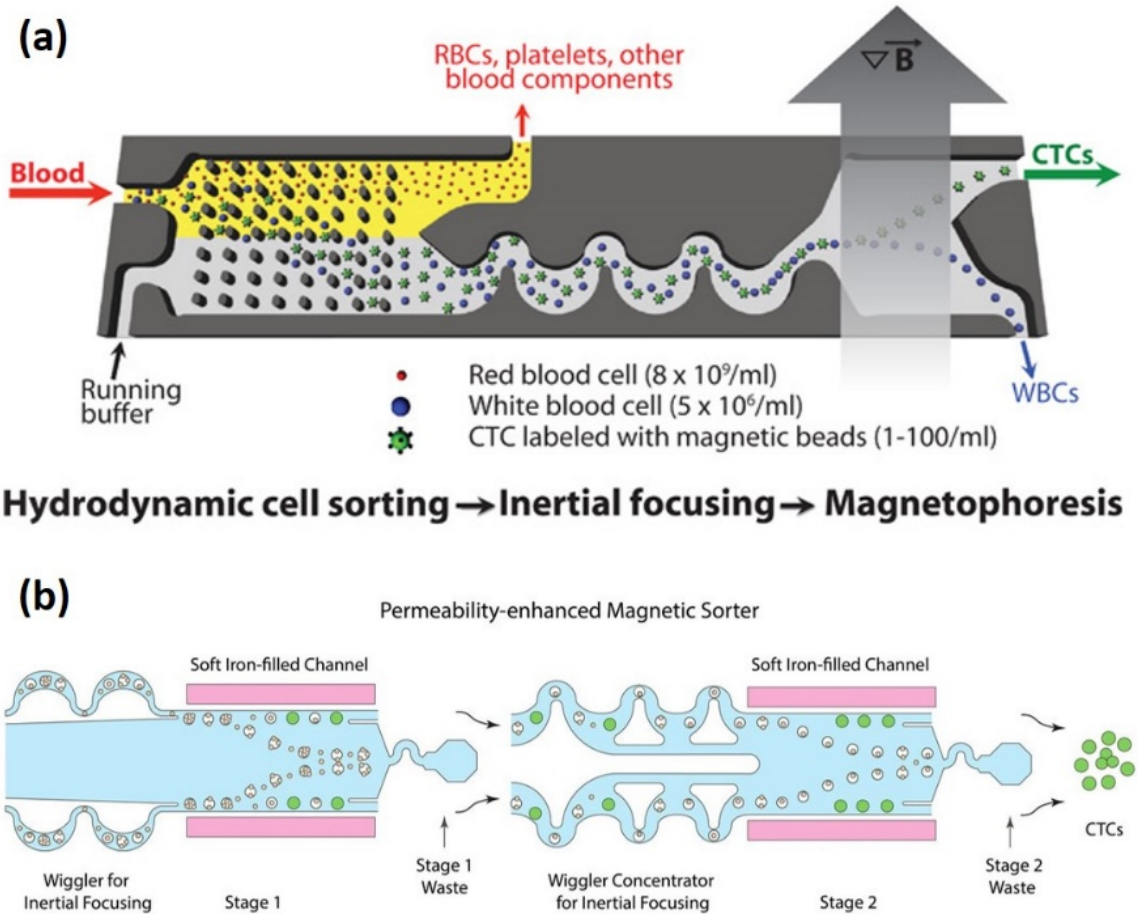

Figure 1.4. (a) CTC-iChip detection strategy, where a positive selection is shown [62]. Three components of the CTC-iChip are shown schematically. Whole blood premixed with immunomagnetic beads and buffer comprises the inputs. Small blood cells and components were sorting out by hydrodynamic force. CTCs and WBCs were aligned in a single central stream. Magnetophoresis to positively select CTCs. (b) ^{LP}CTC-iChip (LP: leukapheresis product) detection strategy [63]. It has similar inertial focusing as the CTC-iChip and an enhanced magnetic sorter section, and can process the entire leukapheresis volume of 65 mL.

Kim *et al.* developed a microfluidic device named "SIM-Chip" that integrates magnetophoretic enrichment of CTCs bound with immunomagnetic nanobeads, size-based identification with an electrical impedance cytometer, and isolation using a single-cell microshooter [65]. The "SIM-Chip" can achieve an isolation yield of 82% and purity of 92% with respect to WBCs using cancer cell line. Though the efficiency is satisfied, the throughput of this platform is too low, it typically uses 200 μL blood diluted to 1 mL, which is insufficient for processing standard blood sample. Chen *et al*. built an optimized immunomagnetic microchip for CTC detection, which integrates with an inkjet-printed micromagnet array that significantly

enhances the magnetic attractive force [66-68]. The design of the micromagnet array for enhanced CTC capturing ability is delicate and efficient, the detection yield can be as high as 96% with cancer cell line. However, without any size-filtration or surface treatment, the plain microchip surface largely limits the concentration of immunomagnetic beads used and the purity is gathered to be unsatisfied. Vermesh *et al.* reported a novel in vivo CTC capturing system by developing a flexible magnetic wire that can retrieve CTCs from vein [69]. The wire is inserted and removed through a standard intravenous catheter and can capture CTCs that have been previously labelled with injected magnetic particles. This system is not restricted by the volume of a standard clinical sample, which is the main limitation in vitro systems, so that it could detect more CTCs theoretically. However, the safety and efficiency of the system when applying to human need to be further studied and addressed.

Another popular type of immunoaffinity-based CTC detection system is based on a principle like immunosorbent assays. In these systems, antibodies or ligands that target CTCs are attached to a solid surface, and CTCs are captured and "anchored" while the blood sample flows through the surface. For example, Tseng Group presented four generations of "NanoVelcro" CTC system that uses nanostructures coated with antibodies or aptamers for CTC enumeration, isolation, and purification, as shown in Figure 1.5 [70]. They presented a unique concept of "NanoVelcro" cell-affinity substrates named after the Velcro tape, and the nanostructured substrates are coated with anti-EpCAM or aptamer to capture CTCs. A PDMS chaotic mixer is designed to introduce helical flows in the microchannel to enhance CTC-substrate contact probability. After capturing on the substrate, the CTCs are isolated and retrieved using several different methods: laser capture microdissection (LCM), temperature-dependent purification, or surface chemistry with competitive binding. Different substrates (SiNS, polymer) and coating materials are used to improve the purification and isolation efficiency of CTCs. The system can achieve a detection yield of >85% and is proved to possess clinical potential including successful downstream molecular analysis of the captured cells. However, since this method utilizes a "2D" contact between the target CTCs and the substrate, the flow speed and throughput are largely limited (typically 1 mL/h) in order to maintain the detection yield, makes it not so practical dealing with standard volume blood samples.

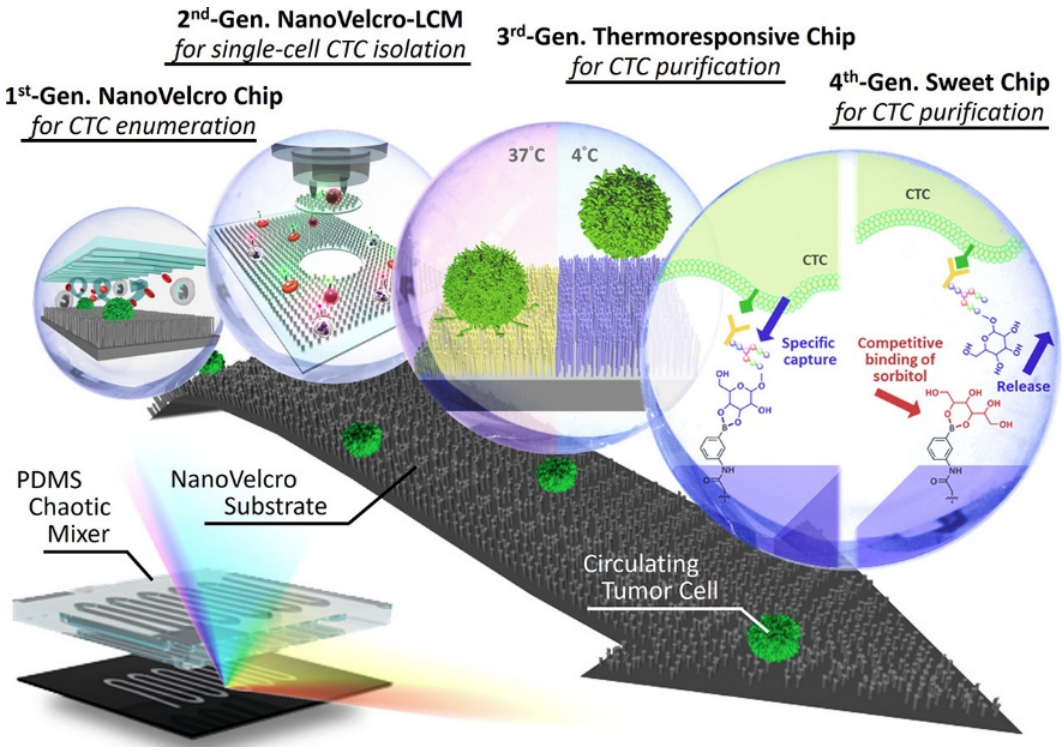

Figure 1.5. Graphic illustration of the NanoVelcro CTC assays [70]. 1st-Gen: SiNS nanosubstrates for CTC enumeration. 2nd-Gen: polymer nanosubstrates, LCM technique for single CTC isolation. 3rd-Gen: thermoresponsive polymer brushes coated on substrates for CTC release. 4th-Gen: Competitive binding surface chemistry used for CTC release.

Generally, the immunoaffinity-based detection systems have a higher sensitivity and detection yield, thanks to the specificity of antibody-antigen binding. But as discussed above, CTCs have high heterogeneity in phenotype, which means the expression of surface markers (antigens) differs a lot, hence these systems potentially miss CTC subpopulations especially when only one kind of antibody is used for capturing. The throughput of these systems is also low with a typical flow rate in the unit of μL/min. Moreover, the functional assays and devices are usually delicate but complex, and require a lot of training work to process.

1.2.2 Label-free Methods

Instead of relying on biomarkers, CTCs can also be detected based on their dissimilar morphologies to achieve label-free cell detection. These systems employ some form of micro-filter or microfluidic channel; whereby the blood sample is forced through the micro-structure, and the target CTCs are separated from other blood cells, based on their physical parameters such as size,

deformability, or density [71-75]. Another CTC sorting method based on physical properties uses the principle of dielectrophoresis (DEP) which relies on CTCs having different dielectric properties than other cells [76,77]. Some other label-free technologies available for CTC detection including fluorescent in situ hybridization (FISH) assay [78]; EPISPOT assay, which distinguishes between apoptotic and viable CTCs by detecting proteins secreted/released/shed from single epithelial cancer cells [79]; and droplet-based microfluidic device that can isolate CTCs by measuring the abnormal metabolic behavior of single cells [80].

Size-based microfluidic separation devices are the most common label-free systems. One of the popular principles for size-based CTC isolation is inertial focusing. Inertial focusing, as the name suggests, uses the effect of fluid inertia to focus/align cells at high flow rates. A well-designed microchannel is used to generate the flow and let the dispersed particles run through, during which the cells are subjected to two inertial lift forces: shear-gradient force that focuses the cells toward the channel wall, and wall effect force that repels the cells against the wall and to the channel centerline. The combination of the two forces makes particles migrate to specific dynamic equilibrium positions. Cells with different sizes experience different forces and end up in different positions between the centerline and the wall [64]. CTCs usually have larger size than other blood cells, hence can be separated by inertial focusing.

As a typical system, Elodie *et al.* reported a microfluidic device named “Vortex Chip” that uses micro-scale vortices and inertial focusing to isolate CTCs from blood with high purity based solely on their size [64,65]. The schematic of the Vortex Chip is shown in Figure 1.6. In the first part, the sample flows through the microchannels and CTCs dynamically focus to different equilibrium positions from the other blood cells due to the inertial focusing effect discussed above. The second part of this technology has expansion-contraction reservoirs placed in series and parallel to generate micro-vortices. Target cells larger than a defined cut-off size can be selectively isolated in reservoirs and continuously orbit stably in the vortices, while other cells remain in the mainstream and are washed away. After wash, the trapped cells can be released from the reservoirs by using a lower flow rate. The microchannel dimensions and flow rates are optimized for a maximum capturing efficiency, and the device is characterized by detecting spiked cancer cell line. The system can process blood samples with a high throughput (8 mL/min), and have a high enrichment purity of >80%. However, to reach the high purity, a large cut-off size is chosen, leads to a low detection yield of <30%. Even with high dilution rate (as high as 40X), which sacrifices

the throughput, the detection yield can just improve to around 35%, meaning a large portion of target cells with small size are missed. The application of this system to detect CTCs from advanced prostate cancer patient samples has been reported [65], which demonstrates its clinical potential. However, due to the low sensitivity, it is not suitable for scenarios where there are few CTCs.

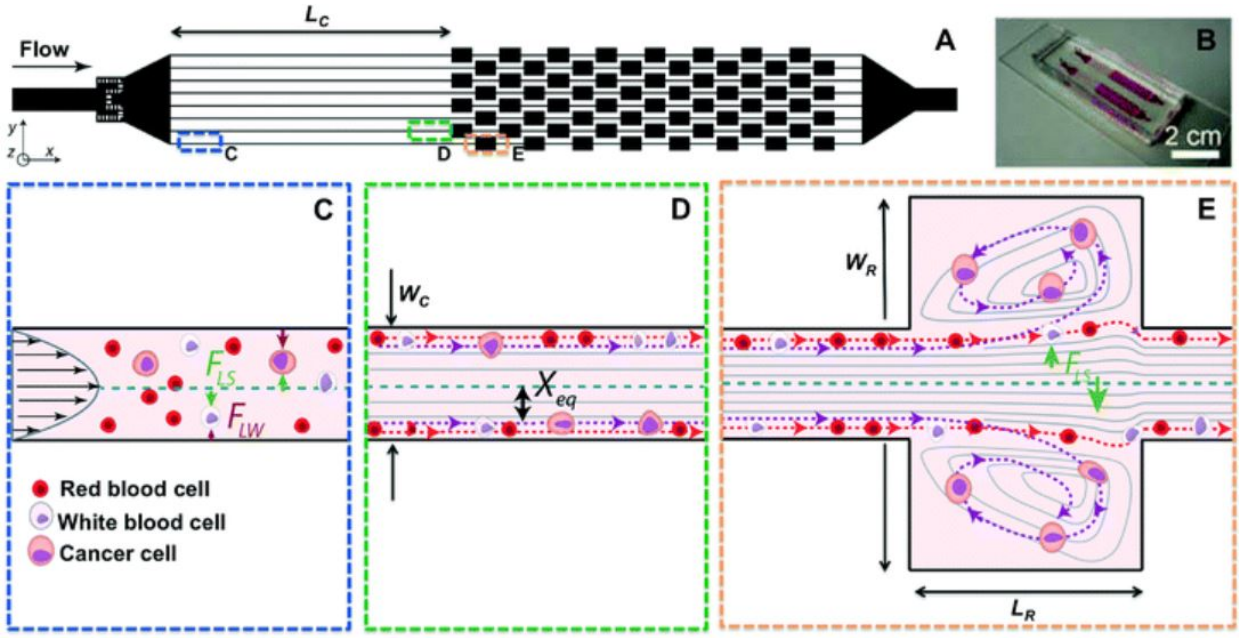

Figure 1.6. Schematic of the Vortex chip [64]. A) and B) The Vortex chip consists of 8 parallel microchannels and 8 reservoirs on each channel. C) Cells experience two opposing lift forces in the channel: shear-gradient lift force F_{LS} and wall effect force F_{LW}. D) Cells focus to different dynamic lateral equilibrium positions Xeq, based on their different sizes. E) At the reservoir, larger cells like CTCs are pushed into the vortices and trapped there for they experience a larger F_{LS}, while smaller cells remain in the mainstream.

Even though elimination of antibodies also eliminates all affinity-based uncertainties and result in systems that are generally simpler and therefore more scalable, relying on physical parameters is highly risky when target entities are too rare in nature. High heterogeneity of CTCs can result in some of them being physically different from others (e.g., in size), and the typical size range of CTCs (10 ~ 30 μm) overlapped a lot with that of WBCs (10 ~ 17 μm), which easily lead to miss smaller CTCs and/or capture too many unwanted blood cells.

1.3 Challenges and Objectives

1.3.1 Challenges

Despite significant efforts by numerous groups, detection of CTCs is still challenging. The challenges lie in CTCs' fundamental characteristics: scarcity and heterogeneity. CTCs are extremely rare in the circulation of cancer patients, typically 1 to 100 per 7.5 mL of human whole blood, and the number is usually lower in patients with early-stage disease, compared with ~ 4×10^7 WBCs and ~ 5×10^{10} RBCs in the same amount of blood [81,82]. CTC heterogeneity occurs both at the phenotypic and morphological levels and directly influences the detection process. The expression of protein markers on the surface of CTCs varies significantly in different cancer types and stages, as well as during metastatic progression [83]. Morphologies like size and deformability also differ significantly among CTCs, even when they originate from the same patient or same tumor lesion. Moreover, studies have shown that CTCs may form clusters that possess more aggressive metastatic propensity, which also increases the detection difficulty [25,84,85].

Immunoaffinity-based detection methods usually have a high detection sensitivity, but their speed and throughput are quite low, typically in the unit of μL/min. It would easily take several hours for these systems to process one tube of whole blood. To shorten the time, preparation steps such like centrifugation are usually involved, which may cause unwanted lose or damage of CTCs. Moreover, the functional assays or devices usually have limitations in terms of system complexity and robustness, fabrication cost, and operation difficulty,

Label-free detection methods are relatively easy to process, and the entry level is low. Besides, they can usually maintain a high process speed in the scale of mL/min. But the main issue of these systems is the trade-off between purity and detection yield, which usually cannot be achieved simultaneously. The reason is that CTCs' physical properties are not that distinguishing, especially the overlapped range of size with that of WBCs'.

1.3.2 Research Objectives

The challenging characteristics of CTCs discussed above warrant that the detection system meet some equally challenging demands: 1) sensitivity: the system should be able to detect as little as one single cancer cell from a 10 mL tube of blood; 2) purity: the system should discard or

deplete most if not all of the unwanted red and white blood cells; and 3) scalability and throughput: the system should have a streamlined workflow with minimal sample preparation and allow processing of large volumes (typically ~ 7.5 mL). It is very difficult to fulfil all the requirements above, from both biological and engineering points of view. The current detection platforms have advantages in some ways while always have some drawbacks at the same time. Some of them have a high sensitivity but can only achieve a fair purity, others may possess a good scalability and purity at cost of a lower sensitivity and detection yield. Based on our review of current available CTC detection techniques, there is not a single reliable system that can meet all the challenging demands above simultaneously. We conclude that to make CTC detection a standard and reliable tool remains a delicate yet interesting job. The main goal of this thesis is to develop a fast, simple, and robust CTC capturing system that can maintain excellent detection sensitivity and purity.

1.4 Proposed Strategy

We proposed a microfluidic system for CTC detection and isolation that integrates positive immunomagnetic capturing, high-throughput parallel flow and size-based filtration. We adopted immunoaffinity as our capturing principle because it is specific, rather simple and versatile, as well as capable of integrating with high-throughput process. Immunoaffinity, or antigen-antibody affinity, is a specific chemical interaction between antibodies and antigens during immune agglutination, originally in blood. An antibody is a Y-shape high molecular weight glycoprotein, also called an immunoglobulin, that binds specifically to another molecule (antigen) through non-covalent bonding with high affinity. Each antibody can bind only to a particular type of antigen due to their specific chemical constitutions. Antibody and antigen bind to each other through complementary binding sites: paratopes and epitopes. The paratopes on antibodies, which is situated at the variable region of the polypeptide chain, uniquely recognize and interact with the epitopes on antigens. CTCs express specific antigens on their cell surface that can be targeted by corresponding antibodies. Antibodies can be conjugated with magnetic beads in advance, and the antibody-beads bound target cells can be captured by applying magnetic force. The schematic of immunomagnetic capturing of the target cells is shown in Figure 1.7.

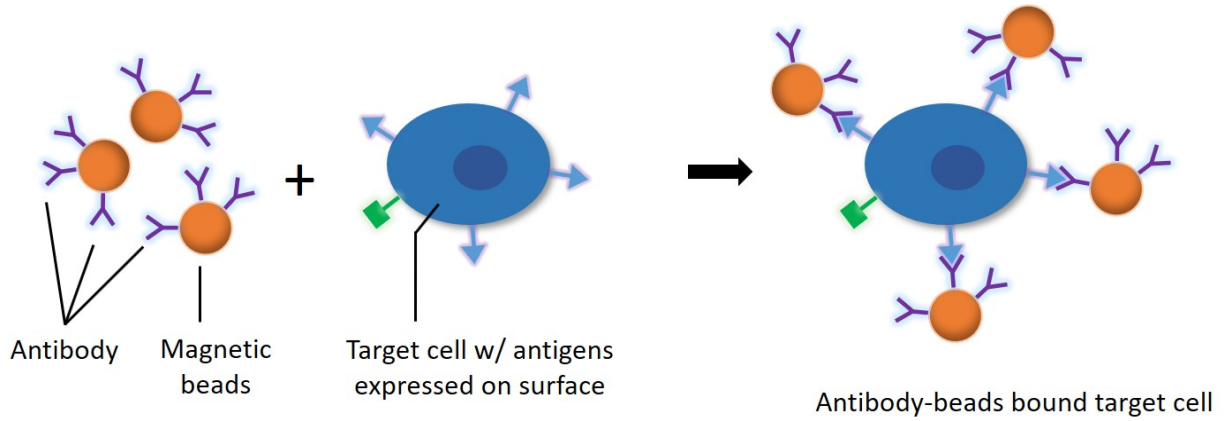

Figure 1.7 Schematic of the immunomagnetic capturing strategy. The target cell is captured with antibody conjugated magnetic beads. The antigens expressed on the target cell surface are targeted using specific antibodies.

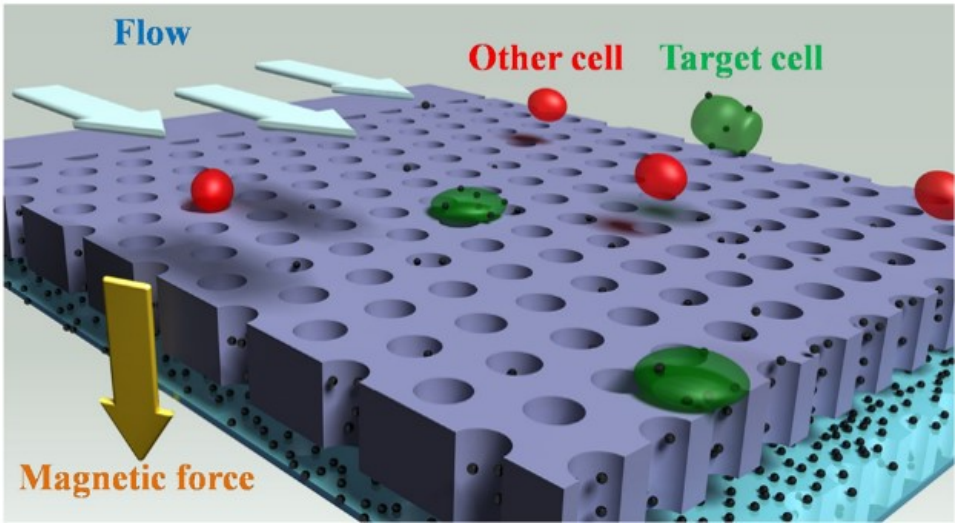

Figure 1.8. Schematic of the detection strategy combining immunomagnetic capturing, high-throughput flow, and size-based filtration. Blood sample passes through a fluid chamber under a flow that is perpendicular to the magnetic field, antibody-beads bound cells are captured on the chip surface, while free magnetic beads go through the micro-apertures on the chip. Blood cells that are not bound with any beads are washed away by the parallel flow.

The schematic of the whole detection system is shown in Figure 1.8. After incubation with antibody-beads, the blood sample passes through a fluid chamber under a parallel flow which is perpendicular to the magnetic field; the bottom of the fluid chamber is a microchip to seize the captured cells and keep them in place. A high-throughput flow is used to wash away unwanted

blood cells that are not bound with any antibody-beads. The high flow rate ensures processing a large volume of blood in a short time. The microchip needs to be delicately designed. A flat chip surface significantly limits antibody-beads amount added to the blood sample, since all the beads would pile up on the magnetic area to close over the captured cells, and increases the chance for non-specific bound with blood cells. Therefore, micro-apertures are fabricated on the chip which work as size-based filters. The dimension of the apertures is set to be smaller than the size of CTCs, while bigger than the free beads to allow them to pass through. Moreover, the chip surface needs to be passivated to reduce non-specific binding of blood cells and impurities to further guarantee a high detection purity.

1.5 Organizational Overview

In Chapter 2, our first-generation microchip system for CTC detection and isolation is presented. Detection strategy, device fabrication and assembly, and experiment protocol are introduced successively. The optimal experiment parameters are determined by sequential tests. The system is characterized with respect to detect and isolate very few CTCs by capturing deterministically spiked cells in whole blood. To demonstrate the clinical utility of the system, we apply it to a challenging phase II clinical trial and the results are presented.

The second-generation system is presented in Chapter 3. The upgraded device and protocol are introduced first. Then the system and the forces acting on the cells are modeled numerically. The improved detection efficiency is verified by both simulation and characterization result. Result of CTC detection using the second-generation system as part of a phase I clinical trial is then presented to demonstrate its clinical potential. Finally, the system is used to explore a novel 4-marker panel for CTC detection from mTNBC patient samples.

Chapter 4 presents the CTC downstream analysis ability of our system, discusses the possible directions of future work, and concludes the whole study.

2. FIRST-GENERATION SYSTEM

This chapter presents the first-generation microchip system for CTC detection and isolation from whole blood samples. The detection strategy and system setup are first illustrated and explained in section 2.1. Section 2.2 describes the materials and experimental methods used. The ability of the system to detect the spiked MCF-7 cell lines from a tube of whole blood is presented in section 2.3, by demonstrating the parameter optimization and system characterization experiments. Finally, the clinical utility of the system was presented by applying it to a rather challenging clinical trial, and the result is shown in section 2.4.

2.1 Introduction

As discussed in section 1.4, the detection strategy of our system combines immunomagnetic capturing, high-throughput flow, and size-based filtration. The system not only uniquely combines the advantages of all three approaches, but also possesses the simplicity of structure and streamlined workflow. The system enables processing whole blood directly, and significantly reduces sample preparation steps by eliminating centrifugation, while achieving a high CTC detection yield and purity.

In an earlier publication [86], we reported a preliminary system applying our unique detection strategy which was able to detect CTCs from stage IV metastatic lung and pancreatic cancer patient blood samples. Modeling and preliminary characterization of the system were also presented. The preliminary system required pre-processing of the blood sample including centrifugation, and was not designed for maximization of purity. Compared to the previous version, our first-generation system has distinct advantages: First, the chip surface is coated with a super-hydrophilic polymer layer that has ultralow fouling properties, which significantly reduces the number of unwanted WBCs and other impurities captured on the chip surface. Therefore, the detection purity increases by two orders of magnitude (to a >99.9998%, or 5.7-log depletion of leukocytes), while maintaining a reliable super-hydrophilic surface that can be re-used for multiple experiments. Second, blood sample is processed directly without centrifugation or any other pre-filtration. This optimized detection protocol and simplified process flow minimizes the chance of

losing target cells and increases the detection yield (from less than 90%) to over 95% while reducing the unwanted capture of WBCs on the chip surface.

We used one kind of antibody for capturing in the first-generation system: antibody against epithelial cell adhesion molecule (anti-EpCAM). EpCAM is frequently overexpressed on tumor-initiating malignant cells like CTCs, rendering it the most widely used surface marker of CTCs to target [87]. To mimic real CTCs for parameter optimization and system characterization experiments, we used breast cancer cell line MCF-7 cells, which are known to highly express EpCAM on the surface.

To find the optimal experimental parameters, we studied the relationship between detection yield and incubation time for three different amounts of anti-EpCAM-beads by detecting known numbers (75 ~ 95) of MCF-7 cells from a tube of whole blood (7.5 mL). We then presented the system's efficiency in capturing extremely small numbers of (1, 10 and 100) cells spiked deterministically into a tube of whole blood. Finally, we demonstrated the clinical potential of our system by presenting CTC detection result from 182 blood samples obtained from 124 early-stage triple-negative breast cancer (TNBC) patients that have received chemotherapy as well as surgery.

2.1.1 Detection Strategy

The detection strategy for the first-generation system is shown in Figure 2.1. Anti-EpCAM conjugated superparamagnetic beads are added directly into the blood sample and incubated in the original blood collection tube, without any pre-processing like centrifugation or transferring. CTCs in the blood are bound with the anti-EpCAM-magnetic beads via antibody-antigen affinity. The sample then flows through the fluid chamber at a high flow rate (typically 2 mL/min). Parallel to the flow is a microchip with 8 μm apertures that are larger than free magnetic beads but smaller than the CTCs. The chip surface is coated with a super-hydrophilic polymer layer to minimize non-specific fouling of blood cells and impurities. A permanent magnet is placed underneath the fluid chamber to establish a magnetic field that attracts the magnetic beads (free ones as well as those attached to CTCs) to the microchip. Due to this attraction, target cell-beads complexes that are larger than the apertures are captured on the chip surface along with a small number of blood cells that are non-specific bound with few beads; while free beads are filtered via the apertures to the bottom chamber, so that they would not pile up on the chip surface and block the captured cells. Most of the blood cells that are not bound with any beads are flushed out of the chamber due to

the high flow rate of the parallel flow. Captured cells are then identified and counted by immunofluorescence analysis while still on the chip, without the need to open the chamber or transfer the cells to a microscope slide, which risks losing the ultra-rare target cells. However, if needed for applications that require further downstream analysis, the cells can also be released to a secondary microchip device by removing the bottom magnet and applying a high-speed flow and retrieved individually [88]. Due to the super-hydrophilic nature of the polymer layer coated on the chip surface, the captured cells are easily lifted and carried away by the flow without the magnetic field underneath, so that this retrieving process has minute chance of losing cells.

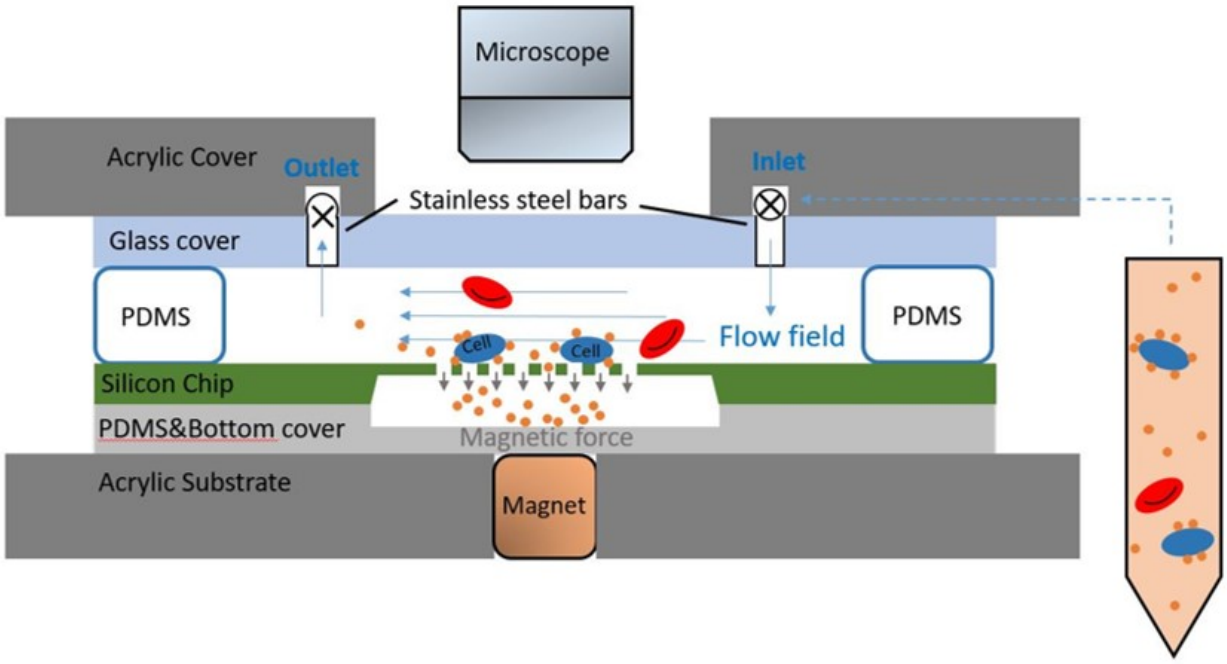

Figure 2.1. Schematic of the first-generation microchip system, and cross-section view of the fluidic chamber.

2.1.2 System Setup

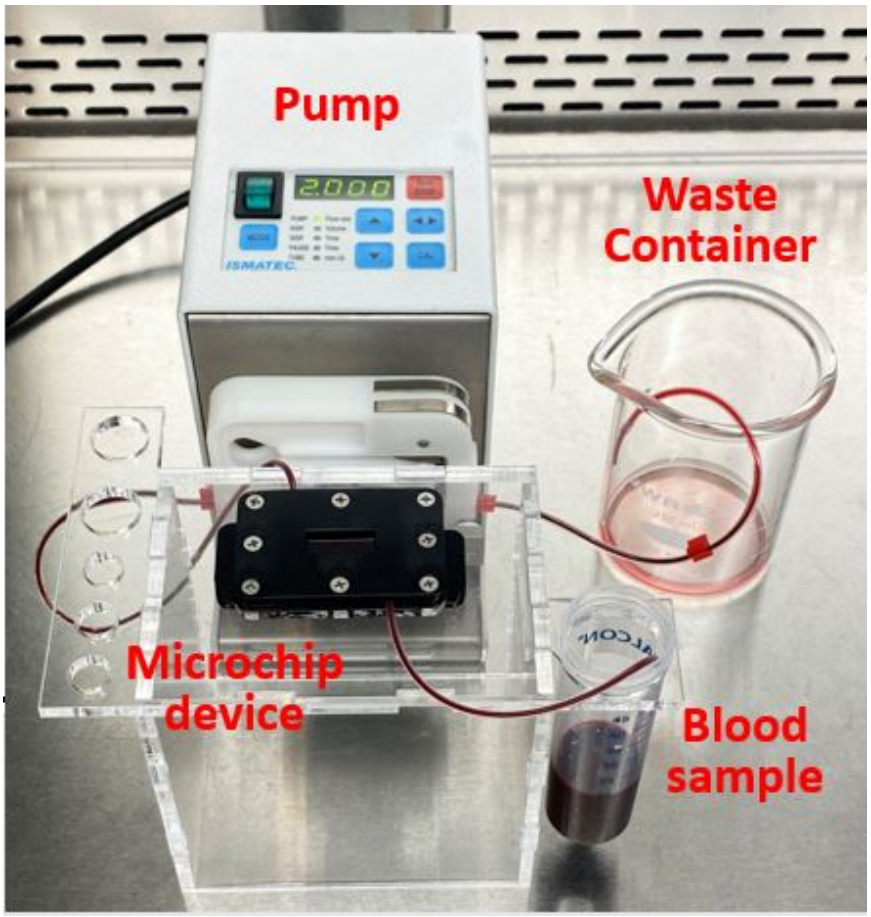

Figure 2.2. Experiment setup. The microchip device is seated on the top of a permanent magnet. The inlet tubing of the device is inserted in the blood sample and outlet tubing connected to a peristaltic pump. The sample fluid flows through the microchip device and goes into the waste container. The flow rate of the pump is set to be 2 mL/min in the image. The device and the 50 mL sample tube are placed on an acrylic stand.

The configuration of the experiment setup is shown in Figure 2.2. A sandwich-structured microfluidic device was first assembled. A 1 mm thick PDMS layer with a groove opened in the center was placed on a micro-aperture chip with its surface passivated by coating a polymer layer, and capped by a glass slide to construct the fluid chamber. Elbow shape stainless steel bars were inserted and glued to the openings drilled on the glass slide as inlet and outlet of the fluid chamber. The other arms of the bars were connected to silicone tubing. The bottom chamber was patterned and sealed by another layer of thin PDMS and a transparent sheet. The fluid chamber was then mounted and held in place in between two pieces of acrylic stands, which were gently fastened by

screws and nuts. The bottom acrylic stand had a window opened in the middle to allow insertion of a permanent magnet underneath the chamber. The inlet tubing was inserted to sample fluid or solutions, while the outlet was connected to a peristaltic pump (Ismatec, ISM596B) that creates the flow and drained to a waste container. A stand made with transparent acrylic sheet is used to hold the device and sample tubes, holes with different sizes were made on the stand to fit different tubes, as can be seen in Figure 2.2. The whole detection system is designed to be compact and streamlined, and rather user-friendly.

2.2 Materials and Methods

2.2.1 Microchip Design and Fabrication

The 40 mm by 20 mm microchip has a 9 mm by 3 mm porous area in the center with micro-apertures. The micro-apertures have a diameter of 8 μm, which is smaller than CTCs (typical size of 10~30 μm) and bigger than free magnetic beads (1 μm) and red blood cells (6~8 μm). The porous area works as a size-based filter by allowing the free beads and red blood cells to go through the apertures to a trapezoid bottom chamber, while keeping the captured CTCs on chip.

The microchip was fabricated on a <100> SOI (silicon on insulator) wafer with a thickness of 500 μm using a conventional fabrication procedure. The process flow was presented in a previous study of our group, as shown in Figure 2.3 [88]. In brief, an array of cylindrical cavities was first etched on the front side of the chip by Deep Reactive Ion Etching (DRIE), the etching depth was 50 μm which served as the thickness of the porous area in the end; then a window was defined on the back side of the chip for wet etching, and a layer of silicon nitride was deposited using low-pressure chemical vapor deposition (LPCVD) to protect other chip surface area; finally, the silicon was wet etched from the back side through the window and stopped till the bottom of the cavities.

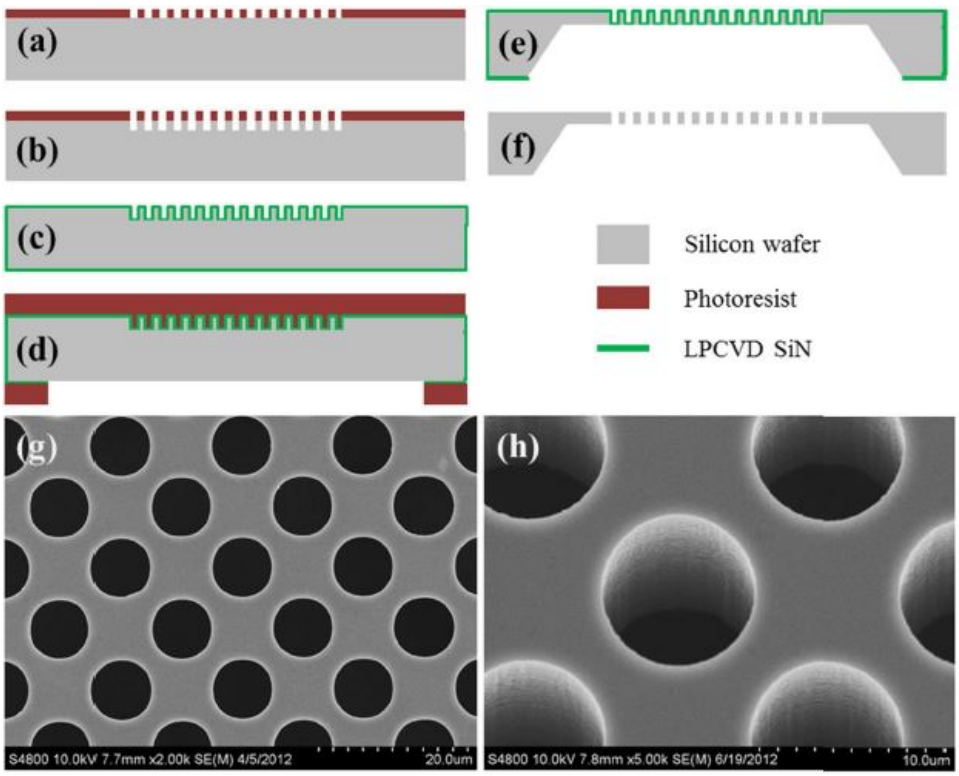

Figure 2.3. (a-f) Fabrication process flow and (g-h) SEM images of a fabricated micro-aperture chip. Each aperture is 8 μm in diameter.

2.2.2 Chip Surface Coating with a Super-hydrophilic Polymer Layer

Polyzwitterionic materials have been widely used in biomedical and engineering applications involving human blood contact because of their great biocompatibility and non-fouling properties [90-93]. In order to minimize the non-specific fouling of blood cells, proteins and other blood impurities to the microchip surface, a high-density layer of zwitterionic sulfobetaine methacrylate polymer (p-SBMA) was coated on the chip surface using surface-initiated atom transfer radical polymerization (SI-ATRP) [94,95]. The coating scheme is shown in Figure 2.4. The microchip was first cleaned by Piranha solution (H_2SO_4:H_2O_2 = 1:1) and buffered oxide etch (BOE), followed by RCA-1 silicon wafer cleaning (H_2O:NH_4OH:H_2O_2 = 5:1:1) to further remove organic residues and hydroxylate the chip surface. Using anhydrous toluene as solvent, trichlorosilane ([11-(2-Bromo-2-methyl)propionyloxy]undecyl-trichlorosilane, Gelest), an alkyl bromide that works as the ATRP surface tethered initiator was deposited on the chip surface under the effect of silanization.

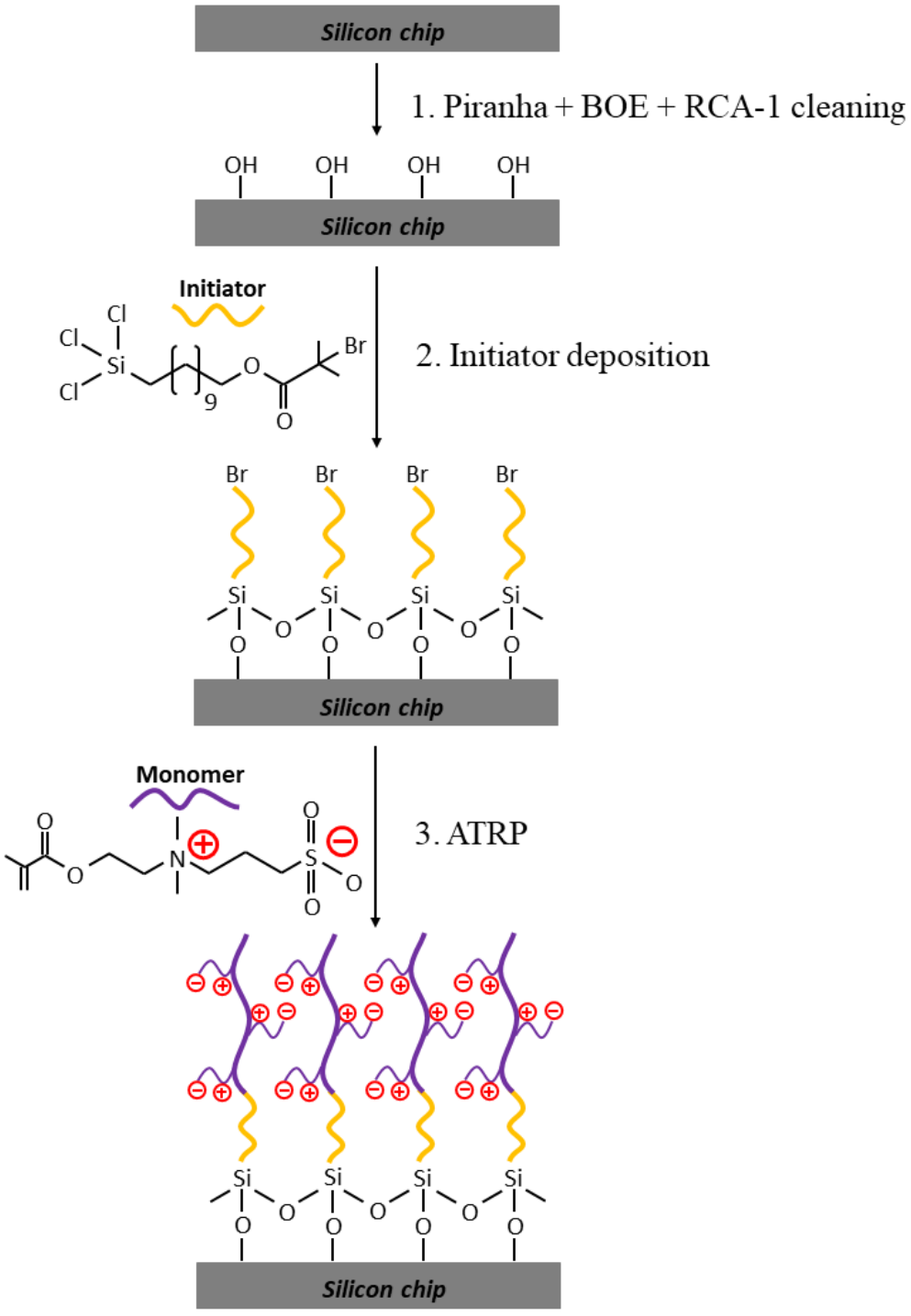

Figure 2.4. Schematic of the zwitterionic polymer layer coating process. 1. Chip cleaning and surface hydroxylation. 2. Surface tethered initiator deposited by silanization. 3. ATRP reaction: SBMA monomer grafted on the initiator and propagated in the presence of copper halide catalysts and BPY ligands.

The chip was then immersed in nitrogen-purged methanol-water solution (4:1), and the zwitterionic monomer, SBMA ([2-(Methacryloyloxy)ethyl]dimethyl-(3-sulfopropyl)ammonium hydroxide, Sigma-Aldrich), was grafted on the initiator and propagated in the presence of copper halide catalysts (CuCl and $CuCl_2$) and BPY (2,2′-Bipyridine) ligands, which is used to solubilize the copper halide and to adjust the redox potential of the copper. The non-fouling nature and the reusability of the polymer layer were related mainly to its thickness and density. We conducted multiple tests on the coated chips with human blood to achieve the optimal range of thickness and density. The polymer layer 15 ~ 20 nm thick with a refractive index unit (RIU) of 1.40 ~ 1.45 was determined to provide the best performance that minimizes the fouling of blood cells and impurities. Thickness and refractive index were measured using an ellipsometer (J.A. Woollam Co., Inc., VASE). The SBMA monomer dosage and reaction time were precisely controlled to yield the wanted thickness and density. The coated chip was rinsed thoroughly with DI water and immersed in PBS overnight, then washed again and stored in vacuum and placed in a 4°C fridge to protect the polymer layer.

2.2.3 Device Assembly

The assembly schematic of the device and a picture of an assembled device are shown in Figure 2.5. The sandwich-structured device consists of three major parts: fluid chamber defined by a microchip, top PDMS, and glass cover, and bottom chamber patterned with bottom PDMS and transparent sheet; acrylic cover and substrate; as well as permanent magnet and its stand.

Fluid Chamber

Fluid channel was first defined on the microchip by placing a layer of 1 mm thick PDMS (Polydimethylsiloxane, Dow Corning 184 Silicone Elastomer) with a 30 mm by 4.3 mm groove cut in the center, which enclosed the porous area. Next the chamber was capped by a 1 mm thick glass slide with inlet and outlet holes drilled. Short arms of the elbow shape stainless steel bars were inserted into the holes and glued to the glass cover with epoxy, and the long arms were connected to the inlet and outlet silicone elastomer tubing (0.04" I.D., 0.085" O.D.). The bottom chamber was patterned with another layer of 0.1mm thick PDMS with a 10 mm by 4.3 mm groove in the center. Bottom PDMS was cured on a transparency film (3M, PP2500) for sealing.

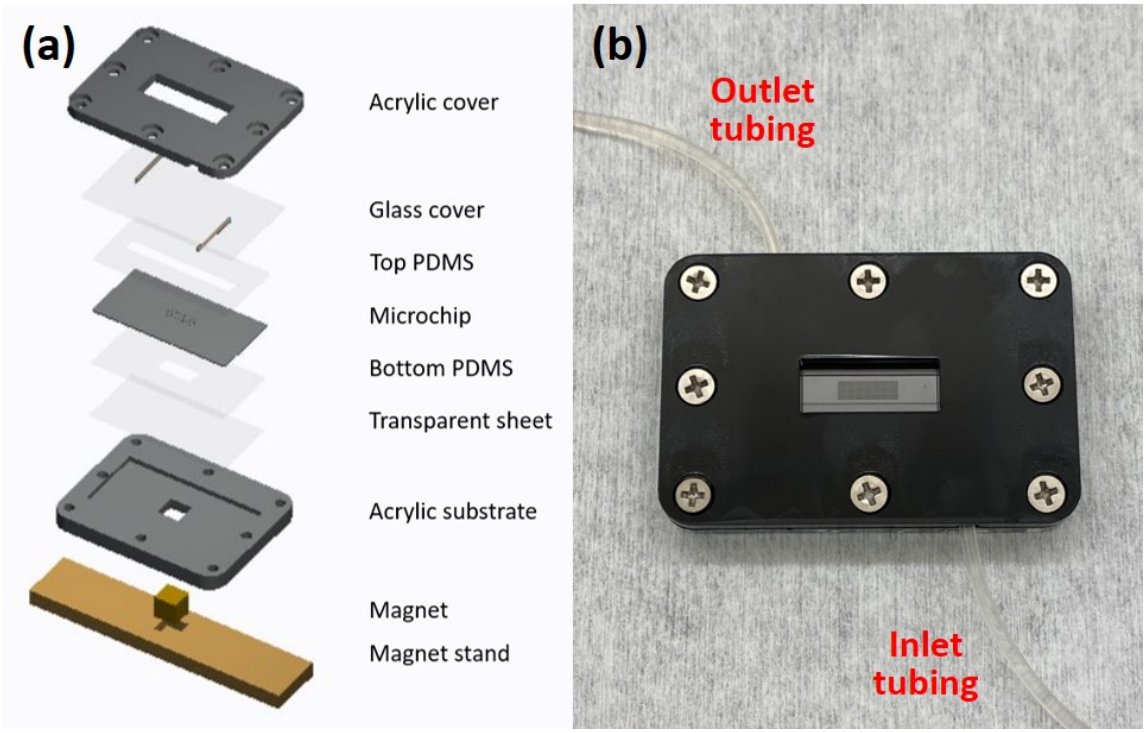

Figure 2.5. (a) Assembly schematic of the microfluidic device and the bottom magnet setup. (b) Top view of an assembled device. The porous area (small dark-grey rectangular) in the center of the microchip can be scanned through the opening on the acrylic cover. The fluid channel defined by top PDMS can also be seen.

Acrylic Cover and Substrate

The fluid chamber was placed into a two-piece acrylic stand consisting a cover and a substrate, and gently fastened by 8 pairs of screws and nuts. Two blind grooves were engraved on the on backside of the acrylic cover to accommodate inlet and outlet bars and tubing. An opening on the acrylic cover facilitated direct microscopic scanning of the chip surface. The acrylic substrate also had a window opened in the center which allowed a permanent magnet to be placed underneath the fluid chamber. We chose acrylic as the material of our device stand because of its excellent impact and scratch resistance, light weight, and rigidity. In addition, acrylic is easily patterned by laser cutter.

All PDMS and acrylic components were machined using a laser cutter (Universal Laser System, Inc., Professional Series).

Permanent Magnet

We placed a block N52 neodymium permanent magnet (K&J Magnetics, Inc.), with the size of 1/4"×1/4"×1/4", right underneath the bottom chamber to generate the magnetic field to pull the cell-beads complexes as well as the free beads down to the chip surface. Neodymium magnet is made from an alloy of neodymium, iron, and boron (NdFeB), and is the most powerful permanent magnet. We chose grade N52, the highest grade of neodymium magnet currently available, for a maximum pulling strength. The magnetic field strength at the surface of the block magnet we used is 6451 Gauss. A stand made of acrylic and metal sheet was used to hold the magnet.

Improvements

Inlet and outlet tubing were placed on the sides (instead of on the top as were in the previous generation device), leaving a much wider room for microscopic scanning within the opening of the acrylic cover. This also made the device compatible with high magnification microscope lenses that require shorter working distances. Stainless steel bars were used as inlet and outlet connectors (while the silicone tubing was glued on the glass slide directly in the previous device), rendering more firmly connection after gluing in place on the glass cover, and making the device more impact resistant and more robust for transportation. The acrylic stand is also relatively thin (3") and more compact, which makes the device more user-friendly.

Device Storage and Priming

After the assembly, we stored the device in plastic bags filled with nitrogen at 4°C for facilitating preservation and transportation. The priming of the device was performed by flowing ethanol, DI water and phosphate buffered saline (PBS, Invitrogen) through the chamber. The inlet tubing was pinched several times during priming to suck out the air in the bottom chamber and allow the solutions to go through the apertures and fill the whole chamber. The outlet tubing of the chamber was connected to a peristaltic pump that generated the flow, while the inlet tubing was inserted into the sample fluid.

2.2.4 Preparation of Anti-EpCAM-conjugated Magnetic Beads

Filtration of the Magnetic Beads

Dynabeads MyOne Streptavidin T1 superparamagnetic beads with 1μm diameter (Invitrogen) were chosen for immunomagnetic capturing because of their rapid liquid-phase reaction kinetics, efficient magnetic pull for a quick separation, and large surface area and high capacity. In preliminary tests, we found that there were some big beads clusters in the original suspension, as shown in Figure 2.6 (a). These clusters could be an interference during cell detection and observation, for they may increase the nonspecific binding of blood cells, clog the micro-apertures, or generate clusters of cells and beads on the chip surface. To remove beads clusters, the original suspension was first filtered through a 5-μm low protein binding membrane filter (Durapore) using a syringe, then washed three times on a magnetic stand (PerkinElmer, Germany) with wash buffer (PBS + 0.1% BSA, bovine serum albumin + 0.02% NaN3), and stored at 4°C at its original volume in the same wash buffer to prevent further cluster formation. The filtered beads are free of clusters, as can be seen in Figure 2.6 (b).

To find out the beads' concentration after filtering, we did an image digital processing. First, the beads suspension was thoroughly pipetted and 1:10 diluted with PBS, 1 μL of the suspension was deposited on a glass side to form a thin layer. Then we took picture of the beads under bright field microscope, and the picture was converted to grayscale then binary image; after binarization, the number of black pixels in the image would represent bead concentration in the original picture. We took three pictures each of un-filtered and filtered beads suspension and conducted the processing. The average concentration ratio between the filtered and un-filtered beads was 92% $\pm$ 3%. This indicates a filtration loss rate of around 8%, which is acceptable, and approved to have little effect on the subsequent detection process.

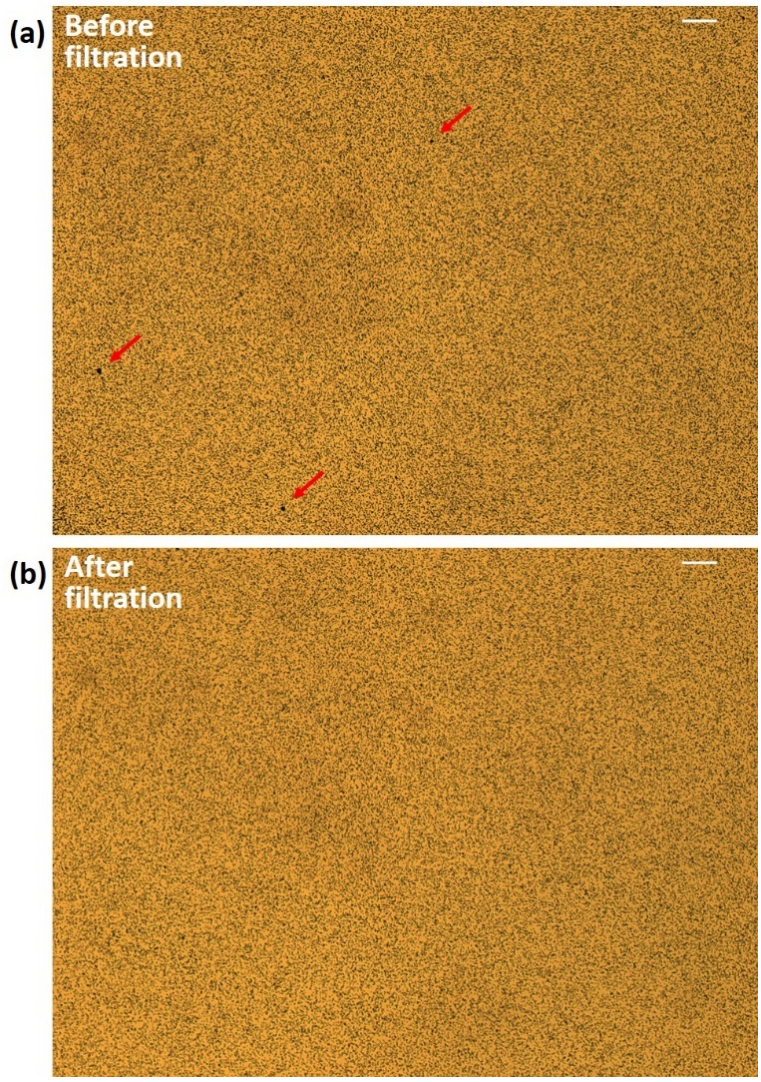

Figure 2.6. Bright field images of 1:10 diluted beads suspensions. (a) Un-filtered beads. Three clusters with size of ~ 5 μm are indicated in the image by red arrows. (b) Filtered beads. Free of beads clusters. Scale bars indicate 20 μm.

Conjugation of Anti-EpCAM and Magnetic Beads

The filtered streptavidin-coated magnetic beads were then conjugated with biotinylated polyclonal antibodies against human EpCAM (R&D Systems). The conjugation was achieved due to the extraordinarily high binding affinity of the streptavidin-biotin interaction, which is one of the strongest known non-covalent interactions, once formed, it is hardly affected by harsh conditions or agents. The conjugation was also very rapid.

The anti-EpCAM was stored at -20°C in PBS solution at a concentration of 0.2 mg/mL after purchasing. 1 mg of Dynabeads MyOne Streptavidin T1 typically binds with ~20 μg antibodies,

according to the information provided by the vendor. To maintain the maximized magnetic capturing capacity, we saturated the magnetic beads (40 μL, ~368 μg after filtration) with excess anti-EpCAM (50 μL, 10 μg), and the mixture was washed three times with PBS using a magnetic stand to remove the Wash Buffer, and incubated in PBS for 1 hour at room temperature. The mixture was placed on an end-over-end rotator during incubation to yield a sufficient encountering and conjugation between the beads and antibodies. After incubation, the mixture was rinsed three times with PBS on the magnetic stand to get rid of unbound antibodies, and finally re-suspended in 400 μL PBS, stored at 4°C and used within a week.

2.2.5 Preparation of MCF-7 Cells

MCF-7 is one of the most used breast cancer cell lines in research. It is approved to be suitable as a model mammary cell line for breast cancer study [96]. MCF-7 cells are known to be with epithelial phenotype and overexpress epithelial markers like EpCAM on their surface [97].

Culturing

The MCF-7 cell line was purchased from American Type Culture Collection (ATCC, HTB-22), and cultured in Eagle's Minimum Essential Medium (EMEM, ATCC 30-2003) with 10% fetal bovine serum (FBS, ATCC 30-2020) as recommended. Before spiking, cultured cells were harvested by Trypsin-EDTA (ATCC 30-2101), centrifuged and re-suspended in culture media to form cell suspension.

Spiking

There were two methods we used for MCF-7 spiking: 1) *average spiking method*, where the concentration of the cell suspension was estimated as the average of multiple small volume samplings; and 2) *deterministic spiking method*, where individual cells were picked with a micro-pipette and spiked one by one into blood using a microaspiration system. In average spiking, we deposited 3 μL of thoroughly pipetted cell suspension on a glass slide to form a thin layer, then counted the number of MCF-7 cells on the slide under a bright-field microscope and calculated the concentration. We took the average of five such samplings as the approximate concentration. A volume of the suspension that contained the desired number of MCF-7 cells was added into

blood. As for deterministic spiking, we used a microcapillary based single-cell manipulation system reported by our group that was optimized to pick up and dispense nanoliter volumes of liquid [97]. The whole picking and spiking process was monitored under a bright-field microscope to ensure the accurate spiking quantitation. We first transferred the cell suspension to a petri dish containing culture media to render a low cell concentration and waited till the cells sank to the bottom of the petri dish and be stable. Then we located single cells under microscope and picked them up individually and spiked into blood.

2.2.6 Detection of MCF-7 cells Spiked in Healthy Human Blood

We conducted system parameter optimization and characterization experiments by spiking MCF-7 cells into human blood samples and measuring the detection yield. Healthy human blood with K2-EDTA acting as anti-coagulant was purchased from Biochemed Services (10761WB-EK2-FI), the blood was stored in 4°C until cell spiking. Known number of MCF-7 cells were spiked into 7.5 mL of blood, and the anti-EpCAM-beads were added into the blood sample and incubated under room temperature. The blood tube was put on an end-over-end rotator to benefit the anti-EpCAM-beads and cells encountering. After incubation, the blood sample was transferred to a 50 mL centrifuge tube and diluted 1:1 with PBS solution to a total volume of 15 mL to reduce the dynamic viscosity, and then flowed into the fluidic chamber at a 2 mL/min flow rate using a peristaltic pump with the bottom magnet in position. To increase the chance of capturing, we circulated the blood sample in the chamber by inserting the outlet of the peristaltic pump back into the sample tube. After 8 minutes of blood circulation (equivalents to passing the entire sample through the chamber once already) through the fluidic chamber, the sample flowed out and the chamber was washed with 3 mL of PBS solution. During the wash, a second magnet was placed on top of the chamber and moved back and forth slightly to align the free beads and/or bead-bound small blood cells with the apertures on the chip surface, and facilitate their discarding into the bottom chamber, as discussed in the previous study [86]. To get rid of the remaining red blood cells, 500 μL of red blood cell Lysis Buffer (G-Biosciences) was introduced into the chamber, incubated for 5 minutes, and washed by PBS. The captured cells were fixed with 4% paraformaldehyde solution in PBS (4% PFA, Santa Cruz Biotechnology, Inc.) and permeabilized with 0.1% Triton X-100 (Sigma-Aldrich) to prepare for immunofluorescence analysis to identify

the MCF-7 cells. A thorough PBS wash was adopted after fixation and permeabilization, respectively.

2.2.7 Detection of CTCs from TNBC Patient Blood Samples

We verified the clinical potential of our system by applying it to a clinical trial. The BRE12-158 study was a randomized phase 2 clinical trial of genomically directed therapy after preoperative chemotherapy for patients with TNBC. Triple-negative breast cancer (TNBC) is defined by the absence of estrogen-receptor (ER), progesterone-receptor (PR), and human epidermal growth factor receptor 2 (HER2) over-expression [43,99,100]. This trial enrolled patients with TNBC treated with neoadjuvant chemotherapy who had residual disease at the time of surgery. Blood samples for the possible detection of ctDNA and CTCs were obtained either prior to treatment or at the routine visits of the patients.

182 blood samples from 124 early-stage TNBC patients were collected for CTC detection (all patients assessed in this study were consented as part of the IRB-approved BRE12-158 trial protocol [43]). Patient blood samples were collected in 10 mL CellSave Preservative tubes ((7900005, Menarini Silicon Biosystems) and stored under room temperature. Detection was conducted within 72 hours of collection. 150 μL of anti-EpCAM-beads was added into a tube of whole blood sample and incubated for 90 to 120 minutes. The rest of the detection protocol was the same as that of MCF-7 spiking experiment discussed above, except there was no fixation step since the cells were already fixed in the CellSave tube.

2.2.8 Immunofluorescence Analysis

The technique of immunofluorescence is for specifically labeling a target antigen by fluorophore attached antibody within a sample, and then observing with a fluorescence microscope. The detection is based on antibody-antigen affinity and specificity, and the distinguish of the antigens depends on the fluorophore types attached to the antibodies.

After fixation and permeabilization, the captured cells were stained with fluorescent dyes in situ. Two kinds of anti-cytokeratin (CK)-fluorescein isothiocyanate (FITC) (Miltenyi Biotech; BD Biosciences) were used to label the captured target cells, for cytokeratin is keratin protein found exclusively in the cytoskeleton of epithelial cells and not of blood cells; anti-CD45- phycoerythrin

(PE) (Miltenyi Biotech) was used as negative control to eliminate the white blood cells; and 4,6-diamidino-2-phenylindole (DAPI, Sigma-Aldrich) was used to label nucleated cells. This was accomplished by mixing the fluorescent reagents in 100 mL of PBS, introducing the mixture into the chamber, and incubating for 10 minutes under room temperature, followed by a thorough wash with 3 mL of PBS. Finally, the chip with fluorescent-labeled cells was scanned under a fluorescence microscope (ECLIPSE 80i, Nikon) for identification of the cells.

2.2.9 Reuse of the Device

Although the fluidic chamber (including the microchip) is intended as a disposable, the polymer coating on the chip surface allows reusing it. The chip surface can be cleaned and regenerated after each use in situ without opening the fluidic chamber. After each use, the device was cleaned by flowing plenty of DI water through the fluidic chamber, then rinsing with and soaking for 10 minutes in diluted RBS detergent (RBS 35 Concentrate, Thermo Scientific). This was followed by flushing with DI water and ethanol (alternating the two several times) and finally filling the chamber with DI water. Blood and free beads in the bottom chamber were pulled out through the apertures by pinching the inlet tubing several times. The entire washing procedure was performed under a high flow rate (10 mL/min) to help thoroughly clean the chamber. The chip surface was scanned under both bright-field and fluorescent microscopes to make sure there was no cell or impurity residues from the last detection process. We found that this cleaning procedure allows reusing the device at least 5 times before it has to be disassembled, and the chip cleaned and coated again as discussed above.

2.3 Parameter Optimization and System Characterization

2.3.1 Parameter Optimization

Efficiency of our system, including both detection yield and purity, depends on three essential experimental parameters: 1) amount of antibody-beads added into each blood sample; 2) incubation time of antibody-beads in blood; and 3) flow rate.

Here, we fixed the flow rate to be 2 mL/min based on our previous work [86], in which a simulation and a preliminary test were done to figure the relationship between detection yield and flow rate, and focused on studying the relationship between efficiency of the first two parameters.

Typically, tens of millions of antibody-beads are added in one blood sample, and a target cell (MCF-7 or CTC) can only bound to tens to hundreds of beads. Hence most of the beads end up as free beads and that do not bound with any cells. (That is one of the main reasons we designed micro-apertures on the chip, to allow the free beads to go through.) So that there is a subtle balance between the system performance and the amount and incubation time of antibody-beads, as illustrated in Figure 2.7. The two parameters need to be sufficient to ensure encountering and attachment with all target cells, to achieve a high detection yield, but not too high/long to cause excess non-specific binding with blood cells which will decrease the purity.

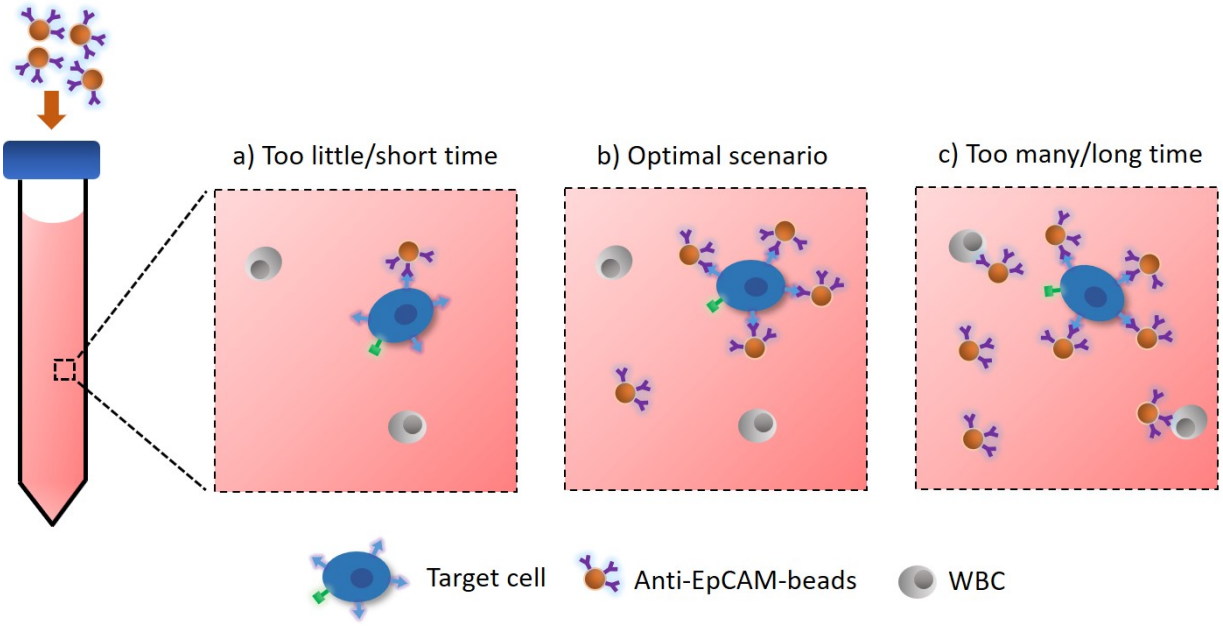

Figure 2.7 Schematic of different incubation scenarios. a) Not sufficient anti-EpCAM-beads or incubation time: target cells only bound with a small number of antibody-beads, leading to a low detection yield. b) Optimal scenario: the surface antigens on the target cell are fully exploited and mostly bound with beads, while there are few non-specific bindings of WBCs. c) Too many anti-EpCAM-beads or incubate for too long: plenty of blood cells non-specifically bound with antibody-beads, making them easier to foul on the chip surface and rendering a lower purity eventually.

To determine the optimal parameters, a known number of MCF-7 cells ranged from 75 to 95 were spiked into 7.5 mL of blood using average spiking method described in section 2.2.6. Based on a preliminary selection using small volume of blood, three different amounts, 100 μL, 150 μL, and 200 μL of anti-EpCAM-beads was then added into the blood and incubated. For each

bead amount, the incubation time started from 15 minutes and increased at a 15-minute interval for sequential experiments. After detection, we counted the MCF-7 cells captured on the chip surface to calculate the detection yield. We determined the incubation time to be sufficient for capturing when the detection yield exceeded 90%, a criterion that is commonly used in CTC detection studies. And we stopped the sequential experiments for each amount of the anti-EpCAM-beads when the detection yield was over 90% for two consecutive time points to take the safe side.

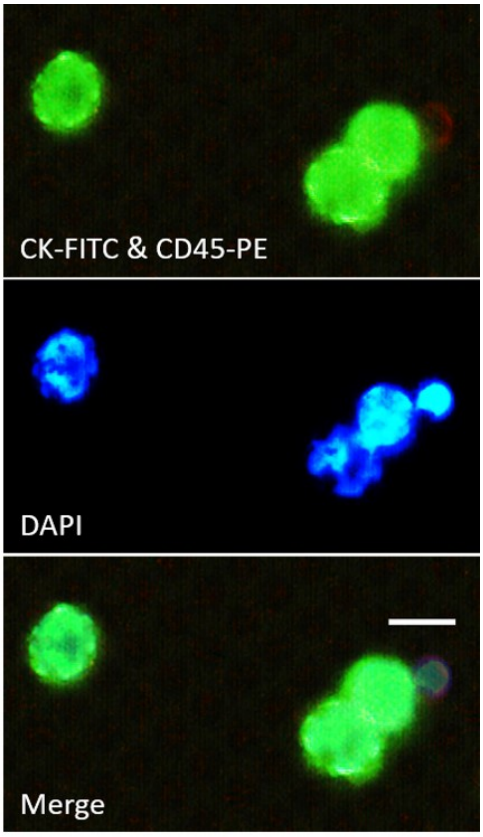

Figure 2.8. Fluorescent and merged images of cells detected from blood spiked with MCF-7 cells. MCF-7 cells are stained with anti-CK-FITCs and show green fluorescence; while WBCs are stained with anti-CD45-PE and show red fluorescence. Both CTCs and WBCs are stained with DAPI. Scale bar indicates 20 μm.

Figure 2.8 shows the fluorescent images of a few cells captured on the chip surface. We identified the cells by their fluorescence: an MCF-7 cell was green (CK+), the color of FITC dye, and blue (DAPI+) with no red (CD45-), while a WBC showed red (CD45+), the color of PE dye, and blue (DAPI+). We also used size (typically 10 ~ 30 μm) and shape (nearly circular) as additional confirmation of identification. Detection yield against incubation time for each amount

of anti-EpCAM-beads is plotted in Figure 2.9. The data was normalized to 100%. Each data point represents the mean of three measurements, and error bars indicate standard deviations. As expected, both larger amount of anti-EpCAM-beads and longer incubation time result in higher detection yield. 30 minutes is determined to be sufficient for capturing with 200 μL anti-EpCAM-beads, and 45 minutes and 60 minutes for 150 μL and 100 μL, respectively. We attribute the 45 min-150 μL datapoint (99%) being slightly higher than the 60 min-150 μL one (96%) to possible uncertainties in the average spiking method. We conducted one more test using 75 min-150 μL and got a peak detection yield of 100%, which was in accordance with the general trend. The number of captured WBCs sometimes varied depending on the blood sample's condition (e.g., donor's health, number of days after blood-draw). But in general, greater number of anti-EpCAM-beads and longer incubation times both increased the number of WBCs we found on chip.

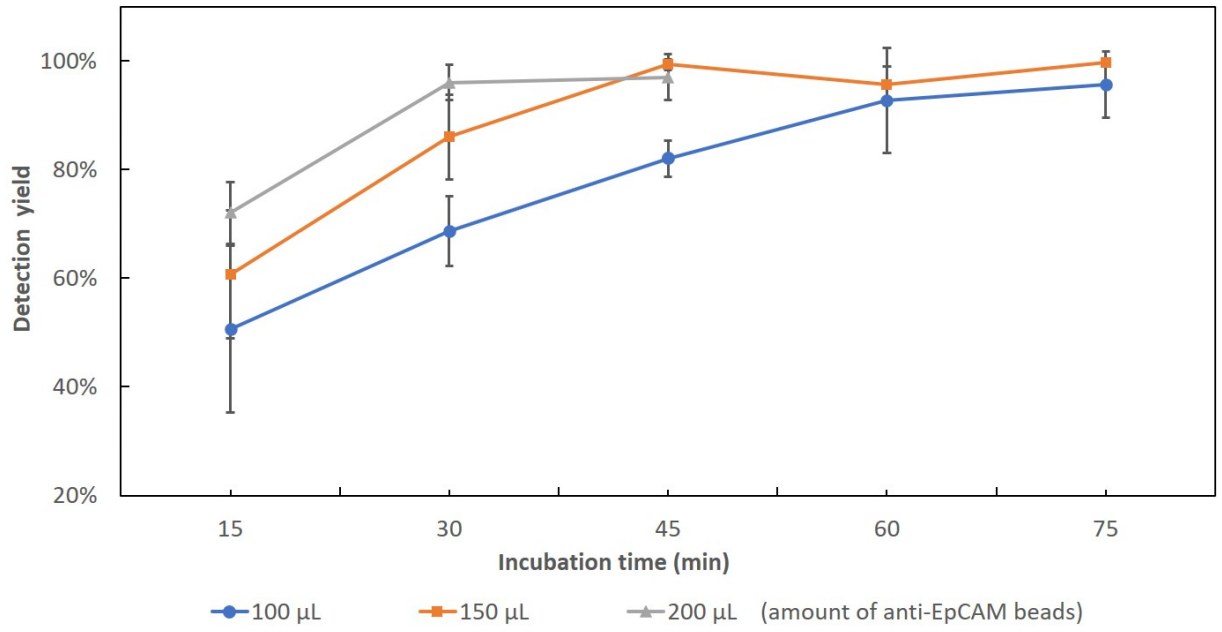

Figure 2.9. Detection yield of spiked MCF-7 cells vs. incubation time using different amounts of anti-EpCAM-beads. Blue, orange, and gray line indicates 100 μL, 150 μL, and 200 μL anti-EpCAM-beads dosage, respectively, added to the spiked blood sample. Each data point represents the mean of three measurements, and error bars indicate standard deviations.

Based on the results described above, we determined the optimal dosage of anti-EpCAM-beads to be 150 μL and incubation time to be 45 minutes (which yielded a detection yield of 99%). These parameters yield the best balance between cell detection yield and non-specific capture of

WBCs. We have also found that while most WBCs are attracted to the chip surface due to having bound to a small number of beads non-specifically, a robust hydrophilic coating on the chip surface allowed washing them away easily during PBS wash.

2.3.2 System Characterization

We next challenged our system to verify its capability of detecting as few as one single target cell from 7.5 mL of whole blood. To mimic the real clinical scenario where the number of CTCs is extremely low, and study the system's detection range, we spiked exactly 1, 10, and 100 single MCF-7 cells into 7.5 mL of blood using deterministic spiking method. Based on the optimization results, we used a 2 mL/min flow rate, 150 μL anti-EpCAM-beads and 45-minute incubation time as experimental parameters. We performed six independent experiments with only one single MCF-7 cell spiked, and three experiments each with 10 and 100 cells spiked. A negative control, using the same protocol for detection with no cell spiked, was also conducted three times.

The detection result is listed in Table 2.1. In all six one-cell spiking experiments, the target cell was successfully detected every time, which resulted in a detection yield of 100% and displayed an excellent reproducibility of our system; the fact that a single cell can be captured among tens of millions of WBCs and tens of billions of RBCs demonstrated the system's ultra-high sensitivity. For 10-cell and 100-cell spiking experiments, the average detection yields were 96.7% and 95%, respectively; no target cells were captured in any of the negative control tests. The result is plotted and linear fitted in Figure 2.10. A linear fit to the data indicates that the system can detect more than 95% of the target cells within a broad detection range, which across two orders of magnitude, and can maintain the excellent detection yield with consistency.

Table 2.1. Detection result of first-generation system characterization experiments.

# of MCF-7 Cells Spiked in 7.5 mL Blood	**# of MCF-7 Cells Detected**						**Average Detection Yield (%)**	**STDEV (%)**
	exp 1	**exp 2**	**exp 3**	**exp 4**	**exp 5**	**exp 6**		
0	0	0	0				N/A	N/A
1	1	1	1	1	1	1	100	0
10	10	10	9				96.7	0.47
100	100	91	94				95	3.74

As discussed in the last section, there was a large amount of free anti-EpCAM-beads filtered to the bottom chamber and not bound with any cell. In addition, compared to the porous area for detection, the occupied area by 100 cells is very small, leaving wide space for capturing more target cells. Due to the versatility of the detection strategy and our system, it is not unreasonable to believe our system can capture hundreds of or even thousands of target cells easily in just one detection, which renders our system scalability and potential to handle much larger volume of blood samples that contains more target cells. This immense detection ability and capacity, combined with the high throughput (in mL/min), give our system a significant advantage compared with other microfluidic CTC detection systems, which are mostly confined to process small volume blood with a low flow rate (in μL /min), and can typically only handle dozens of target cells.

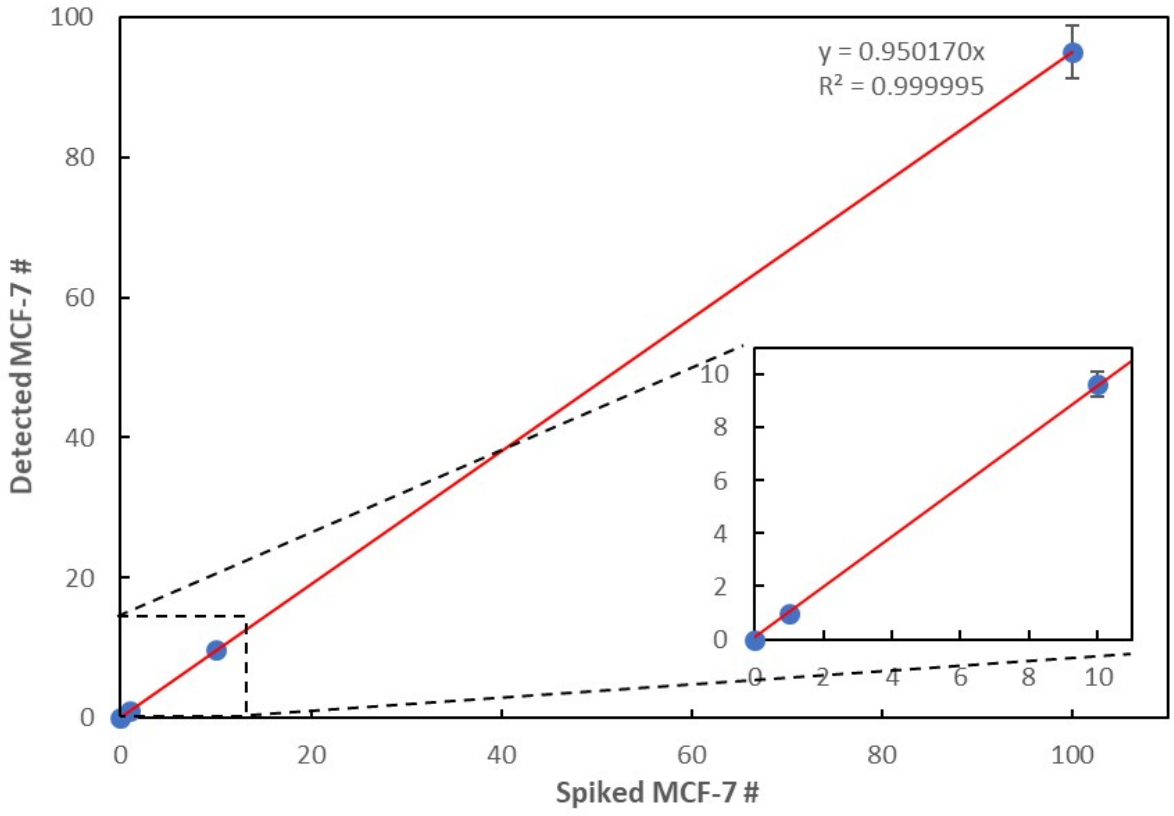

Figure 2.10. System characterization result: detected number of MCF-7 cells vs. spiked number (0, 1, 10, and 100) in 7.5 mL of human blood. Error bars indicate standard deviations from 3 measurements.

2.4 CTC Detection from TNBC Patient Blood Samples

2.4.1 Enumeration of CTCs

To demonstrate the clinical application of our system, we presented CTC detection in a total of 182 blood samples from 124 early-stage TNBC patients (in some cases, a second or third samples were also drawn from the same patient during their routine follow-up visits). The samples were processed during the period of Apr. 2016 to Jul. 2019, as part of a phase II multicenter clinical trial BRE12-158 in a collaboration with Indiana University School of Medicine. The patients recruited for the trial were early-stage non-metastatic (stages I through III) TNBC patients enrolled after completion of neoadjuvant chemotherapy (NAC, the use of chemotherapy to reduce a tumor's size prior to surgery) and surgery. These patients have “residual disease” at surgery where the analysis of the mass removed at surgery shows non-necrotic tumor but otherwise have no other tumor burden detectable. Therefore, these patients are clinically cancer free, and normally very few to no CTCs should be expected. However, these patients are known clinically to be at high-risk of disease relapse. Hence this constituted an especially challenging scenario to test our platform. We detected CTCs from patient blood samples to explore the presence of minimal residual disease (MRD) and predict which patients may have clinical recurrence.

Unlike the lab-cultured MCF-7 cell line that displays a robust and steady behavior as far as the expression of surface antigens, actual CTCs may vary significantly in the way they express epithelial markers. For example, they could experience reduction or loss of EpCAM expression on cell surface during epithelial-to-mesenchymal transition (EMT), rendering fewer target sites for anti-EpCAM-beads we added for capturing. As such, even though during our characterization experiments we have determined we can capture most of spiked MCF-7 cells with a 45-minute incubation period, we deliberately increased the incubation time to bring the possibility of losing a target CTC to a minimum. We incubated 150 μL of anti-EpCAM-beads with the blood sample for 90 ~ 120 minutes. CTCs and WBCs were identified by fluorescence analysis as described in section 2.2.8. Fluorescent images of detected cells from two patient samples are shown in Figure 2.11 as examples. There is a pair of one CTC and one WBC in Figure 2.11(a), and a cluster of 7 CTCs in Figure 2.11 (b). The cells in the cluster are overlapped, they were enumerated by counting the cell nuclei with circular shape using DAPI image. We also observed a few triple-positive (CK+, CD45-PE+, and DAPI+) cells from some patient samples. These cells were considered as

nucleated blood cells that non-specifically bound with anti-CK-FITC, and were not scored as CTCs.

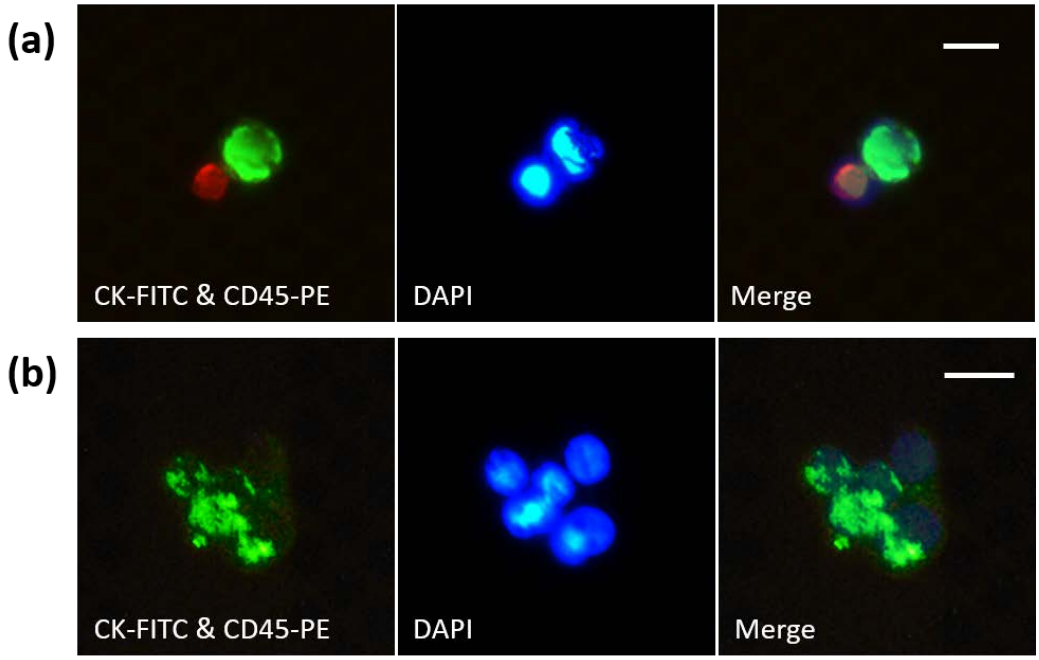

Figure 2.11. Fluorescent and merged images of cells detected from patient blood samples. Cells show both green and blue fluorescence are CK+ and DAPI+, therefore distinguished as CTCs. While WBC show red and blue indicating CD45+ and DAPI+. (a) There is one CTC and one WBC identified in the image. (b) There is a cluster of 7 CTCs identified in the image. The cells were partly overlapped to each other and enumerated by the circular shape nuclei. Both scale bars indicate 20 μm.

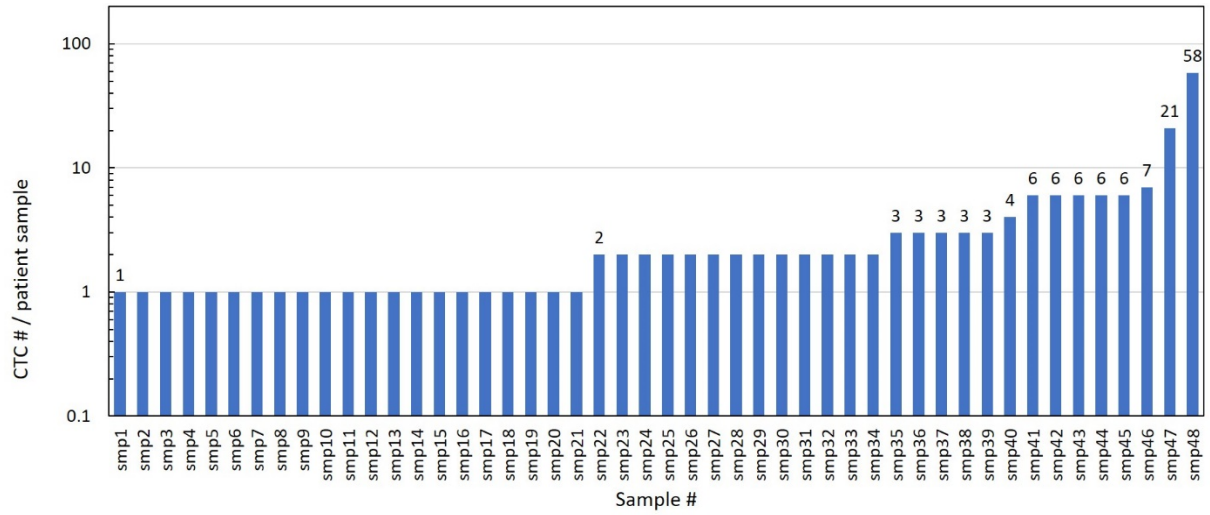

Figure 2.12. Histogram showing number of CTCs detected in each of the 48 positive samples of BRE12-158 trial, ranging from 1 to 58. Y-axis in logarithmic scale.

In 45 out of 124 patients (48 out of 182 samples), we detected at least 1 CTC, which yielded a CTC positivity in 36.3% of patient (26.4% per tube of blood sample). The patient % being slightly higher than per sample % indicates the extreme scarcity of the CTCs and hence their heterogeneous distribution over the blood samples. Figure 2.12 shows the number of CTCs in each positive sample, ranging from 1 to 58. An average of 3.8 CTCs was detected from 48 positive samples (standard deviation, 8.5). Figure 2.13 presents the median (2), upper and lower quartiles (3 and 1) of number of CTCs detected. A major part of the positive samples had very low numbers of CTCs: 21 with a single CTC, and 13 with two CTCs, also met expectations that very few CTCs should present in the blood samples, if there is any. As expected, many samples did not present CTCs indicating that combined chemotherapy and surgery was relatively successful and/or the minimal residual disease burden was sufficiently low. At the same time, a significant proportion of patients had at least one CTC detected, indicating that residual disease was present after chemotherapy and surgery.

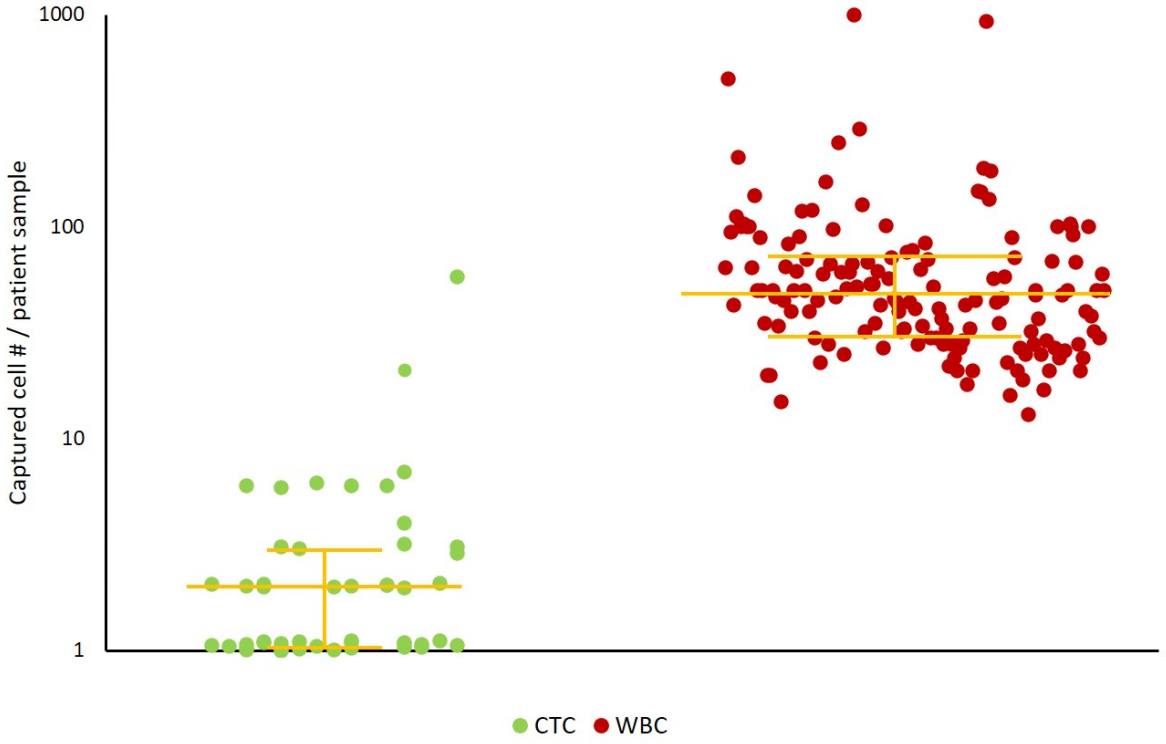

Figure 2.13. The median, upper and lower quartiles of number of CTCs and WBCs detected in patient samples of BRE12-158 trial. CTCs were captured in 48 samples, the number in one tube of blood sample ranged from 1 to 58. WBC counting was available from 147 samples, the number ranged from 13 to 1000. Y-axis in logarithmic scale.

Although the clinical study did not involve it, we also counted the number of captured WBCs from most of the blood samples (147 out of 182) in order to assess our system's detection purity. The WBC counting is presented in Figure 2.13, the number ranging from 13 to 1000, with a median of 48 and upper and lower quartiles to be 72 and 30. Although we deliberately used a longer incubation time (more than doubled the optimal time of 45 minutes), the average number of WBCs was only 75.3 per sample indicating excellent purity (standard deviation, 119.3). Considering a typical concentration of $4 \sim 10 \times 10^7$ WBCs in a 7.5 mL tube of blood, our system can effectively remove >99.9998% (or 5.7-log depletion) of WBCs.

2.4.2 Integrated Result of the BRE12-158 Trial

We matched our CTC detection result with the clinical follow-up information. The integrated result of BRE12-158 trial was presented in a previous published study [43]. The evaluable patient

sample dataset is slightly different from that reported above, because the selection criteria are not exact the same. First, as a phase II clinical trial that stretched for over 5 years, we included samples processed using the specific protocol discussed here. Besides, for the purpose of providing a specialized clinical analysis using both CTC and ctDNA detection result, some data points were reasonably discarded in the published paper. As shown in Figure 2.14, 112 patients had both ctDNA and CTC detection result available, and our system detected CTCs from 62% of the patients who experienced distant recurrence (n = 29). This means the patients had cancer come back at a distant organ, and characterized as stage IV disease that is almost not curable. Besides, an increasing CTC count of the same patient was significantly associated with inferior DDFS (Distant Disease-Free Survival), DFS (Disease-Free Survival), and OS (overall survival), suggesting that the quantitative burden of CTCs could be a good predictor of outcomes. The presence and enumeration of the CTCs detected by our system has a meaning, they can be used as independent markers to predict recurrences and identify the patients with high risk, therefore can help clinicians' decision making and therapy choice.

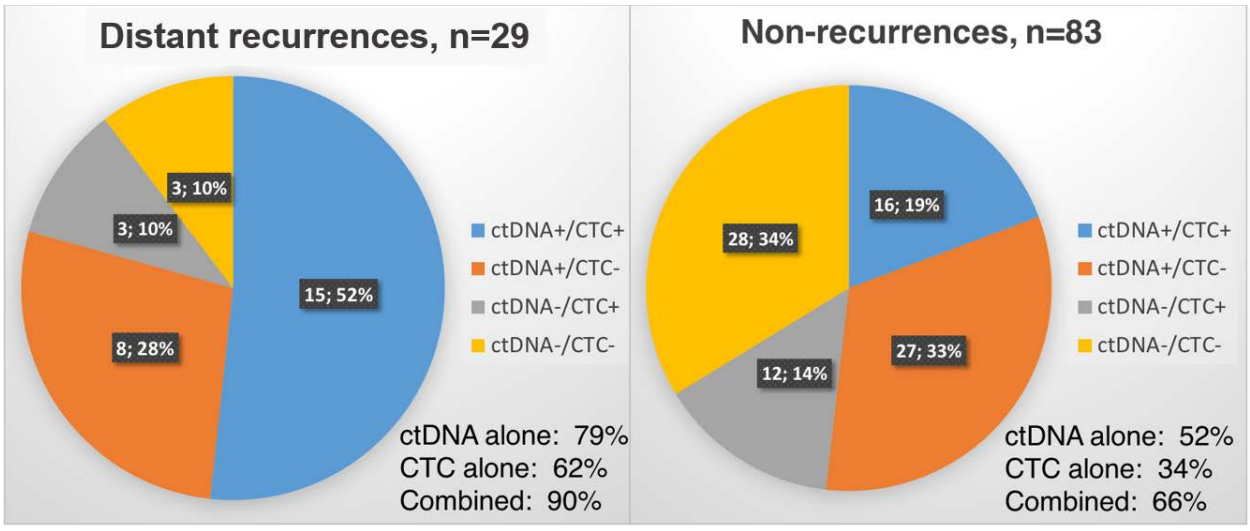

Figure 2.14. Demonstration of detection result from 112 patients from BRE12-158 trial who had both CTC and ctDNA analyzed. The analysis is split by patients who experience a clinical recurrence of distant disease (n = 29) versus those who don't have a distant recurrence at the time of analysis (n = 83).

Our prior results demonstrated that these patients were at high-risk of relapse [43], yet these patients had no clinical symptom nor tumor burden detectable when the blood was drawn for liquid

biopsy detection. In this perspective, CTC and ctDNA are more predictive than any other markers, like original tumor size or disease stage. Based on our knowledge, this is one of the largest clinical trials of the use of CTC and ctDNA markers in MRD prediction. And the results demonstrated the great clinical utility of using CTCs captured by our system as prognosis and predictive markers.

2.5 Summary

We have presented the first-generation microchip system with a highly streamlined whole-blood processing workflow for detection of CTCs. The robust and scalable system design is combined with a streamlined workflow with minimal sample processing steps that exclude centrifugation. This results in high detection yield and purity, while enabling processing whole blood directly and limiting unwanted damage to cells. The cells can be scanned and enumerated on-chip and readily retrieved for further analysis. We performed a number of spiking experiments using the MCF-7 cell line to determine optimal anti-EpCAM-bead dosage as well as incubation times. We then characterized the system by detecting deterministically spiked MCF-7 cells into 7.5 mL of blood. An average of >95% of the MCF-7 cells were captured, while a 100% detection yield was achieved from all six single-cell spiking experiments. We further used the system to the analyze the CTC count in clinical samples obtained from 124 early-stage triple negative breast cancer (TNBC) patients who had completed chemotherapy and surgery, as part of a phase II clinical trial. At least one CTC was found in >36.3% of the patients, indicating that even after chemotherapy and surgery, early-stage patients may still have CTCs in their circulation. The result demonstrates that our system is useful and efficient even under challenging circumstances where CTCs are clinically-expected to be extremely low in number. Its performance in sensitivity and purity, as well as its overall scalability and ease-of-use make this system ideal for a broad range of CTC-related studies.

Though the first-generation system achieves a high detection yield and sensitivity, and has been verified efficient in detecting CTCs from patient blood samples, there's still room for improvements. First, detecting the spiked MCF-7 cells cannot fully mimic the real scenario for capturing CTCs. MCF-7 cells are known to over express EpCAM on the cell surface, while CTCs have high heterogeneity, and the expression of the surface markers vary a lot. The first-generation system is limited by the presence of EpCAM-negative CTCs, a phenotype that is enriched in CTCs of metastatic cancers. This prompts us to upgrade our system to have a higher detection sensitivity,

particularly to be able to capture the target cells with few surface markers expressed thus bound to few antibody-magnetic beads. Moreover, the capturing strategy using only EpCAM as a single marker has it inherent defect, we want to address this by exploring a panel of biomarkers for CTC detection when applying the second-generation system.

Another area of the first-generation system that requires improvement is although its workflow is already rather streamlined (the whole process flow, from getting a tube of blood sample to CTC detected and identified, only takes 100 minutes), it involves blood circulation in the chamber. We use circulation because it increases the detection sensitivity by allowing the targeted cells to pass the chamber more than once and be captured. We want to get rid of the circulation step since 1) it is time consuming; 8 minutes is not long but we want to streamline the process as much as we can; and 2) it involves manual operation which is not very user-friendly, the outlet of the pump needs to be inserted into the blood sample tube first, after 8 minutes circulation, the outlet is taken out and put in the waste container to drain the sample. This can be addressed by improving the microchip and microfluidic device.

Finally, except for their presence and enumeration, CTCs can also be used for downstream analysis, like single cell culturing. That demands the captured cells to be alive. In the first-generation protocol, we used antibody-dyes that target intracellular markers to stain the cells for identification, requiring fixation and permeabilization, which are meant to kill the cells. We want to adopt a new staining method that can preserve cells and benefit downstream applications.

The reasons mentioned above prompted the development of the second-generation system.

3. SECOND-GENERATION SYSTEM

In this chapter, the second-generation microchip system for CTC detection and isolation from whole blood samples is presented, and the improvement on the first-generation are focused on. The new system employs a similar detection principle as the previous generation, with some upgrades to further improve the detection efficiency. The upgraded detection strategy and protocol are first explained in section 3.1. Section 3.2 emphatically describes the materials and experimental methods that are different from those of the first-generation. System modeling and simulation result for detection sensitivity is presented in section 3.3. In section 3.4, characterization result is first presented to verify the improved sensitivity; then, to demonstrate the clinical utility of the second-generation system, CTC detection result from metastatic Triple-negative breast cancer (mTNBC) patient samples of a phase I clinical trial is discussed; finally, the CTC detection result using a novel 4-marker panel from mTNBC patient samples is reported.

3.1 Introduction

Though our first-generation CTC detection system had reached some high achievements, we believe there is still some room for improvement, as discussed at the end of chapter 2, which prompted the development of the second-generation. The new system employs the same detection strategy of combining immunomagnetic capturing, high-throughput flow, and size-based filtration. However, an upgraded micro-aperture chip and device is developed, and the detection protocol is also modified accordingly.

As introduced in chapter 1, the surface marker expression level on CTCs varies a lot due to their heterogeneity, especially when they are going through metastases. Thus, we put forward the goal of detecting CTCs bound with very few magnetic beads for the second-generation system. In addition, though our protocol is already streamlined, we want to further optimize and simplify it by getting rid of the circulation. These require a further enhancement of the detection sensitivity, while maintaining the purity and high-throughput of the system.

The microchip was first upgraded by enlarging the aperture area in both length and width direction. The larger micro-aperture area enables more magnets to be placed underneath, generating a stronger and larger magnetic area for capturing. The width of the fluid channel was

increased therewith. It benefits the detection efficiency because, while maintaining the same flow rate, the wider fluid channel decreased the flow speed as well as the drag force acting on the cells in the fluid channel. Smaller drag force means the cells are less likely to be carried away by the flow. Thus, a higher detection sensitivity can be achieved. As a result of the increased sensitivity, the target cells are expected to be captured during the first time they pass through the fluid chamber, so that the circulation process can be removed. However, the enhancement comes at a cost of lower detection purity. When the target cells attached to few beads can be detected, the chance of non-specific capturing of blood cells also extends correspondingly. We attribute this to be acceptable. A higher sensitivity is more important to the system since our detection objects are too rare in the blood, and the top priority is to detect CTCs as many as possible. Nevertheless, a balance between the sensitivity and purity must be maintained well.

Another bottleneck of further improving the detection performance lies in the strategy of using a single type of antibody for capturing, which was raised to our attention when applying the first-generation system to detect CTCs of TNBC. From a clinical perspective, TNBC is known to possess disproportionately higher morbidity and mortality including increased frequency of distant metastasis, it is characterized by broad heterogeneity [101,102]. In addition, TNBC is particularly variable in epithelial-to-mesenchymal transition (EMT) , which is associated with increased capacity for metastasis, while mesenchymal-like CTCs are characterized by loss of expression of the EpCAM [103]. Hence a major goal and application of the second-generation system is to explore a novel panel of biomarkers for CTC detection instead of using anti-EpCAM alone. The principle of utilizing a cocktail of antibodies to encompass the heterogeneity of CTCs is illustrated in Figure 3.1. Instead of relying on one surface marker whose expression level varies a lot, a panel of antigens are targeted with specific antibody-beads, such that more magnetic beads can attach to a single target cell. By using a cocktail of antibodies, we anticipate both detection sensitivity and system robustness would be improved.

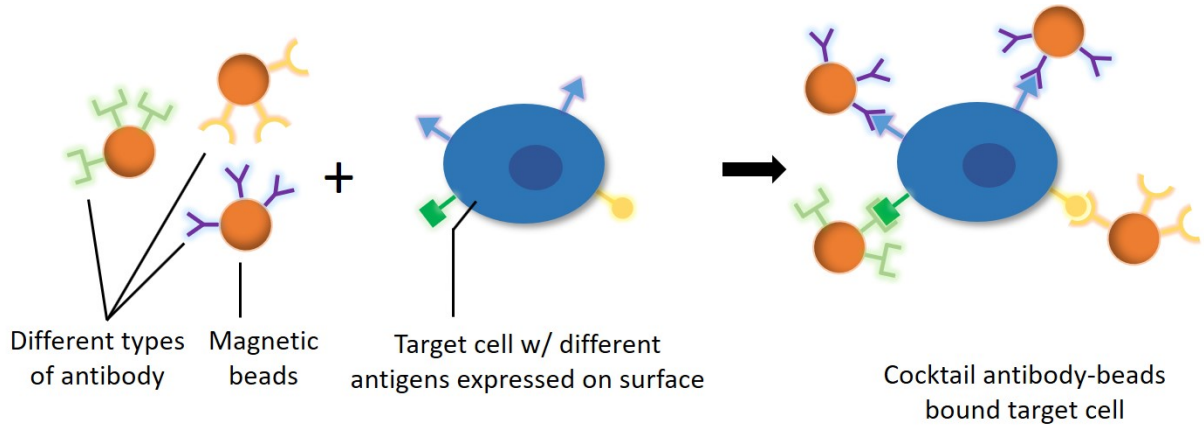

Figure 3.1 Schematic of the capturing of target cells with a cocktail of antibodies conjugated magnetic beads. Different shapes, triangle, rectangle, and circle, illustrate different types of antibody, which are used to specifically target different antigens expressed on the cell surface.

3.2 Upgraded Materials and Methods

3.2.1 Upgraded Microchip and Device

We first got down to upgrade the micro-aperture chip and the fluid channel, as shown in Figure 3.2. The micro-aperture area for cell capturing is 4 times larger than the first-generation, which benefits the detection sensitivity because 1) the effective cell capturing area is larger, which also help increase the isolating purity, 2) more magnets can be used to generate a longer and stronger magnetic field, and 3) larger dosage of antibody-beads is allowed since the bottom chamber is bigger together with the micro-aperture area. At the same time, the whole chip size is smaller, rendering the microfluidic device more compact (the fluid channel length is slightly smaller from 30 mm to 28 mm). The fabrication is also more cost-effective, 10 microchips can be fabricated on a 4" wafer now instead of 6 chips of the first-generation. By widening the fluid chamber (4.3 mm to 8 mm) while keeping the same thickness (1 mm), the flow *velocity* (in the unit of mm/min) in the chamber can be reduced almost by half under the same flow *rate/throughput* (in the unit of mL/min). The drag force acting on the cells is reduced correspondingly, too.

The second-generation microfluidic device has the same sandwich structure as the first-generation, the only difference is in size, as shown in Figure 3.3. Besides, there are two block N52 neodymium permanent magnets with the size of 1/4"×1/4"×1/4" underneath the bottom chamber.

Chip fabrication, polymer layer coating, device assembly and reusage are all the same as described in Chapter 2, and will not be reiterate here.

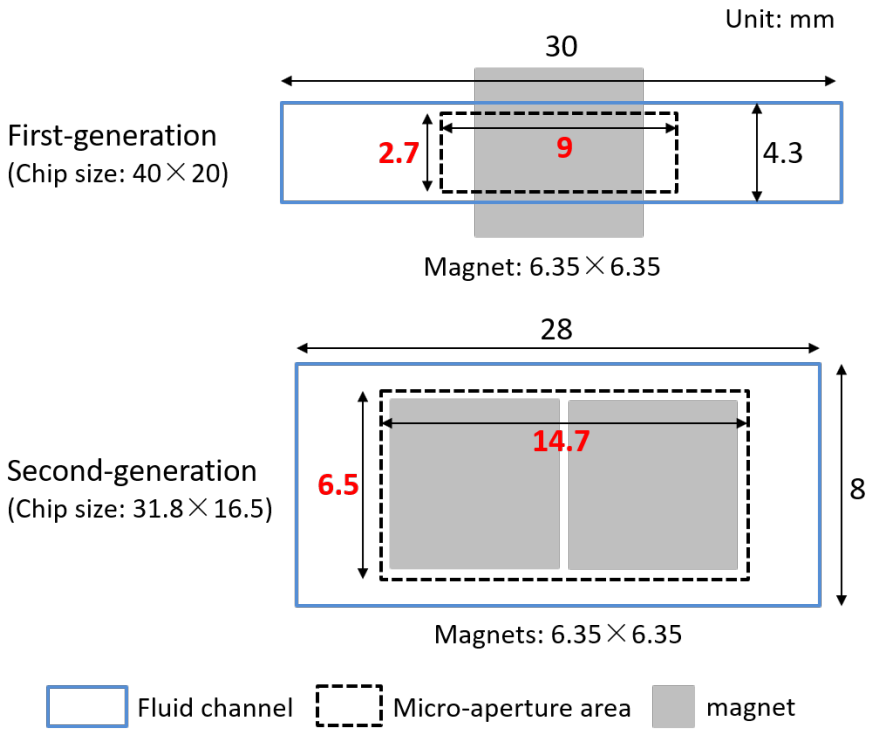

Figure 3.2. Micro-aperture area of the chip and fluid channel comparison between first- and second-generation system.

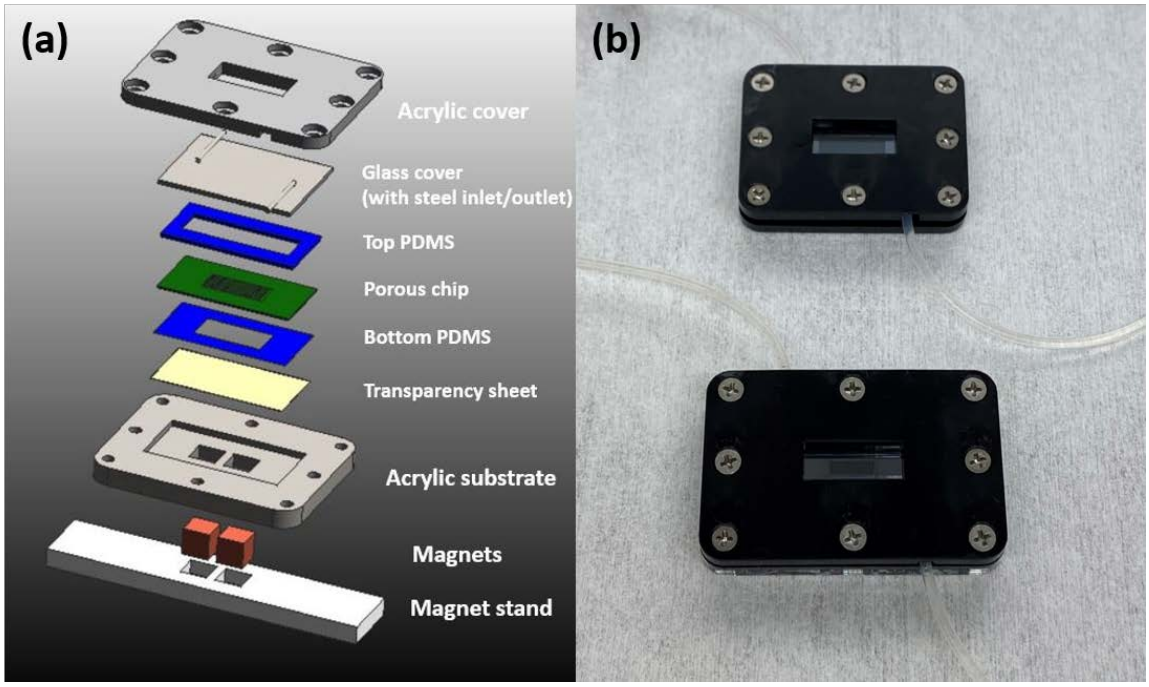

Figure 3.3. (a) Assembly schematic of the second-generation microfluidic device. (b) Assembled devices: second-generation (up) and first-generation (bottom).

3.2.2 Preparation of Antibody-conjugated Magnetic beads

In the exploration of the novel 4-marker panel for CTC detection, four kinds of antibody-beads need to be prepared. Same as anti-EpCAM-beads, we saturated the magnetic beads (20 μL, 200 μg) with excess anti-EGFR, anti-N-Cadherin, and anti-TROP2 (5 μg each) to maximize the capturing capacity. Biotinylated antibodies targeted the 4-marker panel were conjugated with the filtered T1 magnetic beads through the same process as shown in section 2.2.4. After conjugation, the antibody-beads were all re-suspended in 200 μL PBS to maintain the same concentration as the anti-EpCAM-beads.

3.2.3 Preparation of JEG-3 and JAR Cells

JEG-3 and JAR are both human placental choriocarcinoma cell lines; they are commonly used as models to mimic either CTCs or circulating trophoblast cells, which is another type of rare cells that can be retrieved from maternal blood. Both JEG-3 and JAR cell line were purchased from American Type Culture Collection (ATCC, HTB-16 and HTB-144), and cultured in recommended medium (EMEM, ATCC 30-2003, for JEG-3, and RPMI-1640 Medium, ATCC 30-2001, for JAR) with 10% FBS (ATCC 30-2020). Cell trypsinization and spiking in blood process were the same as described in section 2.2.5 for MCF-7. In characterization experiments of the second-generation system, we only used the average spiking method.

3.2.4 Detection of Spiked JEG-3 and JAR cells

To characterize the second-generation system as well as compare it with the first-generation, we detected JEG-3 or JAR cells spiked into either cell culture medium or healthy human blood and measured the detection yield. Known number of JEG-3 or JAR cells were spiked into 2 mL of cell culture medium/7.5 mL of healthy human blood, 20 μL/150 μL of anti-EpCAM-beads was then added, followed by a 60 to 90 minutes incubation. After incubation, the blood sample was transferred to a 50 mL centrifuge tube and diluted 1:1 with PBS solution to a total volume of 15 mL, while the medium sample was flowed directly with no dilution. The sample was flowed through the fluid chamber without circulation. The rest of the detection process, including the immunofluorescence analysis was the same as that of the first-generation as described in section 2.2.6.

3.2.5 Detection of CTCs from mTNBC Patient Blood Samples

To verify the clinical utility of the second-generation system, we applied it to a clinical trial. IUSCC-0613 was a phase 1 dose escalation clinical trial for exploring a novel combination of cancer drugs against mTNBC. The recruited patients were all with mTNBC, not early-stage disease as in the BRE12-158 trial. 10 patients with mTNBC were recruited (all consented as part of the IUSCC-0613 trial protocol), from whom 102 blood samples were collected for CTC detection. Multiple samples were collected from the same patients during a certain period. Patient blood samples were collected in standard blood collection tubes, and detection were conducted within 48 hours of collection. 150 μL of anti-EpCAM-beads was added into a tube of whole blood sample and incubated for 60 to 90 minutes. The sample was then flowed through the fluid chamber at a flow rate of 2 mL/min without circulation. After washing and WBC lysis, the captured cells were not fixed or permeabilized as in the first-generation system, but were immuno-stained using antibody dyes targeting cell surface markers, as will be described later in section 3.2.7.

3.2.6 Exploration of a Novel 4-marker Panel by Detecting CTCs from mTNBC Patient Blood Samples

To address the detection efficiency problem of using only anti-EpCAM for capturing, we explored a novel 4-marker panel for CTC detection from mTNBC patients in a study collaborated with Indiana University School of Medicine. The four target markers: EGFR, EpCAM, N-Cadherin, and TROP2 were preliminary screened out by a comprehensive search of publications. Then the four markers were characterized across 11 TNBC cell lines by flow cytometry, and at least 1 marker from our panel was positive in every cell line assessed. EpCAM was detected with 8/11 cell lines positive yet 3/11 lines negative, illustrating that the panel of markers had robust potential to tackle the TNBC heterogeneity than EpCAM alone. Two EpCAM-positive and four EpCAM-low or -negative lines were assessed by spiking into cell culture medium and detected using our system. It was reported that the capture efficiency was constantly better using the panel markers across the EpCAM-low or -negative lines, and the panel markers were proved to be superior to EpCAM only [97].

Next, we proceeded to conduct CTC detection from real mTNBC patient samples using the second-generation system. 13 patients were consented and recruited from the clinics at Indiana University School of Medicine. Blood samples were drawn and preserved in 10 mL CellSave

Preservative tubes. Paired comparison was done between using panel markers and anti-EpCAM only for detection. For the paired analysis, 2 CellSave tubes of blood were drawn per patient, stored at room temperature, and analyzed within 72 hours. Before detection, two tubes of blood were thoroughly mixed, and then split into two tubes evenly to eliminate the original stochastic error between tubes. The ratio of used antibody-beads was 2:1:1:1 (EpCAM: EGFR: N-Cadherin: TROP2), which means 100 μL of anti-EpCAM-beads together with 50 μL of each of the rest three antibody-beads was added into the 4-marker panel tube; and 150 μL of anti-EpCAM-beads was added into the EpCAM-only tube. After an incubation of 70 minutes, the sample was flowed through the fluid chamber at a flow rate of 2 mL/min, followed by PBS wash and WBC lysis. The captured cells were then immuno-stained on-chip, as will be described later in section 3.2.7.

3.2.7 Surface Marker Staining for Immunofluorescence Analysis

In section 2.2.8, we described the protocol for immunofluorescence analysis of the captured CTCs using antibody-dyes targeting an intracellular antigen, cytokeratin. However, to allow the anti-CK-FITC to get through the cell membrane and stain the intracellular antigen, the cell needs to be fixed and permeabilized beforehand, which will damage the live cell. To preserve the health of and vital information in captured CTCs, we adopted antibody-dyes targeting cell surface antigens for immunofluorescence identification, which can avoid the fixation and permeabilization and keep the captured cells alive. Moreover, previously we used DAPI for cell nucleus staining to identify nucleated cells. DAPI is cell-impermeant and requires fixation. Hence for surface immuno-staining, Hoechst 33342 (62249, Thermo) was chosen as an alternate since it is a cell-permeant nuclear counterstain for live cell staining. Anti-CD45-PE was still used to label the WBCs, for CD45 is a membrane glycoprotein that expresses on the cell surface of leukocytes which does not require fixation nor permeabilization for targeting.

For identification of cells detected from mTNBC patient samples of IUSCC-0613 trial, anti-EpCAM-FITC and TROP2-FITC were used. They were mixed with anti-CD45-PE in 200 mL of PBS, introduced into the chamber, and incubated for 15 minutes under room temperature. After the first staining reagents were thoroughly washed with PBS, Hoechst 33342 in 200 mL of PBS was introduced into the chamber and incubated for another 10 minutes then washed with PBS. Finally, the chip with fluorescent-labeled cells was scanned under a fluorescence microscope for cell identification.

In detection of CTCs for exploration of the 4-marker panel with mTNBC patient samples, different staining methods were used for the paired experiments. Cells captured with the 4-marker panel were surface immuno-stained with FITC-labeled antibodies against all four markers, anti-CD45-PE, and Hoechst 33342. The staining process is the same as that used for IUSCC-0613 trial above. Cells captured with anti-EpCAM-only were immuno-stained using the same protocol of the first-generation system (with anti-CK-FITC, anti-CD45-PE, and DAPI), as described in section 2.2.8, only the volume of mixed fluorescent reagents was 200 mL instead of 100 mL since the second-generation fluid chamber has a larger volume.

3.3 Modeling and Simulation

To better understand the underlying physics and find the optimal configuration, we performed modeling and numerical simulation of the system. For simplicity, we treated the target cell attached with magnetic beads as a cell-beads complex, so that it can be modeled as a single mathematical particle. First of all, the forces experienced by the cell-beads complex need to be studied. The governing equation is the Newtonian Law, as shown in Eq. (3.1), and there are four major forces acting on the cell-beads complex: magnetic force $\overrightarrow{F_m}$, Stokes drag force $\overrightarrow{F_d}$, gravity force $\overrightarrow{F_g}$, and buoyant force $\overrightarrow{F_b}$ [104,105].

$$m_p \frac{\partial \overrightarrow{V_p}}{\partial t} = \overrightarrow{F_m} + \overrightarrow{F_d} + \overrightarrow{F_g} + \overrightarrow{F_b} \tag{3.1}$$

where m_p and $\overrightarrow{V_p}$ are the mass and velocity of the complex. The mass of a single MCF-7 cell bound with N beads is (1433 + N) pg [86]. The gravity force and the buoyant force are constant and easy to model.

$$\overrightarrow{F_g} = m_p \vec{g} \tag{3.2}$$

$$\overrightarrow{F_b} = -\rho \vec{g} V \tag{3.3}$$

where ρ is the density of the cell-beads complex, which is approximately equal to the density of the fluid. And V is the volume of the complex.

Thus, two main forces affect the complex trajectory are magnetic force and the Stokes drag force. Magnetic force is calculated by Eq. (3.4):

$$\overrightarrow{F_m} = N \times \frac{V\chi}{2\mu_0} \nabla \vec{B} \cdot \vec{B} \tag{3.4}$$

where N is the number of beads per cell, χ is the magnetic susceptibility of beads, μ_0 is the vacuum permeability, and $\vec{B}$ is the magnetic flux density. 2 mL/min flow rate equals to a flow speed of 4.17 mm/s in the fluid chamber. The experimental parameters and chamber dimensions yield a Reynold's number of 1.75, indicating the flow in the fluid chamber is laminar, and the Stokes drag force equation can be applied, as shown in Eq. (3.5):

$$\overrightarrow{F_d} = 6\pi\eta r_p(\vec{U} - \overrightarrow{V_p}) \tag{3.5}$$

where η is the fluid dynamics viscosity ($2.5 \times 10^{-3}[kg \cdot m^{-1} \cdot s^{-1}]$), r_p is the radius of the complex, and $\vec{U}$ and $\overrightarrow{V_p}$ are velocities of the fluid and the complex, respectively.

We then proceeded to conduct a numerical simulation of our system using COMSOL Multiphysics software involving multiple physics domains. The fluid chamber with a dimension of 28 mm by 8 mm by 1 mm was first modeled. We simulated the stationary magnetic field generated by a pair of block N52 Neodymium permanent magnets. Two side-by-side magnets configurations: poles same direction and poles opposite direction, were studied to find the optimal setup in regard of the attractive magnetic force experienced by the cell-beads complex within the chamber. Next, the flow field in the fluid chamber was simulated. As introduced above, a peristaltic pump was used to create the flow, which is not a stationary but really pulsatile flow. Finally, by coupling of multi-physics fields, the trajectories of the cell-beads complexes can be calculated with the Newton's equation and simulated using the particle tracing module of the software. Detection yield is measured by counting how many complexes ended up reaching the chip surface.

3.3.1 Magnetic Field and Magnetic Force Acting on Cell-beads Complex

The stationary magnetic field was first simulated. Two block N52 neodymium permanent magnets were created in the model, placing side-by-side underneath the fluid chamber along the flow direction, with a small gap of 3 mm between each other as in the real system setup. Residue magnetic flux density (B_r) and relative permeability (μ_r) of the magnets were entered into simulation as 1.45 T and 1.05, respectively, according to the material characteristic list.

As shown in Eq. (3.4), the magnet force depends on the magnetic flux density. For a pair of side-by-side placed magnets, different configurations yield different magnetic fields. Two configurations, either same poles or opposite poles of the magnets facing upwards, were studied.

Figure 3.4 shows the magnetic flux density patterns on the chip surface of the two configurations. (a) In poles same direction configuration, due to the repulsion of the same polarity, magnetic induction lines are concentrated on the far-side edges of the magnets and yields high flux density there. (b) On the contrary, magnetic induction lines are concentrated on the near-side edges because of the attraction of the opposite polarity in the second configuration, where the high flux density area is formed in between two magnets, and the maximum density norm (T) is ~20% larger than that of poles same direction configuration.

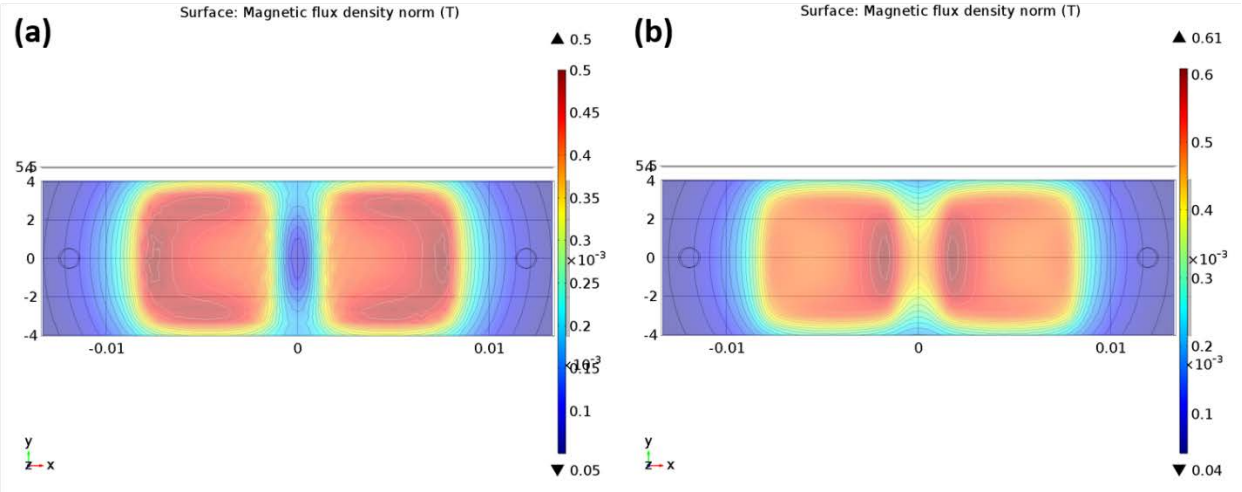

Figure 3.4. Top view of magnetic flux density maps along chip surface of two side-by-side magnets configurations. (a) Poles same direction. (b) Poles opposite direction.

Next, we studied the magnet force acting on a single magnetic bead in the system. According to Eq. (3.4), magnetic susceptibility χ of the beads needs to be determined first. Due to their superparamagnetism, the susceptibility of the beads varies under different magnetic field strength. Based on the magnetic hysteresis (M(emu/g) vs B(G)) provided by the manufacturer (not shown here), the function between the susceptibility χ and the magnetic flux density B can be derived and fitted by a 6-order polynomial function ($R^2 = 0.9999$), as shown in Eq. (3.6).

$$\mathrm{M} = -47775B^6 + 83760B^5 - 58459B^4 + 20727B^3 - 3953.9B^2 + 405.72\mathrm{B} + 0.0018 \quad (3.6)$$

The magnet force experienced by a single bead along the central axis (flow direction) on the chip surface is shown in Figure 3.5 under two different magnet configurations. The blue lines indicate vertical direction magnetic forces which are the attractive forces to pull the bead down to the chip.

The maximum forces in both configurations are about 9.1 pN, but the poles same direction configuration yields four peaks, which indicates larger and more distributed capturing area, while the poles opposite direction configuration only has two peaks. Thus, we chose poles same direction configuration as our experimental setup.

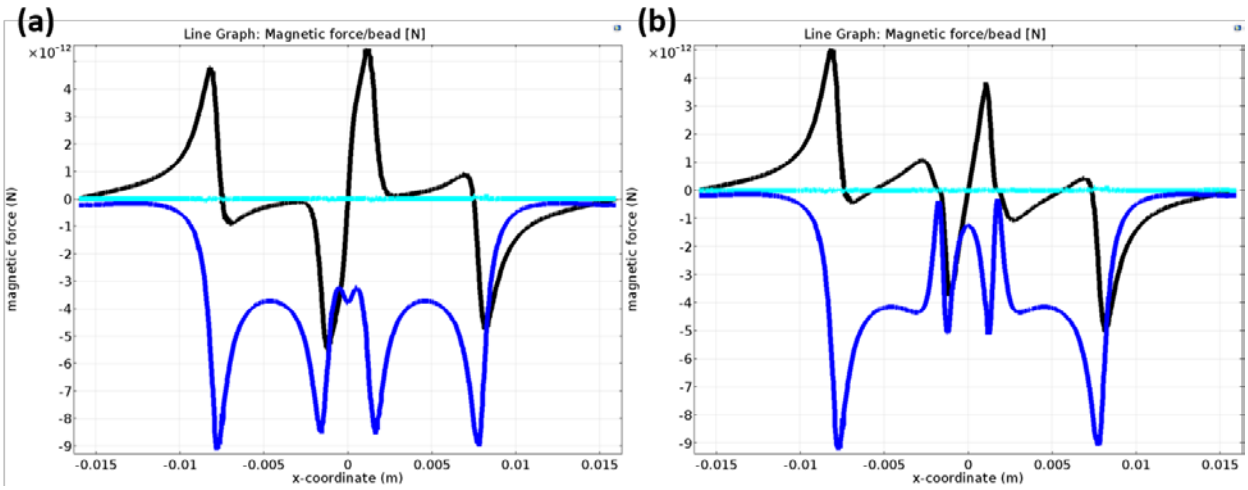

Figure 3.5. Magnetic force acting on one magnetic bead under two side-by-side magnets configurations. (a) Poles same direction. (b) Poles opposite direction. Black, cyan, and blue lines indicate magnetic forces on x (along the flow), y, and z (vertical) direction.

3.3.2 Flow Field

The flow in the chamber has a Reynolds number of 1.75, indicating a laminar flow. However, in reality, though the peristaltic pump can be set to generate a rather smooth flow and maintain a constant flow rate, it is rather a pulsatile rather than steady flow. To simulate the pulsatile flow field, working mechanism of the peristaltic pump was first studied. The pump we used has 12 rollers. When started, the rotating rollers squeeze the tube which is made of flexible materials; with the rollers rotating forward, the fluid within the contacting section of the tube follows the motion, the flow is then generated by the continuing rotating rollers. The force density of one engagement of one roll can be modeled as a Gaussian distribution load [106]. To further simplify the function entered for calculation, we used a sinusoidal function, in the form of $A + Bsin(\omega t)$, to approximate the Gaussian distribution. At a volume flow rate of 1 mL/min, the function of the input flow was found to be:

$$0.895 + 0.165 \times abs(\sin(6\pi t))\ [mL/min] \tag{3.7}$$

Figure 3.6 presents the simulation result of the flow field at a certain time. X-component of the velocity in xz-plane (the axial plane of the fluid chamber) and xy-plane (chip surface) are shown. It can be seen that the maximum velocities appear near the inlet and outlet.

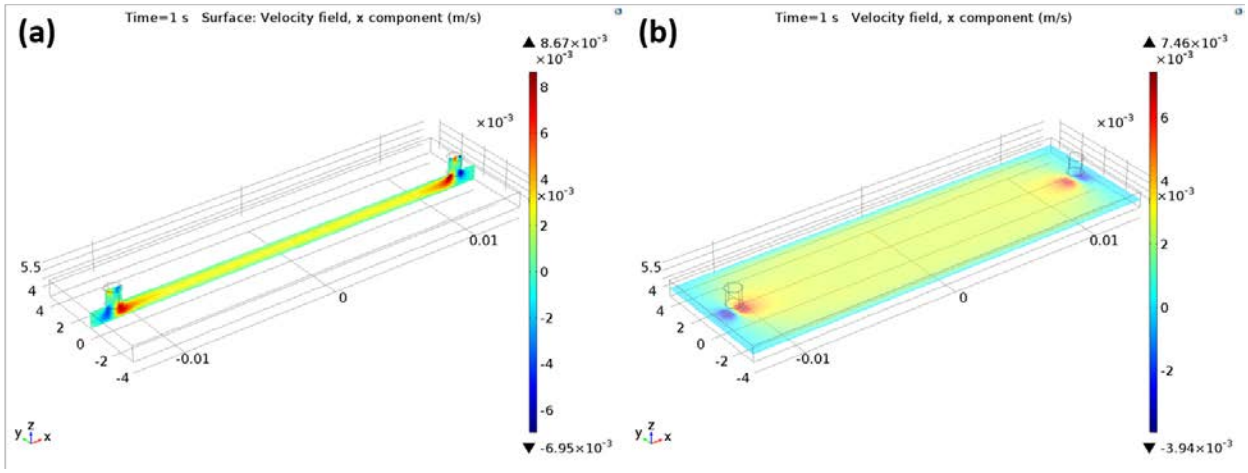

Figure 3.6. Velocity field in the fluid chamber in x-direction (along the flow direction). (a) Velocity field in xz-plane. (b) Velocity field in xy-plane.

3.3.3 Particle Tracing

By coupling the magnetic field and flow field, the forces acting on the cell-beads complexes can be calculated and simulated properly to solve for the complex trajectories. We released 20 complexes through the inlet of the fluid chamber in each simulation and measured the detection yield. Trajectories of 20 complexes with 4 magnetic beads per cell is shown in Figure 3.7. As can be seen in the image, 19 complexes ended up on the chip surface, while one complex escaped through the outlet, rendering a detection yield of 19/20 = 95%.

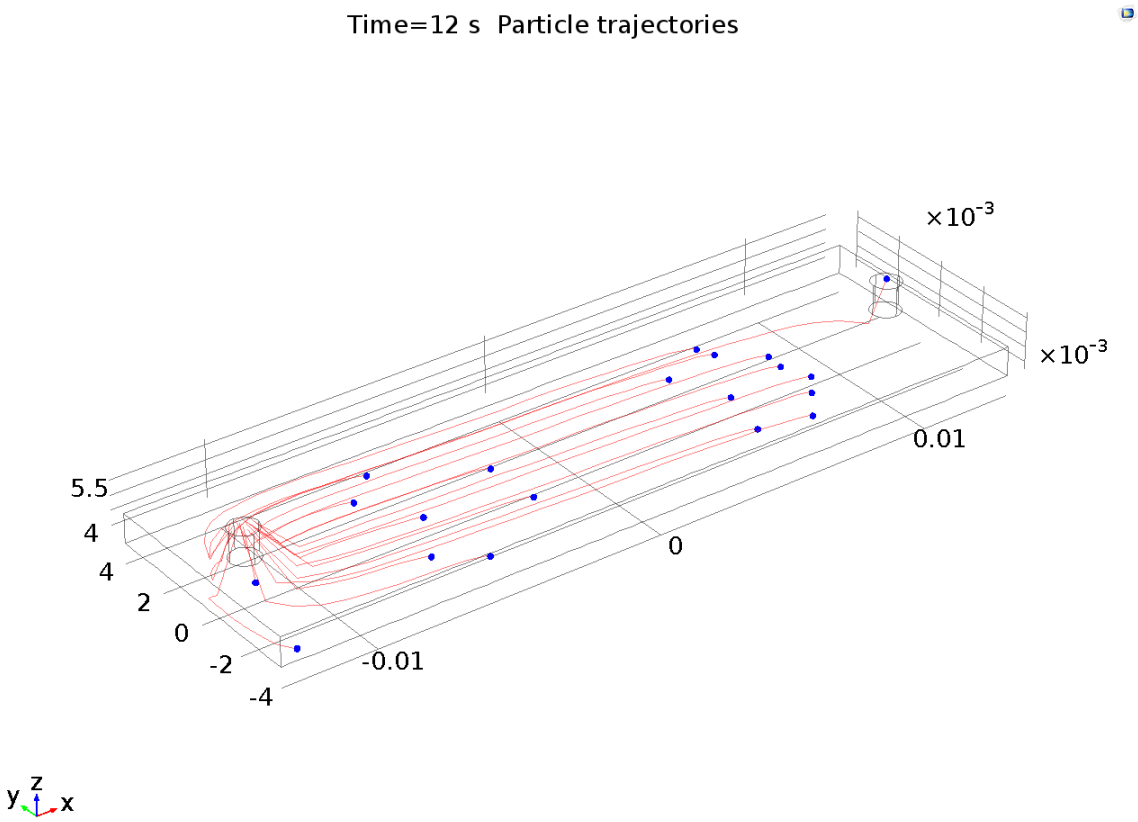

Figure 3.7. Trajectories of 20 cell-beads complexes in the fluid chamber.

We studied the detection yield for complexes attached to different number of beads. Results of both first- and second-generation system are shown in Figure 3.8 for comparison. Under simulation conditions, the second-generation can capture 95% of the released complexes with 4 beads/cell, and 100% of the complexes with 5 beads/cell. While the first-generation system can capture only 40% with the same number of beads bound to one cell. (The first-generation reached a detection yield of >90% with ~20 beads/cell. Note that there was no circulation included in the simulation.) It is concluded from the simulation result that the second-generation achieves a higher sensitivity, and especially more efficient than the previous generation when capturing target cells attached to very few numbers of magnetic beads.

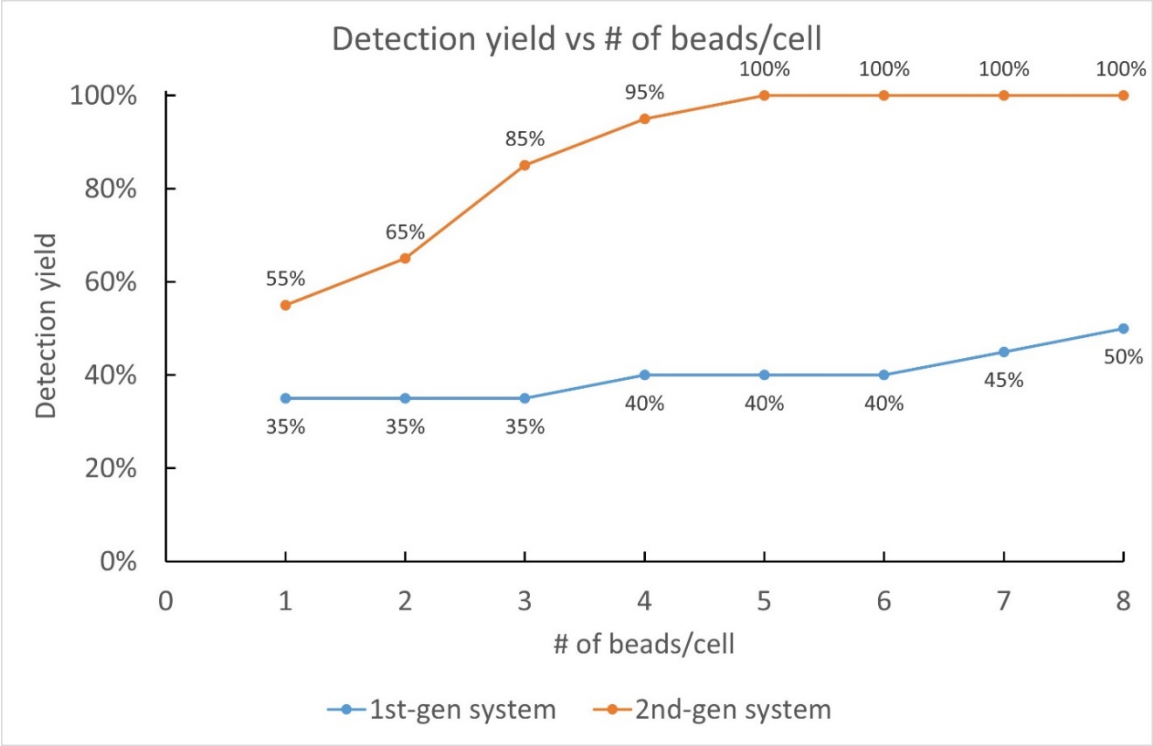

Figure 3.8. Simulated detection yield of cell-beads complexes with different number of beads. Blue and orange line indicate the results using the first- and second-generation system, respectively.

3.4 Results and Discussion

3.4.1 System Characterization and Comparison

From the modeling and simulation result, we conclude that the second-generation has higher detection sensitivity than the first-generation. To further prove it and characterize the second-generation system. We did cell spiking experiments to measure the detection yield under different flow rate. 50 ~ 100 JEG-3 or JAR cells were spiked in 2 mL of cell culture medium first for preliminary test, and 7.5 mL of human blood to mimic the real CTC detection scenario from a whole tube of blood. The detailed detection protocol was discussed in section 3.2.4.

The characterization result from medium spiking experiment is shown in Figure 3.9. Without circulation, the first-generation had a detection yield of 83% under a flow rate of 2 mL/min, and the detection yield decreased with increased flow rate, to 44% at 5 mL/min. In the first-generation ,only cells attached with a lot of beads can be captured, while the others with fewer beads were washed away by the high-speed flow. Under the same condition, the second-generation system can maintain a 100% detection yield under a flow rate as high as 3 mL/min, and the yield

deceased to 90% at 5 mL/min. A student's t-test analysis (paired, one-tailed) on the two generation systems revealed a p-value of 0.006, indicating a statistically significant difference between the detection efficiencies.

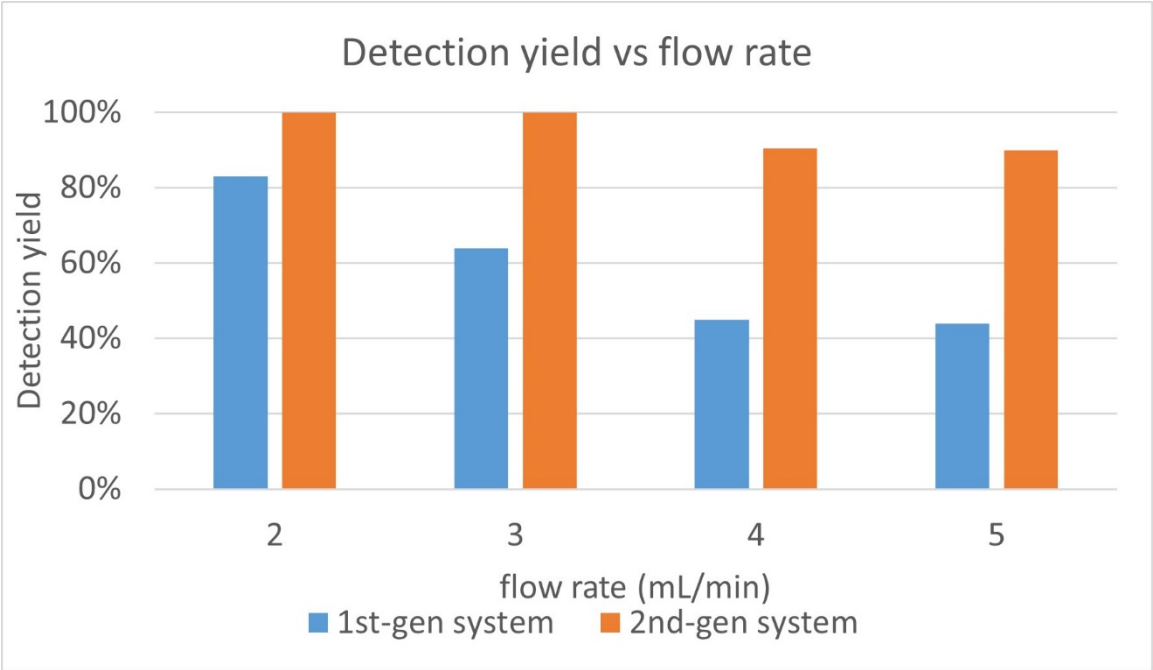

Figure 3.9. System characterization result: comparison of detected yield of spiked JEG-3 or JAR cells in 2 mL cell culture medium using first- and second- generation system.

The characterization result from 7.5 mL blood spiking experiment is shown in Figure 3.10. For the blood-based characterization using first-generation system, we only tested it at 2 mL/min flow rate and got an averaged detection yield of 68%. While the second-generation system can still maintain 100% detection yield at 3 mL/min, this throughput was so high that it only took our system about 5 minutes to run a whole tube of blood (after dilution) through and capture all spiked cells.

Combing the paired test results, the second-generation system has a >20% higher detection yield than the first-generation. The encouraging result demonstrates the solid improvement which prompted us to apply the upgraded system to clinical applications.

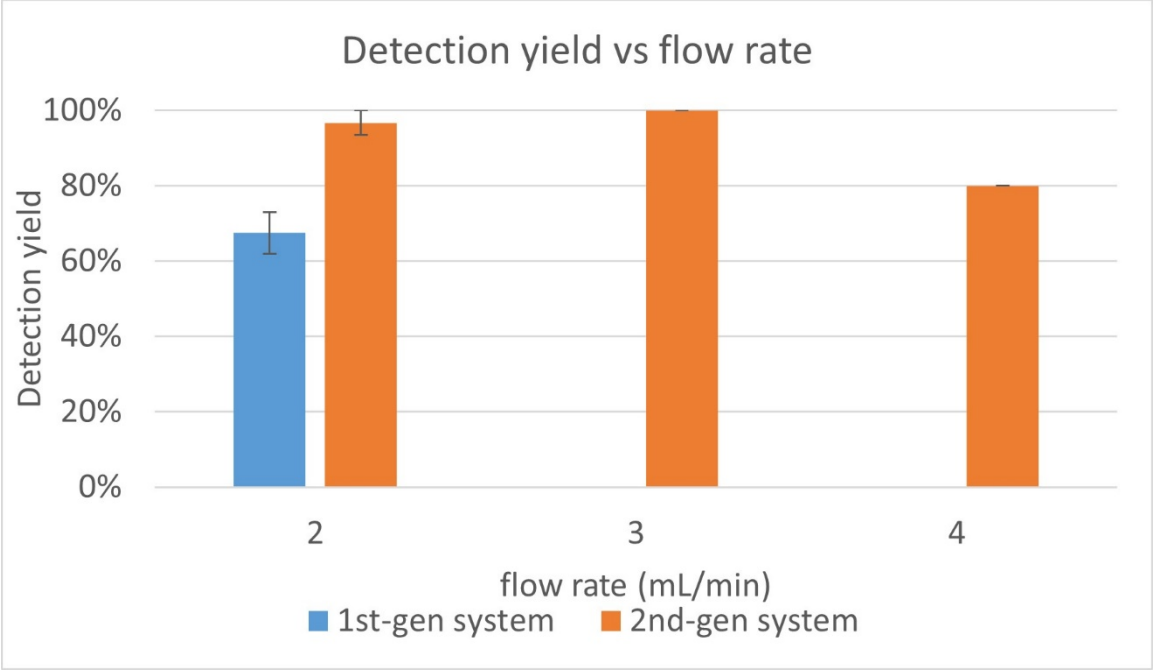

Figure 3.10. System characterization result: comparison of detected yield of spiked JEG-3 or JAR cells in 7.5 mL human blood using first- and second- generation system. Error bars indicate standard deviation.

3.4.2 CTC Detection from mTNBC Patient Blood Samples Using Anti-EpCAM Only

After verifying that the second-generation system has a higher detection sensitivity, we applied it to another challenging clinical trial. We first presented CTC detection result from a total of 102 blood samples from 10 mTNBC patients. The samples were processed during the period of Feb. 2018 to Dec. 2018, as part of a phase I clinical trial IUSCC-0613 in a collaboration with Indiana University School of Medicine. Studies have shown the EpCAM expression in TNBC is ~60% [107], and the expression level is even lower on CTCs from metastatic patients because they could loss EpCAM expression during epithelial-to-mesenchymal transition (EMT) [108]. With less EpCAM expressed on the cell surface, targeting sites are fewer, hence there are fewer magnetic beads attached to a single CTC, which requires the detection system to be highly sensitive.

We determined the detection parameters based on our experience detecting CTCs using the first-generation system with a few adjustments. The incubation time (60 ~ 90 minutes) is shorter than that used for first-generation for the purpose of reducing non-specific binding, yet it is still long enough to have a maximum detection yield based on the simulation and characterization result. CTCs and WBCs were identified by immuno-staining as described in section 3.2.7. Fluorescent

images of two detected single CTCs are shown in Figure 3.11 as an example for the surface staining result.

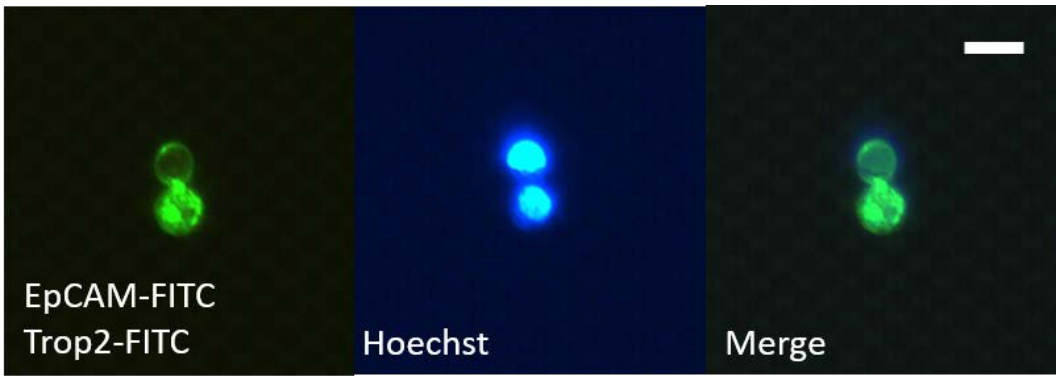

Figure 3.11. Fluorescent and merged images of cells detected from mTNBC patient blood samples of IUSCC-0613 trial. Cells show green and blue fluorescence are EpCAM+/Trop2+ and DAPI+, therefore distinguished as CTCs. There is a cluster of 2 CTCs identified in the images. Scale bar indicates 20 μm.

At least 1 CTC was identified in 48 out of 102 samples (8 out of 10 patients), yielding a CTC positivity in 47% of samples (80% of patients). Figure 3.12 shows the number of CTCs identified in each of the 48 positive samples, ranged from 1 to 212, with a median of 6 and an average of 25 CTCs per sample (standard deviation, 41). We compared the result with that of BRE12-158 trial (plotted in Figure 3.12, too) we introduced in chapter 2, of which the patients also had TNBC, but were with early-stage and non-metastatic disease, and had gone through chemotherapy and surgery. In BRE12-158 trial, we detected CTC in 26.4% of samples (36.3% of patients), and the average CTC number per tube is 3.8. Both CTC positivity rate and average CTC number are lower than those of IUSCC-0613 trial. And a significant association ($p = 0.001$, student's t-test, paired, one-tailed) were found between the number of CTCs detected from the samples of two trials. The result indicates that early-stage TNBC patients who had completion of chemotherapy and surgery did have lighter cancer burden than metastatic TNBC patients who had not received surgery. On the other hand, the enumeration of CTCs detected by our system have solid potential as a diagnosis marker to reflect the cancer status and disease progression.

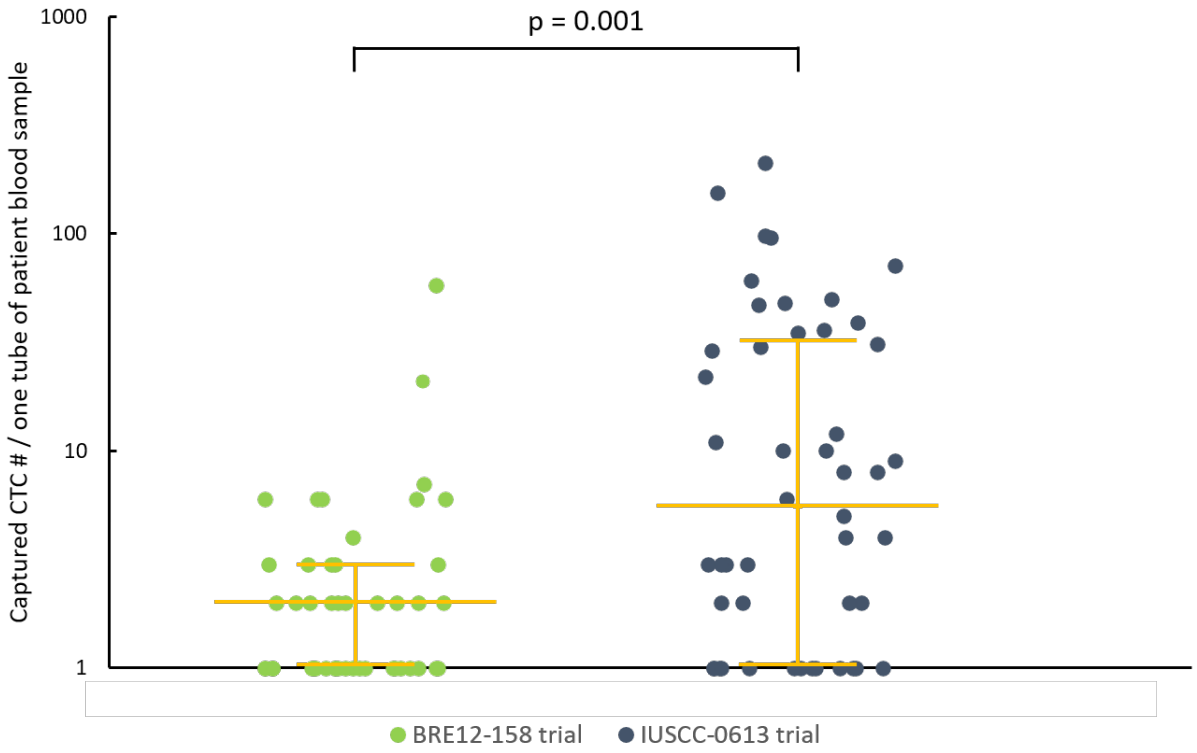

Figure 3.12. The median, upper and lower quartiles of number of CTCs detected in patient samples of BRE12-158 trial and IUSCC-0613 trial. BRE12-158 trial: CTCs were captured in 48 samples, the number ranged from 1 to 58. IUSCC-0613 trial: CTCs were captured in 48 samples, the number ranged from 1 to 212. Y-axis in logarithmic scale.

The number of CTCs identified in positive samples from each of the 8 patients is plotted in Figure 3.13. A student's t-test (paired, one-tailed) revealed a p-value of 0.003 on patient 7 and 8, and 0.007 on patient 6 and 7, indicating the significant association between CTC numbers of the patients. The statistical significance illustrates that the enumeration of CTCs captured by our system can reflect it when the CTC concentrations have a difference between different patients at the first place.

However, the result exposes the issue again of using a single type of antibody for detection: when the target surface antigen expression level on CTCs is low or no expression at all, the system cannot capture the CTCs though it is already very sensitive. This conclusion prompts us to explore a new panel of markers for CTC detection to bypass the limitation of relying on only EpCAM.

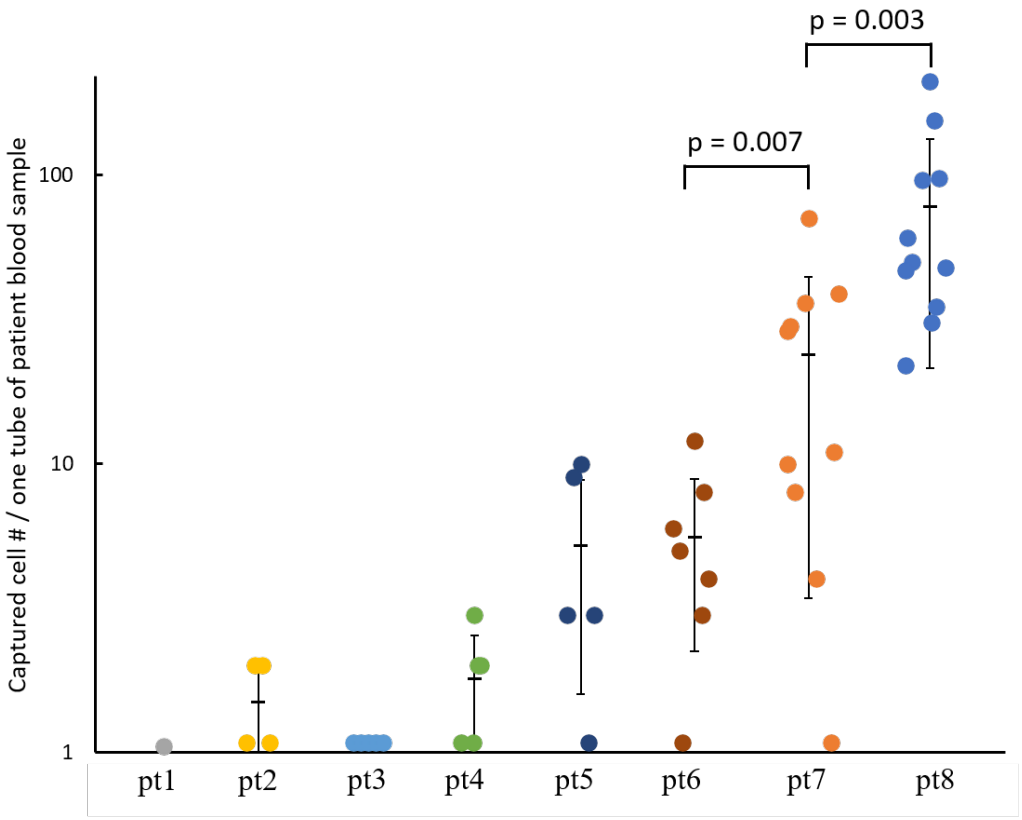

Figure 3.13. Number of CTCs identified in samples from each of the 8 mTNBC patients. Mean values and standard deviations are shown for each patient. Y-axis in logarithmic scale.

To compare with the first-generation system in regard of detection purity, we counted the number of captured WBCs from blood samples of IUSCC-0613 trial (data available in 100 out of 102 samples). The WBC counting is presented in Figure 3.14, the number ranged from 37 to 10,000, with a median of 242 and an average number of 1712 per sample. Compared with an average of 75.3 WBCs per sample detected from the sample of BRE12-158 trial using the first-generation system, the WBC depletion is decreased by 1.3-log. This is anticipated as a consequence of deliberately sacrificing purity in exchange of a higher sensitivity and throughput in the design process. Nevertheless, compared with $4 \sim 10 \times 10^7$ WBCs in a 7.5 mL tube of blood, the second-generation system can still effectively remove >99.996% (or 4.4-log depletion) of WBCs, which is still better than a lot of other CTC detection systems we reviewed. We deem the slightly lower yet still rather competitive detection purity acceptable.

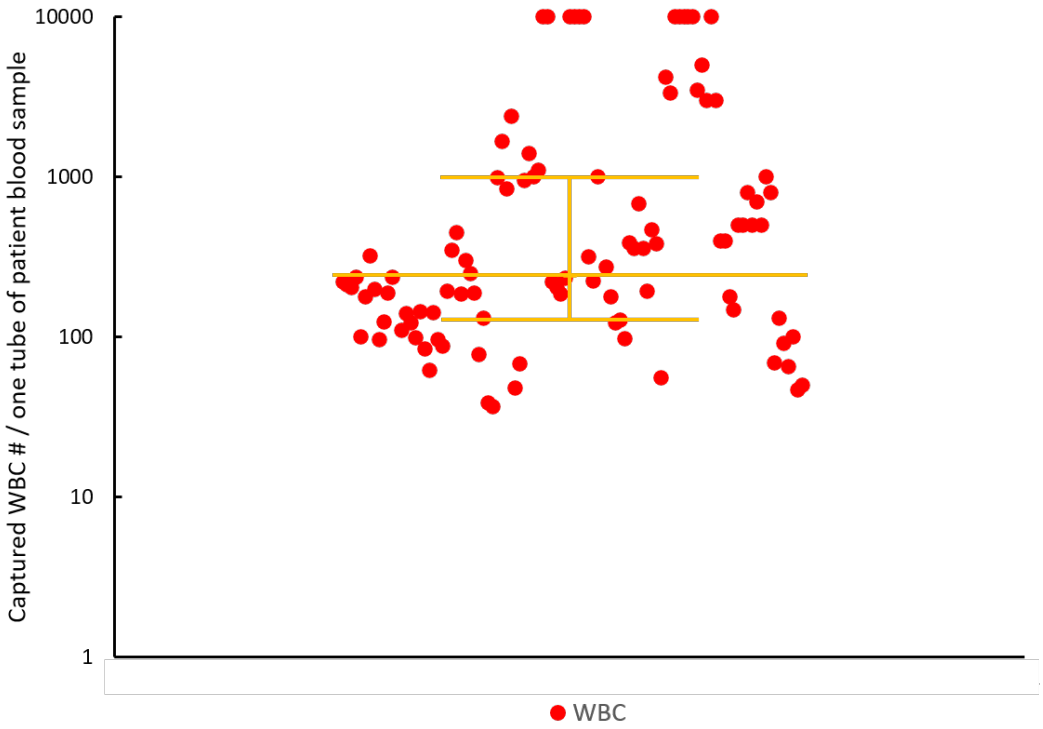

Figure 3.14. Number of WBCs captured from 100 samples, ranged from 37 to 10,000, with a median of 242. Median, upper, and lower quartiles are shown. Y-axis in logarithmic scale.

3.4.3 A 4-marker Panel for CTC Detection from mTNBC Patient Blood Samples

Next, we extend the application of the second-generation system by applying it to a clinical study for exploration of a novel panel of biomarkers for CTC detection from mTNBC. As introduced in the last section, the EpCAM-low or -negative phenotype is enriched in the CTCs of mTNBC, which demands high sensitivity and efficiency of the detection system. 13 patients were recruited, and two tubes of blood were drawn from each for paired analysis. Student's t-test (paired, one-tailed) was used to calculate significance of the association.

Of 8 complete pairs that contain available data from both methods, the 4-marker panel yielded a higher number of CTCs in 5/8, equal number in 2/8, and a lower number in only 1/8, as illustrated in Figure 3.15. The association did not reach significance ($p = 0.08$), but it just slightly missed the significance level. We attribute this to the relative narrow scope of this trial, with only 13 eligible patients. Though this preliminary result cannot be yet treated as a solid proof of the clinical usage of the protocol, it provides confidence in further revisioning. The 4-marker panel has the potential for CTC detection from mTNBC which has not been established previously. We

concluded that this panel of markers returned encouraging improvements in detection sensitivity in patients with mTNBC.

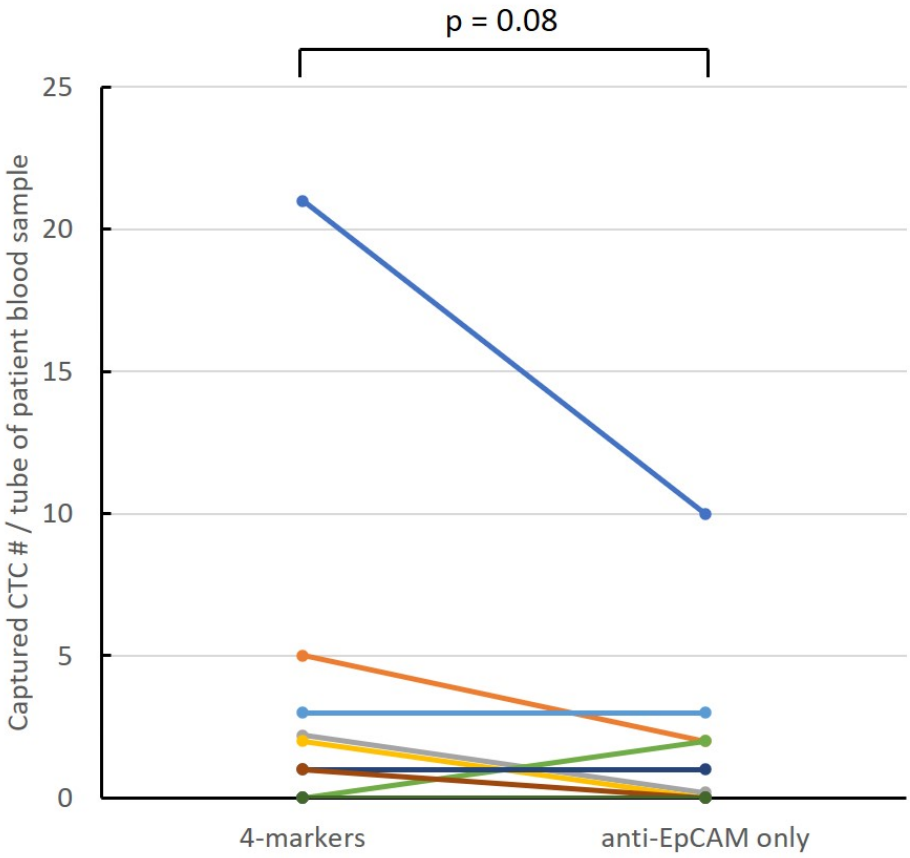

Figure 3.15. Number of CTCs identified in paired comparisons from 8 mTNBC patients. Association significance assessed by Student's t-test (paired, one-tailed).

Furthermore, as shown in Table 3.1, at least 1 CTC was detected using either detection method in 9/13 patients. It yielded a CTC positivity of 69% of patients, which looked like low at first. However, after matching with the patients' clinical follow-up (provided by the clinicians), we found that our system captured CTCs in 9/9 mTNBC patients with confirmed disease progression and 0/4 without progression (demonstrating therapeutic response or disease stabilization). The fact that the presence of CTCs identified by our system agrees well with disease progression illustrating the CTCs captured by our system can be used an independent diagnosis marker to help predict disease follow-up and help doctors' decision-making. The result demonstrated that the second-generation system is rather reliable for clinical utility.

Table 3.1. Paired comparisons of number of CTCs identified from 13 mTNBC patients.

Patient	CTC# detected by 4-marker panel	CTC# detected by anti-EpCAM only	Clinical follow-up
Pt 1	21	10	Confirmed disease progression
Pt 2	5	2	
Pt 3	2	0	
Pt 4	2	0	
Pt 5	3	3	
Pt 6	0	2	
Pt 7	1	1	
Pt 8	1	0	
Pt 9	NA*	6	
Pt 10	0	0	Without progression
Pt 11	0	0	
Pt 12	0	0	
Pt 13	0	0	

Note: Data not applicable due to technical issues.*

3.5 Summary

We have presented the second-generation microchip system for CTC detection and isolation with a higher detection efficiency and more streamlined workflow. By upgrading the device and protocol, the new system scale new heights in sensitivity in regard of capturing CTCs attached to very few beads. Another key improvement of the second-generation system is that it facilitates preservation of the captured CTCs to keep them alive, making them ideal for downstream analysis. We performed modeling and simulation of the system to study the physic behind it and to find the optimal magnet configuration. And the simulation result comparing the two generations verifies the higher sensitivity of the new system. In the characterization experiments, the new system yielded a >20% higher detection yield than the first-generation in capturing spiked cell line cells. We applied the system to CTC detection from 102 mTNBC patient samples as part of a phase I clinical trial, and captured CTCs in 47% of the samples (80% of the patients). The result is in agreement with the conclusions from other studies that EpCAM-low or -negative CTC phenotype is enriched in mTNBC. Yet our system still shows convincing detection efficiency. We further used the system to explore a novel 4-marker panel for CTC detection in mTNBC to tackle the CTC heterogeneity issue. Paired analysis was performed using blood samples from 13 mTNBC patients with 4-marker panel versus anti-EpCAM only. In 5/8 complete pairs, 4-marker panel captured

more CTCs than EpCAM only. Though slightly missed the significance level, the result is encouraging for providing valuable clinical insight. It is concluded that the 4-marker panel possesses robust potential to increase sensitivity in the analysis of CTCs in patients with mTNBC or other high heterogeneous cancers. Moreover, the presence of CTCs shows excellent correlation with these patients' disease progression course. The result that we detected CTCs from 9/9 patients with disease progression and 0/4 patients without progression demonstrates the potential of the system as a trustworthy clinical tool for CTC detection.

4. FUTURE WORK AND CONCLUSIONS

4.1 Introduction

The clinical utility of the first- and second-generation system have been demonstrated in Chapter 2 and 3, respectively, by detecting and isolating CTCs from breast cancer patient samples. In this chapter, we extend the potential of our system by further showing its ability to integrate with downstream applications, and discussing the proposed directions of future work. First, we present that the captured CTCs from the second-generation system can be further purified and individually picked up after readily transferred to a secondary microwell device. The retrieved single cells can be used for downstream analysis like genome sequencing, culturing, and molecular analysis. Future work is discussed regarding two aspects: improvement of the system performance, and a broad range of application areas of the system. The microfluidic device could be perfected regarding its performance by optimizing the fluid and magnetic field, as well as modifying experimental parameters under different conditions. Due to the versatility of our system, we envision it to be ideal for a variety of applications, including exploration of novel biomarkers for CTC detection, detection and isolation of CTC clusters, and detection of other types of rare cells from blood.

4.2 Downstream Applications

The presence and enumeration of captured CTCs by our system have been presented in previous chapters to have solid potential as clinical markers. As discussed in Chapter 1, except for being diagnosis or prognosis markers for cancer, CTCs can also be used for downstream analysis to provide a lot of vital information for both clinical and biology research purpose. To make the captured CTCs available for downstream applications, they need to be as pure as possible, which requires the system to be able to isolate and individually retrieve CTCs as single cells. Although our second-generation system can effectively deplete >99.996% of the WBCs, the detection purity is not ideal because there always are some unavoidable non-specific bindings. We cannot simply release the captured cells in bulk for downstream analysis, otherwise the non-targeted WBCs would reduce the purity (at both cellular and genetic level) by posing as background. So that we

need another downstream device to tackle this purity problem, to further purify the captured CTCs and enabling single cell retrieval.

4.2.1 Further Purification and Individual Retrieval of the Captured CTCs by Releasing to a Second Microchip Device

To achieve this aim, our group has developed a secondary microchip device, accommodating a microwell chip to further isolate all captured cells and enable individual retrieval [89]. Because of the principle of the immunomagnetic capturing we used, the magnetic beads conjugated cells are captured on chip only because of the external magnetic field, and no other chemical or biological connection exists, hence the transferring process can be achieved by manipulating magnets. The transferring process can be described as following: first, two devices are cascaded as shown in Figure 4.1(a), with the outlet of the microwell chip device connected to the pump;

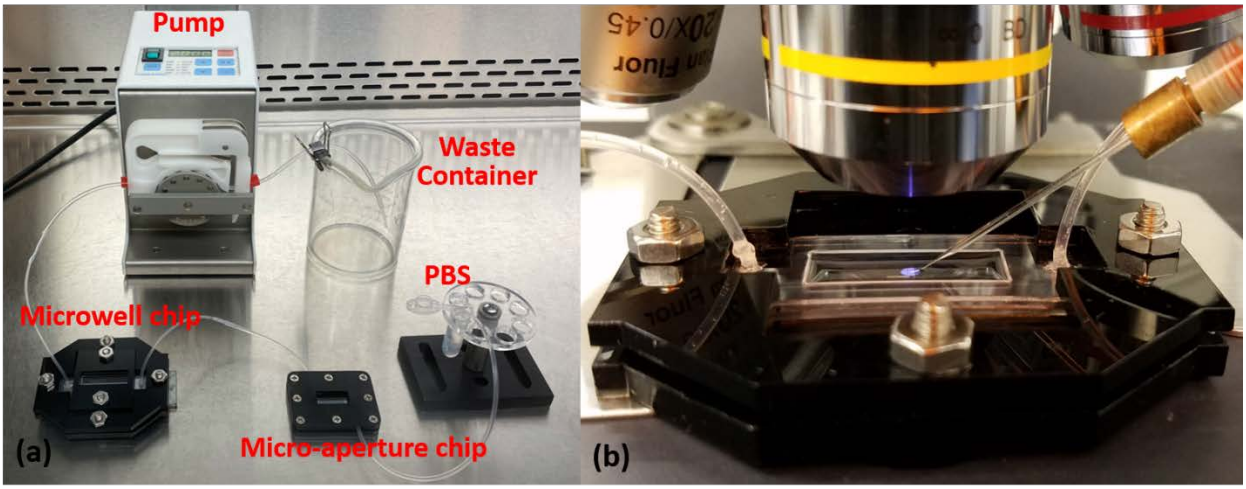

Figure 4.1. (a) Experiment setup for transferring captured cells from micro-aperture chip to microwell chip. (b) Experiment setup for cell retrieval using a micro pipette from an opened microwell chip device under microscope.

second, the magnet underneath the micro-aperture chip is removed, while another N52 permanent magnet is placed underneath the microwell chip; third, the captured cells are released under a PBS wash, and re-captured on the microwell chip; lastly, a manual sweeping of the magnet is conducted to guide the cells toward separate microwells and fall into them when encounter one. Thanks to the polymer layer coated on the chip surface, the captured cells on the micro-aperture chip can be

easily released as long as the magnetic is removed. There are more than 30,000 microwells fabricated on the microwell chip, and their diameters are delicately designed to contain target cells of a broad range of size. Compared with the number of captured cells (typically tens to hundreds) on the micro-aperture chip from a tube of blood, there are more than enough microwells to ensure almost every cell end up in a separate well. Experiments using spiked JEG-3 cells showed that 98% of the re-captured cells having 100% purity [89].

After transferring and re-locating, the top cover of the microwell chip device is opened, allowing a micro pipette to reach the top of the microwells and pick the cells up individually while monitoring under a bright field microscope, as shown in Figure 4.1(b). The picked cells can be subsequently pushed out to another collection vial or independent container and prepared for downstream analysis. This step is achieved using the same microaspiration system that we used for deterministic cell spiking as introduced in Chapter 2.

The process of detection, purification, and retrieval of a single CTC from a mTNBC patient sample is shown in Figure 4.2. (a) The CTC was first captured using our second-generation system, and immuno-stained for verification on chip as described in section 3.2.5. (b) Then we transferred the CTC to the microwell chip through the process described above, and re-located it again in a well with a diameter of 20 μm. (c) The CTC was picked up from the microwell, released to a small vial, and sent to our collaborators at Indiana University School of Medicine for genome analysis. We attribute the small dot of the red fluorescence signal close to the CTC in Figure 4.2(a) to anti-CD45-PE dye debris on background, since it was gone after transferring to the microwell chip.

By conducting the whole process, CTCs can be isolated from a whole blood sample as single cells with 100% purity.

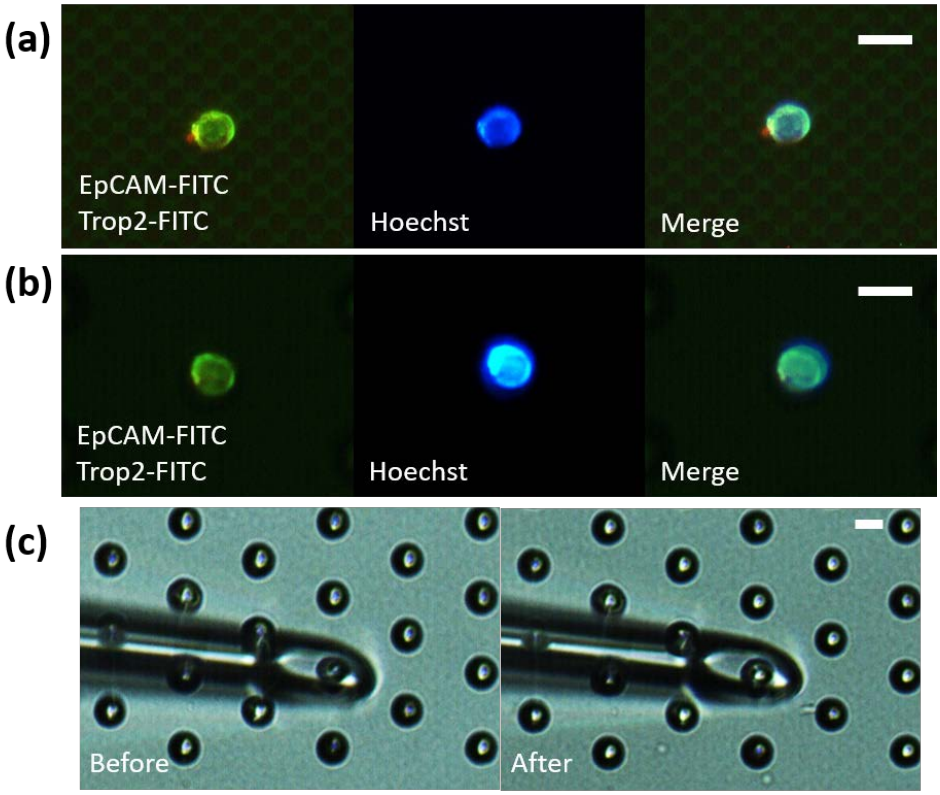

Figure 4.2. The whole process of detection, purification, and pickup of a single CTC from mTNBC patient sample. (a) Fluorescent and merged images of the CTC captured on the microchip surface using the second-generation system. (b) Fluorescent and merged images of the CTC re-located in a 20 μm microwell after releasing from the micro-aperture chip to the microwell chip. (c) Bright field images of the 20 μm microwell before and after the CTC was picked up by the micro pipette. All scale bars indicate 20 μm.

4.2.2 Downstream Analysis of Captured CTCs

As described in Chapter 3, to preserve CTCs, we adopted a surface immuno-staining method for on-chip cell identification, which avoids fixation and permeabilization. Therefore, the captured and individually retrieved single CTCs are viable and possess all vital information, making them ideal for downstream analysis like genome sequencing, molecular analysis, and culturing. For example, the CTCs detected from mTNBC patient samples of IUSCC-0613 trial, like the one shown in Figure 4.3, were picked up, stored in preservation solution, and sent to our collaborators in for DNA/RNA sequencing. Another study conducted by our group focuses on deterministic single cell culturing [98], the retrieved CTCs can be cultured individually and benefit a lot of research purpose like identification of biomarkers, understanding mechanisms of metastasis, and testing new cancer drugs.

4.3 Future Work

Our microchip system has been approved to be fast and robust, and possess excellent sensitivity and purity performing CTC detection and isolation from whole blood samples. There is still some room for improving and extending its application to a broader range of areas. Some of the possible directions of future work are discussed here.

4.3.1 System Performance Improvement

We anticipate that the sensitivity of the second-generation system can be further improved in several ways. First, the detection area on the microchip can be increased by enlarging the fabricated aperture area. Though we decided that the microchip size complies with the law of diminishing marginal utility, a bigger chip can always be used when a higher sensitivity is in demand, like when the expression level of the targeted antigens is very low. Larger detection area would enable usage of more antibody-beads for detection, allow bigger/more magnets to be placed underneath to generate a stronger magnetic field, and make a wider fluid channel possible. All these not only benefit the detection sensitivity, but also shorten the incubation time of antibody-beads. Second, the magnetic field can be enhanced by applying different magnet arrays or combinations, we plan to do further simulation and characterization experiments to find an optimal magnet array configuration. Third, the fluid channel can be modified to improve the detection performance. This can be achieved by designing micro-structures to change the flow and increase the chance of cells entering the area where the magnetic field is stronger.

4.3.2 Exploration of Novel Biomarkers for CTC Detection

Instead of clinical application, our system can also contribute to CTC related biology research. Due to its high sensitivity and reliability, it can be used as a testing tool for exploring new biomarkers, including different kinds of antibodies and synthetical ligands, for CTC detection and identification. As discussed in Chapter 3, using a single antibody to detect CTCs is largely restrained because CTCs have high phenotypic heterogeneity and may partly or entirely loss the expression of a particular antigen. A panel consists of multiple antibodies can tackle this problem to a large extent. The preliminary result discussed in section 3.4.3 has shown potential of our system for exploration of novel biomarker panels for CTC detection from mTNBC. We plan to

continue work with our collaborators at Indiana University School of Medicine to conclude this meaningful trial. We envision our system to be highly beneficial to explore novel biomarkers that expressed on CTCs for both detection and molecular biology purpose.

4.3.3 Detection and Isolation of CTC Clusters

CTC clusters' origin remains unknown, they can arise from either original tumor cell groupings or aggregate during intravascular circulation. And the biology and metastasis mechanisms behind them are largely unclear. However, studies have shown that CTC clusters exhibit dozens of times increased metastatic propensity compared to single CTCs [84,85]. Though even rarer than single CTCs, CTC clusters may possess more important clinical significance and could be a key for metastasis information.

The detection of CTC clusters is more demanding than that of single CTCs in two ways. First, the concentration of CTC clusters in patient blood is even lower than single CTCs, requiring the detection system to have ultra-high detection sensitivity. Besides, the CTC clusters can be so rare that the detection system needs to process larger volume samples (more than a typical 10 mL tube of blood) in order to capture one cluster. In this regard, our system has been proved to have desired high sensitivity and processing scalability. Second, the size of CTC clusters differs a lot depends on how many cells they consist of, hence the detection system must possess a wide size effective range. Many other microfluidic CTC detection platforms have a narrow size effective range, restricted by their delicate microfluidic structures. For example, size-based separation methods usually involve thin microchannels with a width of only tens of micrometers, which could be easily clogged by CTC clusters. On the contrary, our system has a great advantage in dealing with large cell clusters. The fluid channel of our device has dimensions in millimeter scale, which means theoretically there is no upper size limitation for capturing in the scale of cells. In our CTC detection experience from hundreds of patient blood samples, it is not unusual to find clusters with 2 or more CTCs, illustrating the ability of our system for capturing and handling CTC clusters. A giant CTC cluster detected using the second-generation system from a mTNBC patient sample is shown in Figure 4.3 as an example. The CTCs in the cluster are densely overlapped so that the accurate number cannot be counted, but at least 50 CTCs and 2 WBCs can be identified in the images. The dimension in the length direction of the cluster is nearly 200 μm, demonstrating the broad effective range of our system. Thanks to the versatility and high sensitivity of our system,

we anticipate that it can be used to simultaneously detect and isolate both single CTCs and CTC clusters, without much change to the structure or detection protocol. Nevertheless, the experimental conditions like flow rate and magnetic field are optimized aiming at single CTC capturing in this study, careful modeling and experimental characterization regarding cell cluster detection still needs to be done in the future.

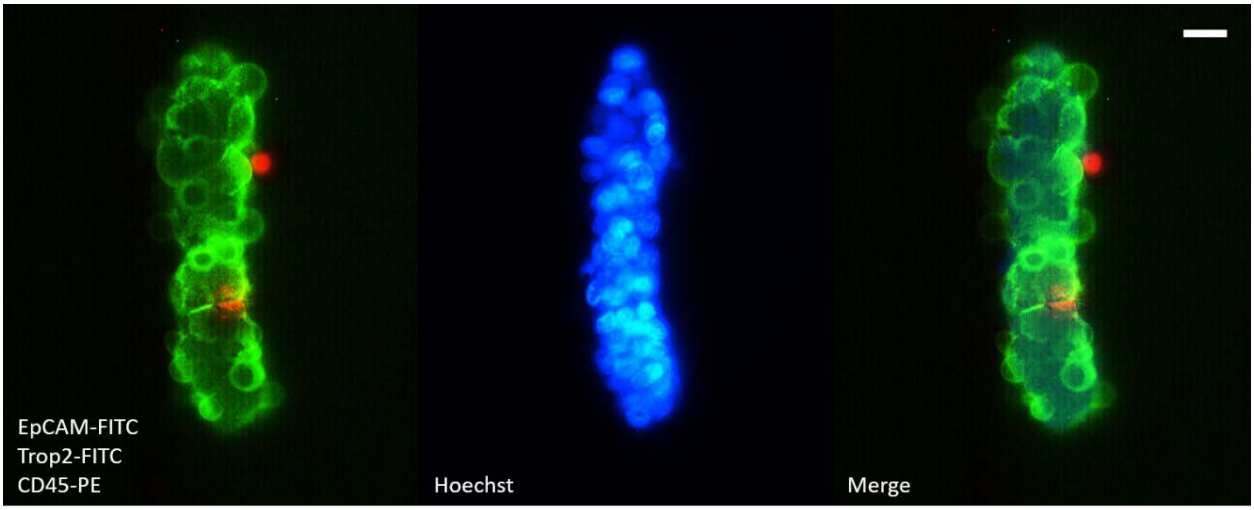

Figure 4.3. Fluorescent images of a big CTC cluster detected from breast cancer patient sample using the second-generation system. The number of CTCs in the cluster cannot be counted accurately due to its 3D shape and a lot of overlap. But at least 50 CTCs and 2 WBCs are identified in the image. Scale bar indicates 20 μm.

4.3.4 Detection and Isolation of Other Types of Rare Cells in Blood

The principle of our detection system is rather versatile, and can be easily transformed for isolating other types of rare cells in blood or body fluid. as long as a distinguished biomarker or a panel of biomarkers is known to separate them from other blood cells. This is especially useful when the target rare cells share similar physical properties with blood cells and are difficult to be separated by label-free methods. To detect other types of cells, the balance between detection sensitivity and purity needs to be specifically addressed for each type respectively, as discussed is section 4.3.1.

For example, isolation of circulating fetal cells (CFCs) from maternal blood is one of the application frontiers of rare cell detection. CFCs are rare cells that contain fetal genetic information while can be retrieved from maternal blood. They can be used for diagnosing chromosomal

abnormalities in fetus by genome analysis. The detection of CFCs is a non-invasive prenatal diagnostic method that could replace invasive clinical ways like amniocentesis. Like CTCs, CFCs are extremely rare in blood [109], and they also need to be isolated as pure single cells for genome analysis. These require the CFC detection system to possess ultra-high sensitivity and purity, which are well met by our system. EpCAM and HLA-G are known to express on the surface of CFCs, and are antigens commonly used for capturing. As introduced in section 3.2.4, JEG-3 and JAR are human choriocarcinoma trophoblastic cell lines, so that our characterization experiments for testing the second-generation system towards detection of CTCs are also applicable for CFCs. We plan to corporate with clinical research labs at Indiana University School of Medicine for detection of CFCs from maternal blood samples.

4.4 Conclusions

CTC detection is a high-yield non-invasive method that can provide vital diagnostic and prognostic information about cancer, yet it is technically challenging because of CTCs' high rarity and heterogeneity. The goal of this thesis is to develop a fast and robust CTC detection and isolation platform that has high sensitivity and purity. We proposed a detection strategy combining positive immunomagnetic capturing, size-based filtration, and high-throughput parallel flow. Employing this strategy, two generations of the microchip system have been developed and applied to achieve the CTC detection from whole blood patient samples.

The first-generation system can capture >95% of the spiked MCF-7 in blood, and it is sensitive to detect as few as one single cell in a tube of 7.5 mL of blood. The system was applied to an extremely challenging phase II clinical trial for CTC detection from 124 TNBC patients who had completion of chemotherapy and surgery and were clinically considered cancer-free. Our system found CTCs in 36.3% of the patients, indicating the existence of minimal residual disease and high risk of cancer relapse in these patients. A purity of >99.9998% depletion of WBCs was achieved by this system.

In order to further improve the detection sensitivity, especially targeting low marker expression CTCs, and further streamline the workflow, we developed the second-generation system. This system can capture >20% more spiked cells with a higher throughput than the previous generation, while maintaining the overall high performance. In addition, the captured cells are kept alive and can be readily released and retrieved as single cells for downstream analysis.

We applied the second-generation system to CTC detection from 102 mTNBC patient samples as part of a phase I clinical trial, although marker-low or -negative CTC phenotype is known to be enriched in mTNBC, we still captured CTCs in 47% of the samples. A novel 4-marker panel for CTC detection from mTNBC was explored using the second-generation system. The panel of markers was proved to improve detection efficiency to encompass CTC heterogeneity.

Our system has ultra-high detection sensitivity and purity, enables high-throughput flow, and possesses overall robustness and scalability. To our knowledge, currently there is no other platform that can achieve all these challenging objectives simultaneously. More importantly, our system has been applied to two clinical trials and a valuable clinical study, in which hundreds of patient blood samples were processed. The presence and enumeration of CTCs detected by our system well agreed with patients' disease course and progression, and the results demonstrate solid clinical implications of our system to assist cancer diagnosis and prognosis, as well as provide important clinical insight. We anticipate our system to be a reliable platform for a broad variety of clinical applications and research, and facilitate CTC analysis towards a standard clinical tool.

REFERENCES

[1] Sung, H., Ferlay, J., Siegel, R. L., Laversanne, M., Soerjomataram, I., Jemal, A., & Bray, F. (2021). Global cancer statistics 2020: GLOBOCAN estimates of incidence and mortality worldwide for 36 cancers in 185 countries. CA: a cancer journal for clinicians, 10.3322/caac.21660.

[2] Crowley, E., Di Nicolantonio, F., Loupakis, F., & Bardelli, A. (2013). Liquid biopsy: monitoring cancer-genetics in the blood. Nature reviews Clinical oncology, 10(8), 472.

[3] Zhang, J., Quadri, S., Wolfgang, C. L., & Zheng, L. (2018). New development of biomarkers for gastrointestinal cancers: From neoplastic cells to tumor microenvironment. Biomedicines, 6(3), 87.

[4] Alix-Panabières, C., & Pantel, K. (2017). Clinical prospects of liquid biopsies. Nature Biomedical Engineering, 1(4), 1-3.

[5] Pantel, K., & Alix-Panabières, C. (2019). Liquid biopsy and minimal residual disease—latest advances and implications for cure. Nature Reviews Clinical Oncology, 16(7), 409-424.

[6] De Rubis, G., Krishnan, S. R., & Bebawy, M. (2019). Liquid biopsies in cancer diagnosis, monitoring, and prognosis. Trends in pharmacological sciences, 40(3), 172-186.

[7] Alix-Panabières, C., & Pantel, K. (2016). Clinical applications of circulating tumor cells and circulating tumor DNA as liquid biopsy. Cancer discovery, 6(5), 479-491.

[8] Karachaliou, N., Mayo-de-Las-Casas, C., Molina-Vila, M. A., & Rosell, R. (2015). Real-time liquid biopsies become a reality in cancer treatment. Annals of translational medicine, 3(3).

[9] Esposito, A., Criscitiello, C., Locatelli, M., Milano, M., & Curigliano, G. (2016). Liquid biopsies for solid tumors: understanding tumor heterogeneity and real time monitoring of early resistance to targeted therapies. Pharmacology & therapeutics, 157, 120-124.

[10] Cohen, J. D., Li, L., Wang, Y., Thoburn, C., Afsari, B., Danilova, L., ... & Papadopoulos, N. (2018). Detection and localization of surgically resectable cancers with a multi-analyte blood test. Science, 359(6378), 926-930.

[11] Buscail, E., Alix-Panabières, C., Quincy, P., Cauvin, T., Chauvet, A., Degrandi, O., ... & Chiche, L. (2019). High clinical value of liquid biopsy to detect circulating tumor cells and tumor exosomes in pancreatic ductal adenocarcinoma patients eligible for up-front surgery. Cancers, 11(11), 1656.

[12] Etzioni, R., Urban, N., Ramsey, S., McIntosh, M., Schwartz, S., Reid, B., ... & Hartwell, L. (2003). The case for early detection. Nature reviews cancer, 3(4), 243-252.

[13] Chaffer, C. L., & Weinberg, R. A. (2011). A perspective on cancer cell metastasis. science, 331(6024), 1559-1564.

[14] Bidard, F. C., Jacot, W., Kiavue, N., Dureau, S., Kadi, A., Brain, E., ... & Pierga, J. Y. (2021). Efficacy of Circulating Tumor Cell Count–Driven vs Clinician-Driven First-line Therapy Choice in Hormone Receptor–Positive, ERBB2-Negative Metastatic Breast Cancer: The STIC CTC Randomized Clinical Trial. JAMA oncology, 7(1), 34-41.

[15] Bettegowda, C., Sausen, M., Leary, R. J., Kinde, I., Wang, Y., Agrawal, N., ... & Diaz, L. A. (2014). Detection of circulating tumor DNA in early-and late-stage human malignancies. Science translational medicine, 6(224), 224ra24-224ra24.

[16] Kang, Y., & Pantel, K. (2013). Tumor cell dissemination: emerging biological insights from animal models and cancer patients. Cancer cell, 23(5), 573-581.

[17] Rhim, A. D., Mirek, E. T., Aiello, N. M., Maitra, A., Bailey, J. M., McAllister, F., ... & Stanger, B. Z. (2012). EMT and dissemination precede pancreatic tumor formation. Cell, 148(1-2), 349-361.

[18] Marusyk, A., & Polyak, K. (2010). Tumor heterogeneity: causes and consequences. Biochimica et Biophysica Acta (BBA)-Reviews on Cancer, 1805(1), 105-117.

[19] Powell, A. A., Talasaz, A. H., Zhang, H., Coram, M. A., Reddy, A., Deng, G., ... & Jeffrey, S. S. (2012). Single cell profiling of circulating tumor cells: transcriptional heterogeneity and diversity from breast cancer cell lines. PloS one, 7(5), e33788.

[20] Yu, M., Bardia, A., Aceto, N., Bersani, F., Madden, M. W., Donaldson, M. C., ... & Haber, D. A. (2014). Ex vivo culture of circulating breast tumor cells for individualized testing of drug susceptibility. science, 345(6193), 216-220.

[21] Contreras-Naranjo, J. C., Wu, H. J., & Ugaz, V. M. (2017). Microfluidics for exosome isolation and analysis: enabling liquid biopsy for personalized medicine. Lab on a Chip, 17(21), 3558-3577.

[22] Wong, R. S. (2011). Apoptosis in cancer: from pathogenesis to treatment. Journal of Experimental & Clinical Cancer Research, 30(1), 1-14.

[23] Howard, E. W., Leung, S. C., Yuen, H. F., Chua, C. W., Lee, D. T., Chan, K. W., ... & Wong, Y. C. (2008). Decreased adhesiveness, resistance to anoikis and suppression of GRP94 are integral to the survival of circulating tumor cells in prostate cancer. Clinical & experimental metastasis, 25(5), 497-508.

[24] Paterlini-Brechot, P., & Benali, N. L. (2007). Circulating tumor cells (CTC) detection: clinical impact and future directions. Cancer letters, 253(2), 180-204.

[25] Giuliano, M., Shaikh, A., Lo, H. C., Arpino, G., De Placido, S., Zhang, X. H., ... & Trivedi, M. V. (2018). Perspective on circulating tumor cell clusters: why it takes a village to metastasize. Cancer research, 78(4), 845-852.

[26] Cen, P., Ni, X., Yang, J., Graham, D. Y., & Li, M. (2012). Circulating tumor cells in the diagnosis and management of pancreatic cancer. Biochimica et Biophysica Acta (BBA)-Reviews on Cancer, 1826(2), 350-356.

[27] Tewes, M., Aktas, B., Welt, A., Mueller, S., Hauch, S., Kimmig, R., & Kasimir-Bauer, S. (2009). Molecular profiling and predictive value of circulating tumor cells in patients with metastatic breast cancer: an option for monitoring response to breast cancer related therapies. Breast cancer research and treatment, 115(3), 581.

[28] Miyamoto, D. T., Sequist, L. V., & Lee, R. J. (2014). Circulating tumour cells—monitoring treatment response in prostate cancer. Nature reviews Clinical oncology, 11(7), 401.

[29] Onstenk, W., Gratama, J. W., Foekens, J. A., & Sleijfer, S. (2013). Towards a personalized breast cancer treatment approach guided by circulating tumor cell (CTC) characteristics. Cancer treatment reviews, 39(7), 691-700.

[30] Yu, M., Bardia, A., Aceto, N., Bersani, F., Madden, M. W., Donaldson, M. C., ... & Wittner, B. S. (2014). Ex vivo culture of circulating breast tumor cells for individualized testing of drug susceptibility. science, 345(6193), 216-220.

[31] Khoo, B. L., Grenci, G., Lim, Y. B., Lee, S. C., Han, J., & Lim, C. T. (2018). Expansion of patient-derived circulating tumor cells from liquid biopsies using a CTC microfluidic culture device. nature protocols, 13(1), 34-58.

[32] Cristofanilli, M., Pierga, J. Y., Reuben, J., Rademaker, A., Davis, A. A., Peeters, D. J., ... & Grisanti, S. (2019). The clinical use of circulating tumor cells (CTCs) enumeration for staging of metastatic breast cancer (MBC): International expert consensus paper. Critical Reviews in Oncology/Hematology, 134, 39-45.

[33] Schochter, F., Friedl, T. W., deGregorio, A., Krause, S., Huober, J., Rack, B., & Janni, W. (2019). Are Circulating Tumor Cells (CTCs) ready for clinical use in breast cancer? An overview of completed and ongoing trials using CTCs for clinical treatment decisions. Cells, 8(11), 1412.

[34] Baek, D. H., Kim, G. H., Am Song, G., Han, I. S., Park, E. Y., Kim, H. S., ... & Cho, Y. K. (2019). Clinical potential of circulating tumor cells in colorectal Cancer: a prospective study. Clinical and translational gastroenterology, 10(7).

[35] Sequist, L. V., Nagrath, S., Toner, M., Haber, D. A., & Lynch, T. J. (2009). The CTC-chip: an exciting new tool to detect circulating tumor cells in lung cancer patients. Journal of Thoracic Oncology, 4(3), 281-283.

[36] Rossi, G., Mu, Z., Rademaker, A. W., Austin, L. K., Strickland, K. S., Costa, R. L. B., ... & Cristofanilli, M. (2018). Cell-free DNA and circulating tumor cells: comprehensive liquid biopsy analysis in advanced breast cancer. Clinical Cancer Research, 24(3), 560-568.

[37] Mehlen, P., & Puisieux, A. (2006). Metastasis: a question of life or death. Nature reviews cancer, 6(6), 449-458.

[38] Fabisiewicz, A., & Grzybowska, E. (2017). CTC clusters in cancer progression and metastasis. Medical Oncology, 34(1), 12.

[39] Follain, G., Osmani, N., Azevedo, A. S., Allio, G., Mercier, L., Karreman, M. A., ... & Goetz, J. G. (2018). Hemodynamic forces tune the arrest, adhesion, and extravasation of circulating tumor cells. Developmental cell, 45(1), 33-52.

[40] Cho, H., Kim, J., Song, H., Sohn, K. Y., Jeon, M., & Han, K. H. (2018). Microfluidic technologies for circulating tumor cell isolation. Analyst, 143(13), 2936-2970.

[41] Ko, J. M. Y., Vardhanabhuti, V., Ng, W. T., Lam, K. O., Ngan, R. K. C., Kwong, D. L. W., ... & Li, W. S. (2020). Clinical utility of serial analysis of circulating tumour cells for detection of minimal residual disease of metastatic nasopharyngeal carcinoma. British Journal of Cancer, 1-12.

[42] Budd, G. T., Cristofanilli, M., Ellis, M. J., Stopeck, A., Borden, E., Miller, M. C., ... & Hayes, D. F. (2006). Circulating tumor cells versus imaging—predicting overall survival in metastatic breast cancer. Clinical Cancer Research, 12(21), 6403-6409.

[43] Radovich, M., Jiang, G., Hancock, B. A., Chitambar, C., Nanda, R., Falkson, C., ... & Schneider, B. P. (2020). Association of circulating tumor DNA and circulating tumor cells after neoadjuvant chemotherapy with disease recurrence in patients with triple-negative breast cancer: preplanned secondary analysis of the BRE12-158 randomized clinical trial. JAMA oncology, 6(9), 1410-1415.

[44] Cristofanilli, M., Budd, G. T., Ellis, M. J., Stopeck, A., Matera, J., Miller, M. C., ... & Hayes, D. F. (2004). Circulating tumor cells, disease progression, and survival in metastatic breast cancer. New England Journal of Medicine, 351(8), 781-791.

[45] Shen, Z., Wu, A., & Chen, X. (2017). Current detection technologies for circulating tumor cells. Chemical Society Reviews, 46(8), 2038-2056.

[46] Sarioglu, A. F., Aceto, N., Kojic, N., Donaldson, M. C., Zeinali, M., Hamza, B., ... & Toner, M. (2015). A microfluidic device for label-free, physical capture of circulating tumor cell clusters. Nature methods, 12(7), 685-691.

[47] Poruk, K. E., Valero III, V., Saunders, T., Blackford, A. L., Griffin, J. F., Poling, J., ... & Wolfgang, C. L. (2016). Circulating tumor cell phenotype predicts recurrence and survival in pancreatic adenocarcinoma. Annals of surgery, 264(6), 1073.

[48] Cheng, Y. H., Chen, Y. C., Lin, E., Brien, R., Jung, S., Chen, Y. T., ... & Yoon, E. (2019). Hydro-Seq enables contamination-free high-throughput single-cell RNA-sequencing for circulating tumor cells. Nature communications, 10(1), 1-11.

[49] Gkountela, S., Castro-Giner, F., Szczerba, B. M., Vetter, M., Landin, J., Scherrer, R., ... & Aceto, N. (2019). Circulating tumor cell clustering shapes DNA methylation to enable metastasis seeding. Cell, 176(1-2), 98-112.

[50] Klotz, R., Thomas, A., Teng, T., Han, S. M., Iriondo, O., Li, L., ... & Yu, M. (2020). Circulating tumor cells exhibit metastatic tropism and reveal brain metastasis drivers. Cancer discovery, 10(1), 86-103.

[51] Gulbahce, N., Magbanua, M. J. M., Chin, R., Agarwal, M. R., Luo, X., Liu, J., ... & Peters, B. A. (2017). Quantitative whole genome sequencing of circulating tumor cells enables personalized combination therapy of metastatic cancer. Cancer research, 77(16), 4530-4541.

[52] Bobek, V., Gurlich, R., Eliasova, P., & Kolostova, K. (2014). Circulating tumor cells in pancreatic cancer patients: enrichment and cultivation. World journal of gastroenterology: WJG, 20(45), 17163.

[53] Zhang, L., Ridgway, L. D., Wetzel, M. D., Ngo, J., Yin, W., Kumar, D., ... & Marchetti, D. (2013). The identification and characterization of breast cancer CTCs competent for brain metastasis. Science translational medicine, 5(180), 180ra48-180ra48.

[54] Woestemeier, A., Harms-Effenberger, K., Karstens, K. F., Konczalla, L., Ghadban, T., Uzunoglu, F. G., ... & Reeh, M. (2020). Clinical Relevance of Circulating Tumor Cells in Esophageal Cancer Detected by a Combined MACS Enrichment Method. Cancers, 12(3), 718.

[55] Alix-Panabieres, C. (2020). The future of liquid biopsy. Nature, 579(7800), S9-S9.

[56] Shields IV, C. W., Reyes, C. D., & López, G. P. (2015). Microfluidic cell sorting: a review of the advances in the separation of cells from debulking to rare cell isolation. Lab on a Chip, 15(5), 1230-1249.

[57] Li, W., Wang, H., Zhao, Z., Gao, H., Liu, C., Zhu, L., ... & Yang, Y. (2019). Emerging nanotechnologies for liquid biopsy: the detection of circulating tumor cells and extracellular vesicles. Advanced Materials, 31(45), 1805344.

[58] Alix-Panabières, C., & Pantel, K. (2014). Challenges in circulating tumour cell research. Nature Reviews Cancer, 14(9), 623-631.

[59] Sharma, S., Zhuang, R., Long, M., Pavlovic, M., Kang, Y., Ilyas, A., & Asghar, W. (2018). Circulating tumor cell isolation, culture, and downstream molecular analysis. Biotechnology advances, 36(4), 1063-1078.

[60] Riethdorf, S., Fritsche, H., Müller, V., Rau, T., Schindlbeck, C., Rack, B., ... & Pantel, K. (2007). Detection of circulating tumor cells in peripheral blood of patients with metastatic breast cancer: a validation study of the CellSearch system. Clinical cancer research, 13(3), 920-928.

[61] Cristofanilli, M., Hayes, D. F., Budd, G. T., Ellis, M. J., Stopeck, A., Reuben, J. M., ... & Terstappen, L. W. (2005). Circulating tumor cells: a novel prognostic factor for newly diagnosed metastatic breast cancer. Journal of clinical oncology, 23(7), 1420-1430.

[62] Ozkumur, E., Shah, A. M., Ciciliano, J. C., Emmink, B. L., Miyamoto, D. T., Brachtel, E., ... & Kimura, A. (2013). Inertial focusing for tumor antigen–dependent and–independent sorting of rare circulating tumor cells. Science translational medicine, 5(179), 179ra47-179ra47.

[63] Mishra, A., Dubash, T. D., Edd, J. F., Jewett, M. K., Garre, S. G., Karabacak, N. M., ... & Stott, S. L. (2020). Ultrahigh-throughput magnetic sorting of large blood volumes for epitope-agnostic isolation of circulating tumor cells. Proceedings of the National Academy of Sciences, 117(29), 16839-16847.

[64] Sollier, E., Go, D. E., Che, J., Gossett, D. R., O'Byrne, S., Weaver, W. M., ... & Di Carlo, D. (2014). Size-selective collection of circulating tumor cells using Vortex technology. Lab on a Chip, 14(1), 63-77.

[65] Kim, J., Cho, H., Han, S. I., & Han, K. H. (2016). Single-cell isolation of circulating tumor cells from whole blood by lateral magnetophoretic microseparation and microfluidic dispensing. Analytical chemistry, 88(9), 4857-4863.

[66] Chen, P., Huang, Y. Y., Bhave, G., Hoshino, K., & Zhang, X. (2016). Inkjet-print micromagnet array on glass slides for immunomagnetic enrichment of circulating tumor cells. Annals of biomedical engineering, 44(5), 1710-1720.

[67] Hoshino, K., Huang, Y. Y., Lane, N., Huebschman, M., Uhr, J. W., Frenkel, E. P., & Zhang, X. (2011). Microchip-based immunomagnetic detection of circulating tumor cells. Lab on a Chip, 11(20), 3449-3457.

[68] Chen, P., Huang, Y. Y., Hoshino, K., & Zhang, X. (2014). Multiscale immunomagnetic enrichment of circulating tumor cells: from tubes to microchips. Lab on a Chip, 14(3), 446-458.

[69] Vermesh, O., Aalipour, A., Ge, T. J., Saenz, Y., Guo, Y., Alam, I. S., ... & Gambhir, S. S. (2018). An intravascular magnetic wire for the high-throughput retrieval of circulating tumour cells in vivo. Nature biomedical engineering, 2(9), 696-705.

[70] Jan, Y. J., Chen, J. F., Zhu, Y., Lu, Y. T., Chen, S. H., Chung, H., ... & Yu, H. H. (2018). NanoVelcro rare-cell assays for detection and characterization of circulating tumor cells. Advanced drug delivery reviews, 125, 78-93.

[71] Warkiani, M. E., Khoo, B. L., Wu, L., Tay, A. K. P., Bhagat, A. A. S., Han, J., & Lim, C. T. (2016). Ultra-fast, label-free isolation of circulating tumor cells from blood using spiral microfluidics. Nature protocols, 11(1), 134-148.

[72] Bagnall, J. S., Byun, S., Begum, S., Miyamoto, D. T., Hecht, V. C., Maheswaran, S., ... & Manalis, S. R. (2015). Deformability of tumor cells versus blood cells. Scientific reports, 5, 18542.

[73] Hur, S. C., Henderson-MacLennan, N. K., McCabe, E. R., & Di Carlo, D. (2011). Deformability-based cell classification and enrichment using inertial microfluidics. Lab on a Chip, 11(5), 912-920.

[74] Zeinali, M., Lee, M., Nadhan, A., Mathur, A., Hedman, C., Lin, E., ... & Nagrath, S. (2020). High-throughput label-free isolation of heterogeneous circulating tumor cells and CTC clusters from non-small-cell lung cancer patients. Cancers, 12(1), 127.

[75] Lin, E., Rivera-Báez, L., Fouladdel, S., Yoon, H. J., Guthrie, S., Wieger, J., ... & Nagrath, S. (2017). High-throughput microfluidic labyrinth for the label-free isolation of circulating tumor cells. Cell systems, 5(3), 295-304.

[76] Gascoyne, P. R., Noshari, J., Anderson, T. J., & Becker, F. F. (2009). Isolation of rare cells from cell mixtures by dielectrophoresis. Electrophoresis, 30(8), 1388-1398.

[77] Gupta, V., Jafferji, I., Garza, M., Melnikova, V. O., Hasegawa, D. K., Pethig, R., & Davis, D. W. (2012). ApoStream™, a new dielectrophoretic device for antibody independent isolation and recovery of viable cancer cells from blood. Biomicrofluidics, 6(2), 024133.

[78] Pailler, E., Faugeroux, V., Oulhen, M., Catelain, C., & Farace, F. (2017). Routine clinical use of circulating tumor cells for diagnosis of mutations and chromosomal rearrangements in non-small cell lung cancer—ready for prime-time?. Translational lung cancer research, 6(4), 444.

[79] Alix-Panabières, C. (2012). EPISPOT assay: detection of viable DTCs/CTCs in solid tumor patients. Minimal residual disease and circulating tumor cells in breast cancer, 69-76.

[80] Del Ben, F., Turetta, M., Celetti, G., Piruska, A., Bulfoni, M., Cesselli, D., ... & Scoles, G. (2016). A Method for Detecting Circulating Tumor Cells Based on the Measurement of Single-Cell Metabolism in Droplet-Based Microfluidics. Angewandte Chemie, 128(30), 8723-8726.

[81] Rack, B. K., Schindlbeck, C., Andergassen, U., Schneeweiss, A., Zwingers, T., Lichtenegger, W., ... & SUCCESS Study Group. (2010). Use of circulating tumor cells (CTC) in peripheral blood of breast cancer patients before and after adjuvant chemotherapy to predict risk for relapse: The SUCCESS trial. Journal of Clinical Oncology, 28(15_suppl), 1003-1003.

[82] Miller, M. C., Doyle, G. V., & Terstappen, L. W. (2010). Significance of circulating tumor cells detected by the CellSearch system in patients with metastatic breast colorectal and prostate cancer. Journal of oncology, 2010.

[83] de Wit, S., Manicone, M., Rossi, E., Lampignano, R., Yang, L., Zill, B., ... & Andree, K. C. (2018). EpCAMhigh and EpCAMlow circulating tumor cells in metastatic prostate and breast cancer patients. Oncotarget, 9(86), 35705.

[84] Wei, R. R., Sun, D. N., Yang, H., Yan, J., Zhang, X., Zheng, X. L., ... & Ding, J. (2018). CTC clusters induced by heparanase enhance breast cancer metastasis. Acta Pharmacologica Sinica, 39(8), 1326-1337.

[85] Aceto, N., Bardia, A., Miyamoto, D. T., Donaldson, M. C., Wittner, B. S., Spencer, J. A., ... & Brannigan, B. W. (2014). Circulating tumor cell clusters are oligoclonal precursors of breast cancer metastasis. Cell, 158(5), 1110-1122.

[86] Chang, C. L., Huang, W., Jalal, S. I., Chan, B. D., Mahmood, A., Shahda, S., ... & Savran, C. A. (2015). Circulating tumor cell detection using a parallel flow micro-aperture chip system. Lab on a Chip, 15(7), 1677-1688.

[87] Eslami-S, Z., Cortés-Hernández, L. E., & Alix-Panabières, C. (2020). Epithelial Cell Adhesion Molecule: An Anchor to Isolate Clinically Relevant Circulating Tumor Cells. Cells, 9(8), 1836.

[88] Chang, C. L., Jalal, S. I., Huang, W., Mahmood, A., Matei, D. E., & Savran, C. A. (2014). High-throughput immunomagnetic cell detection using a microaperture chip system. IEEE Sensors Journal, 14(9), 3008-3013.

[89] Gur, O., Chang, C. L., Jain, R., Zhong, Y., & Savran, C. A. (2020). High-purity isolation of rare single cells from blood using a tiered microchip system. Plos one, 15(3), e0229949.

[90] Schlenoff, J. B. (2014). Zwitteration: coating surfaces with zwitterionic functionality to reduce nonspecific adsorption. Langmuir, 30(32), 9625-9636.

[91] Sin, M. C., Chen, S. H., & Chang, Y. (2014). Hemocompatibility of zwitterionic interfaces and membranes. Polymer journal, 46(8), 436-443.

[92] Ladd, J., Zhang, Z., Chen, S., Hower, J. C., & Jiang, S. (2008). Zwitterionic polymers exhibiting high resistance to nonspecific protein adsorption from human serum and plasma. Biomacromolecules, 9(5), 1357-1361.

[93] Vaisocherova, H., Yang, W., Zhang, Z., Cao, Z., Cheng, G., Piliarik, M., ... & Jiang, S. (2008). Ultralow fouling and functionalizable surface chemistry based on a zwitterionic polymer enabling sensitive and specific protein detection in undiluted blood plasma. Analytical chemistry, 80(20), 7894-7901.

[94] Brault, N. D., Sundaram, H. S., Huang, C. J., Li, Y., Yu, Q., & Jiang, S. (2012). Two-layer architecture using atom transfer radical polymerization for enhanced sensing and detection in complex media. Biomacromolecules, 13(12), 4049-4056.

[95] Brault, N. D., Gao, C., Xue, H., Piliarik, M., Homola, J., Jiang, S., & Yu, Q. (2010). Ultra-low fouling and functionalizable zwitterionic coatings grafted onto SiO2 via a biomimetic adhesive group for sensing and detection in complex media. Biosensors and Bioelectronics, 25(10), 2276-2282.

[96] Comșa, Ș., Cimpean, A. M., & Raica, M. (2015). The story of MCF-7 breast cancer cell line: 40 years of experience in research. Anticancer research, 35(6), 3147-3154.

[97] Hancock, B., Chang, C. L., Zhong, Y., Chen, Y. H., Solzak, J., Bales, C., ... & Radovich, M. (2019). 4-marker positive selection system for improved CTC analysis in metastatic triple-negative breast cancer.

[98] Jain, R., Chittiboyina, S., Chang, C. L., Lelièvre, S. A., & Savran, C. A. (2020). Deterministic culturing of single cells in 3D. Scientific reports, 10(1), 1-13.

[99] Chen, Y. H., Hancock, B. A., Solzak, J. P., Brinza, D., Scafe, C., Miller, K. D., & Radovich, M. (2017). Next-generation sequencing of circulating tumor DNA to predict recurrence in triple-negative breast cancer patients with residual disease after neoadjuvant chemotherapy. NPJ breast cancer, 3(1), 1-6.

[100] Garcia-Murillas, I., Chopra, N., Comino-Méndez, I., Beaney, M., Tovey, H., Cutts, R. J., ... & Turner, N. C. (2019). Assessment of molecular relapse detection in early-stage breast cancer. JAMA oncology, 5(10), 1473-1478.

[101] Dent, R., Trudeau, M., Pritchard, K. I., Hanna, W. M., Kahn, H. K., Sawka, C. A., ... & Narod, S. A. (2007). Triple-negative breast cancer: clinical features and patterns of recurrence. Clinical cancer research, 13(15), 4429-4434.

[102] Liedtke, C., Mazouni, C., Hess, K. R., André, F., Tordai, A., Mejia, J. A., ... & Pusztai, L. (2008). Response to neoadjuvant therapy and long-term survival in patients with triple-negative breast cancer. Journal of clinical oncology, 26(8), 1275-1281.

[103] Yu, M., Bardia, A., Wittner, B. S., Stott, S. L., Smas, M. E., Ting, D. T., ... & Maheswaran, S. (2013). Circulating breast tumor cells exhibit dynamic changes in epithelial and mesenchymal composition. science, 339(6119), 580-584.

[104] Shevkoplyas, S. S., Siegel, A. C., Westervelt, R. M., Prentiss, M. G., & Whitesides, G. M. (2007). The force acting on a superparamagnetic bead due to an applied magnetic field. Lab on a Chip, 7(10), 1294-1302.

[105] Fonnum, G., Johansson, C., Molteberg, A., Mørup, S., & Aksnes, E. (2005). Characterisation of Dynabeads® by magnetization measurements and Mössbauer spectroscopy. Journal of magnetism and magnetic materials, 293(1), 41-47.

[106] Elabbasi, N., Bergstrom, J., & Brown, S. (2011, October). Fluid-Structure Interaction Analysis of a Peristaltic Pump. In COMSOL conference in Boston.

[107] Wu, Q., Wang, J., Liu, Y., & Gong, X. (2019). Epithelial cell adhesion molecule and epithelial-mesenchymal transition are associated with vasculogenic mimicry, poor prognosis, and metastasis of triple negative breast cancer. International journal of clinical and experimental pathology, 12(5), 1678.

[108] Gorges, T. M., Tinhofer, I., Drosch, M., Röse, L., Zollner, T. M., Krahn, T., & Von Ahsen, O. (2012). Circulating tumour cells escape from EpCAM-based detection due to epithelial-to-mesenchymal transition. BMC cancer, 12(1), 1-13.

[109] Krabchi, K., Gros-Louis, F., Yan, J., Bronsard, M., Masse, J., Forest, J. C., & Drouin, R. (2001). Quantification of all fetal nucleated cells in maternal blood between the 18th and 22nd weeks of pregnancy using molecular cytogenetic techniques. Clinical genetics, 60(2), 145-150.

[110] Travers, P., Walport, M., Shlomchik, M. J., & Janeway, M. C. (1997). Immunobiology: the immune system in health and disease (pp. 1-52). Churchill Livingstone.

[111] Huang, W., Chang, C. L., Chan, B. D., Jalal, S. I., Matei, D. E., Low, P. S., & Savran, C. A. (2015). Concurrent detection of cellular and molecular cancer markers using an immunomagnetic flow system. Analytical chemistry, 87(20), 10205-10212.

[112] Huang, W., Chang, C. L., Brault, N. D., Gur, O., Wang, Z., Jalal, S. I., ... & Savran, C. A. (2017). Separation and dual detection of prostate cancer cells and protein biomarkers using a microchip device. Lab on a Chip, 17(3), 415-428.

VITA

Yuan Zhong received the B.S. degree in Department of Precision Instrument from Tsinghua University, Beijing, China in 2015. He is currently working toward the Ph.D. degree in School of Mechanical Engineering at Purdue University. His research focuses on development of novel platforms for cellular and biomolecular detection, which involves bioMEMS, bioinstrumentation and microfabrication.

Yuan got the opportunity to gain industry experience through internships at Savran Technologies Inc. in summer 2019 as lab assistant.